

T-4142

**THE DEGRADATION OF YTTRIA-STABILIZED ZIRCONIA IN
AQUEOUS SOLUTIONS**

by
Todd W. Kube

ProQuest Number: 10783778

All rights reserved

INFORMATION TO ALL USERS

The quality of this reproduction is dependent upon the quality of the copy submitted.

In the unlikely event that the author did not send a complete manuscript and there are missing pages, these will be noted. Also, if material had to be removed, a note will indicate the deletion.



ProQuest 10783778

Published by ProQuest LLC (2018). Copyright of the Dissertation is held by the Author.

All rights reserved.

This work is protected against unauthorized copying under Title 17, United States Code
Microform Edition © ProQuest LLC.

ProQuest LLC.
789 East Eisenhower Parkway
P.O. Box 1346
Ann Arbor, MI 48106 – 1346

T-4142

A thesis submitted to the Faculty and the Board of Trustees of the Colorado School of Mines in partial fulfillment of the requirements for the degree of Master of Science (Materials Science).

Golden, Colorado

Date 1 - 3 - 92

Signed: Todd W Kube

Todd W. Kube

Approved: Dr. Dennis W. Readey

Dr. Dennis W. Readey

Thesis Advisor

Golden, Colorado

Date 08 JANUARY 1992

William D. Copeland

Dr. William Copeland

Program Director,

Materials Science Program

ABSTRACT

The degradation of yttria-stabilized tetragonal zirconia polycrystalline ("Y-TZP") ceramics is characterized by an increased monoclinic content at the ceramic's surface and a drastic decrease in the material's strength. The degradation occurs at slightly elevated temperatures, generally in the 100-300°C range. Until this degradation problem is resolved, applications in which these elevated temperatures are reached and for which Y-TZP ceramics were once thought to be ideal candidates, can no longer be considered.

The research conducted and discussed in this thesis is aimed at understanding the mechanism, or mechanisms, which cause degradation of Y-TZP ceramics and powders. Experiments conducted included the degradation of: Y-TZP powders in 100°C water and 0.01 M HCl solutions; vapor phase sintered yttria in 100°C water and 0.01 M HCl solution; vapor phase sintered Y-TZP in 100°C water, 1.0×10^{-4} M HCl and 0.01 M HCl solutions; dense, polycrystalline Y-TZP samples for morphological investigations in 100°C water and 0.01 M HCl solution; and polycrystalline Y-TZP samples for mechanical investigations in water, 1.0×10^{-4} M HCl and 0.01 M HCl solutions.

The following conclusions and observations were made during these investigations:

- flexural investigations of Y-TZP samples exposed to 100°C water, 1.0×10^{-4} M HCl and 0.01 M HCl solutions show slight strength degradation yet dramatic increases in monoclinic contents in thin surface layers that did not adversely effect the strength;
- fine-grained Y-TZP showed less strength degradation and less monoclinic content than coarse-grained Y-TZP;
- yttrium dissolves preferentially from Y-TZP vapor phase sintered and dense polycrystalline ceramics;

- high silicon concentrations were found in the solutions in which vapor phase sintered ("VPS") samples were degraded;
- yttrium levels in the solutions in which VPS and dense polycrystalline samples were degraded do not appear to correlate to the exposed surface area;
- yttrium levels do not correlate well to idealized grain boundary concentration calculations, however, due to the assumptions made, correlations may exist;
- both SEM and TEM micrographs of polycrystalline Y-TZP indicate that grain boundary dissolution is occurring;
- pure yttria is soluble in water and 0.01 M HCl solutions, showing higher solubility in the acid solution; and,
- Y-TZP powders are unsuitable for degradation investigations due to their extraordinary stability and possible chemical inhomogeneity.

Based on the data presented and discussed in this thesis, the following qualitative degradation model is proposed: initial degradation is caused by the preferential dissolution of yttrium and silicon from grain boundaries; this dissolution reduces the matrix restraint from metastable tetragonal grains allowing them to transform to the monoclinic phase; when the grains transform, micro- and macro-cracks develop which guide the degrading solution into the interior allowing further degradation to occur.

TABLE OF CONTENTS

ABSTRACT	iii
LIST OF FIGURES	vii
LIST OF TABLES	xiv
ACKNOWLEDGMENTS.....	xv
1 INTRODUCTION.....	1
1.1 Y ₂ O ₃ - ZrO ₂ System	1
1.2 Degradation of Y-TZP	4
1.3 Degradation Models.....	9
1.4 Dissolution Behavior.....	14
1.5 Proposed Research.....	16
2 EXPERIMENTAL PROCEDURE	18
2.1 General Objectives	18
2.2 Materials.....	18
2.2.1 Powder Samples	20
2.2.2 Vapor Phase Sintered Samples	22
2.2.3 Polycrystalline Samples	24
2.2.4 Miscellaneous Materials	31
2.3 X-Ray Diffraction Analytical Techniques	33
2.3.1 Equipment, Settings, and Sample Mounting Techniques	33
2.3.2 Analysis of XRD Data.....	34
2.4 ICP - MS and ICP - ES.....	42

3	RESULTS.....	45
3.1	Powder Results.....	45
3.2	Vapor Phase Sintered Results.....	48
3.3	Polycrystalline Results.....	57
3.3.1	Morphological	57
3.3.2	Mechanical Testing.....	68
4	DISCUSSION.....	74
5	CONCLUSIONS.....	85
6	SUGGESTED FUTURE WORK.....	87
7	REFERENCES	88
8	APPENDICES.....	93
	Appendix A	93
	Appendix B	94

LIST OF FIGURES

<u>Figure</u>	<u>Page</u>
1.1	Zirconia rich section of the yttria-zirconia phase diagram 2
1.2	Undegraded Y-TZP ceramic (left) and Y-TZP ceramic degraded in 100°C 0.01 M HCl solution for approximately 260 hours..... 5
1.3	Degradation process of a Y-TZP MOR bar..... 6
1.4	Degradation model as described by Sato and Shimada 9
1.5	Degradation model as described by Yoshimura, Noma, Kawabata and Somiya..... 10
1.6	Degradation model as described by Lepisto and Mantyla..... 12
1.7	Degradation model as described by Lange, Dunlop and Davis 13
1.8	Stable yttrium compounds and predicted solubilities as a function of pH..... 15
1.9	Stable zirconium compounds and predicted solubilities as a function of pH..... 15
2.1	Photomicrograph of initial 3 mol% yttria-stabilized zirconia powder 21

Figure		Page
2.2	3 mol% Y-TZP sample which was vapor phase sintered in 1 atm HCl gas at 1300°C, for thirty minutes.....	23
2.3	Low magnification micrograph of Mines produced Y-TZP flexural test bar	27
2.4	Low magnification micrograph of Coors produced flexural test bar.....	28
2.5	High magnification micrograph of Mines produced flexural test bar.....	29
2.6	High magnification micrograph of Coors produced flexural test bar.....	30
2.7	Experimental matrix for degradation studies	32
2.8	XRD scans of cubic zirconia (8 mol% yttria), monoclinic zirconia (pure zirconia) and undegraded 3 mol% TZP powder	34
2.9	X-ray diffraction pattern for initial 3 mol% yttria-stabilized zirconia powder	35
2.10	Typical analysis of XRD data utilizing a Gaussian fit and linear background subtraction	39
2.11	XRD patterns for monoclinic/ cubic standards.....	40

<u>Figure</u>	<u>Page</u>
2.12	Comparison of volume fraction monoclinic calculations between Garvie, et al., Heuer, et al., Yoshimura, et al., and the ideal situation..... 41
2.13	Comparison of data as determined by ICP-MS and ICP-ES 42
3.1	Monoclinic contents of Y-TZP powder samples exposed to 95°C water 45
3.2	Yttrium and zirconium concentrations in solutions for Y-TZP powder samples in 95°C water 46
3.3	Monoclinic contents of Y-TZP powder samples exposed to 240°C 0.01M HCl solution 47
3.4	Yttrium and zirconium concentrations in solutions for Y-TZP powder samples in 240°C 0.01M HCl solution 47
3.5	Yttrium concentrations in solution for pure yttria samples exposed to 100°C water and 0.01 M HCl solution..... 49
3.6	Monoclinic contents of Y-TZP VPS samples exposed to 100°C water..... 50
3.7	Yttrium concentration in solution per unit surface area for Y-TZP VPS samples in 100°C water..... 50
3.8	Zirconium concentration in solution per unit surface area for Y-TZP VPS samples in 100°C water..... 51

<u>Figure</u>	<u>Page</u>
3.9	Silicon concentrations in solution per unit surface area for Y-TZP VPS samples in 100°C water..... 51
3.10	Monoclinic contents of Y-TZP VPS samples exposed to 1.0×10^{-4} M HCl solution..... 52
3.11	Yttrium concentration in solution per unit surface area for Y-TZP VPS samples in 1.0×10^{-4} M HCl solution..... 53
3.12	Zirconium concentration in solution per unit surface area for Y-TZP VPS samples in 1.0×10^{-4} M HCl solution..... 53
3.13	Silicon concentration in solution per unit surface area for Y-TZP VPS samples in 1.0×10^{-4} M HCl solution..... 54
3.14	Monoclinic contents of Y-TZP VPS samples exposed to 0.01 M HCl solution 55
3.15	Yttrium concentration in solution per unit surface area or Y-TZP VPS samples in 0.01 M HCl solution..... 55
3.16	Zirconium concentration in solution per unit surface area for Y-TZP VPS samples in 0.01 M HCl solution..... 56
3.17	Silicon concentration in solution per unit surface area for Y-TZP VPS samples in 0.01 M HCl solution..... 56
3.18	Monoclinic content of unpolished Y-TZP polycrystalline samples exposed to 100°C water..... 58

Figure	Page
3.19	Yttrium and zirconium concentrations in solutions from unpolished Y-TZP polycrystalline samples in 100°C water..... 58
3.20	SEM micrograph of unpolished Y-TZP sample which was exposed to 100°C water for 19.5 hours..... 59
3.21	SEM micrograph of unpolished Y-TZP sample which was exposed to 100°C water for 29.0 hours..... 60
3.22	SEM micrograph of unpolished Y-TZP sample which was exposed to 100°C water for 47.3 hours..... 61
3.23	SEM micrograph of unpolished Y-TZP sample which was exposed to 100°C water for 125.0 hours 62
3.24	TEM micrograph of two-stage replica from unpolished Y-TZP sample which was exposed to 100°C water for 125.0 hours 63
3.25	TEM micrograph of thin foil section from unpolished Y-TZP sample..... 64
3.26	Monoclinic content of polished Y-TZP sample which was exposed to 100°C 0.01 M HCl solution 66
3.27	Yttrium and zirconium concentrations in solutions from polished Y-TZP polycrystalline samples in 100°C 0.01 M HCl solution 66

<u>Figure</u>	<u>Page</u>
3.28	SEM micrograph of polished Y-TZP sample which was exposed to 100°C 0.01 M HCl solution for 169.0 hours..... 67
3.29	Bending strengths of Y-TZP flexural test bars after degrading in 100°C water 68
3.30	Bending strengths of Y-TZP flexural test bars after degrading in 100°C 1.0 x 10 ⁻⁴ M HCl solution 69
3.31	Bending strengths of Y-TZP flexural test bars after degrading in 100°C 0.01 M HCl solution..... 69
3.32	Monoclinic contents of flexural test bars degraded in 100°C water..... 70
3.33	Monoclinic contents of flexural test bars degraded in 100°C 1.0 x 10 ⁻⁴ M HCl solution..... 70
3.34	Monoclinic contents of flexural test bars degraded in 100°C 0.01 M HCl solution 71
3.35	SEM micrograph cross-section of Mines degraded flexural test sample 72
3.36	SEM micrograph cross-section of Coors degraded flexural test sample 73
4.1	Correlation between yttrium and zirconium concentrations in solution for Y-TZP samples exposed to 95°C water..... 75

<u>Figure</u>		<u>Page</u>
4.2	X-ray absorption as a function of Y-TZP thickness.....	83

LIST OF TABLES

<u>Table</u>		<u>Page</u>
2.1	Chemical composition of initial 3 mol% Y-TZP powder	19
2.2	Initial Y, Zr and Si concentrations in aqueous solutions.....	20
2.3	Standards submitted to Coors Analytical to establish data confidence	43
2.4	Standards from which error bars were determined.....	44
3.1	Surface areas of Y-TZP powder and vapor phase sintered samples.....	48

ACKNOWLEDGMENTS

There are numerous people who have helped me in my work on this project. First of all, I would like to thank Coors for their support of my research. I would also like to thank the people at Coors Analytical laboratories for their excellent and expeditious work. They not only conducted the analytical work, but they expressed an interest in my work and offered many suggestions. I would specifically like to thank Dan Downs and Ed Walters of the Physical Testing portion of Coors Analytical for letting me use their equipment and helping me with my flexural tests. Other people at Coors who have been of great help included Cathy Walters, Mike Letzig, and Don Giovanini.

I would like to thank Dr. Mike Readey and his staff at Carnegie Mellon University for their invaluable help in producing the TEM thin foil section micrographs. The data that they provided was very helpful in understanding what occurs at the grain boundaries during degradation.

I would like to thank the members of my committee for their time and patience. I would like to single out Dr. Mike Haun and Dr. Don Williamson and especially thank them for the help they provided during our many conversations. I would like to thank Dr. Dennis Readey, who as my chief advisor, offered a considerable amount of help during his extremely busy tenure as the Society President. I hope that I am never as busy as you have been in this last year. I would also like to thank my officemate, Marc Ritland, for his friendship and mental sparing.

Finally, I would like to thank two very special people who have shown great patience and support. First, I would like to thank my daughter, Lauren, for being born a healthy, happy baby. God knows what a great baby she has been for the first two months of her life. Other parents have complained that my wife, Robyn, and I have not suffered nearly enough; I suppose our second child will make up for Lauren. Secondly and lastly, I

would like to thank Robyn for her patience during a very stressful time. I would also like to thank her for her sometimes heartless, yet honest, editing of my paper. Without her I would be just another engineer who cannot write.

1 INTRODUCTION

Yttria-stabilized tetragonal zirconia ("Y-TZP") ceramics are used in many applications which require an extremely strong yet reasonably tough material. Examples of such applications include cutting blades (both industrial and culinary), grinding media, die inserts, bearing materials, roller guides, prostheses, engine parts and even tweezers.^{1, 2, 3} Fracture toughness values for Y-TZP ceramics range between 6.0 and 12.0 MPa $\sqrt{\text{m}}$, while flexural strengths range from 1000 to 1500 MPa, depending on the processing parameters.⁴ The combination of Y-TZP's extreme toughness and strength created great excitement in the ceramics world. However, in 1981 Kobayashi, et al., reported that yttria-stabilized zirconias suffered a strength degradation when exposed to approximately 250°C.⁵ This finding cast serious doubt on the ability to use these ceramics in applications in which slightly elevated temperatures are reached. The degradation of Y-TZP ceramics at these slightly elevated temperatures is the focus of the research conducted and reported on in this thesis.

1.1 Y₂O₃ - ZrO₂ System

There are many excellent reviews of Y-TZP ceramics, as well as zirconia-based ceramics in general.^{6, 7, 8} This thesis will make no attempt to cover all aspects of the yttria-zirconia system. However, a few fundamental details, which are pertinent to the research conducted for this thesis, will be reviewed.

Pure zirconia exhibits three polytypes -- cubic, tetragonal and monoclinic. The cubic, or fluorite, phase is stable from 2680°C to 2360°C, while the tetragonal phase is

stable from 2360°C to 1200°C and the monoclinic phase is stable from 1200°C down to room temperature. These three polytypes also occur when zirconia is alloyed with yttria. Fig. 1.1 presents the zirconia-rich portion of the yttria-zirconia phase diagram.

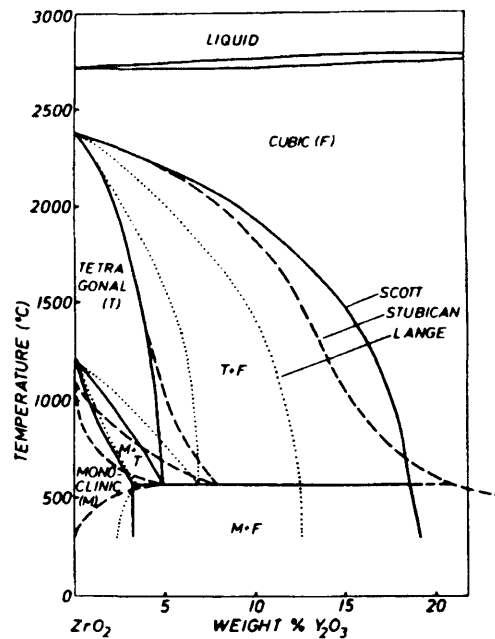


Fig. 1.1 Zirconia rich section of the yttria-zirconia phase diagram.⁹ The three different sets of lines are attributed to different authors and represent some of the uncertainty in the Y-TZP system.

The most interesting feature of the yttria-zirconia system is the phase transformation which occurs between the tetragonal and monoclinic phases at approximately 600°C. This transformation is not unique to the yttria-zirconia system. It also occurs in the magnesia-zirconia system at approximately 1240°C and in the calcia-zirconia system at approximately 1000°C.^{10, 11} The greatly reduced transformation temperature found in the yttria-zirconia system has significant implications for the design and use of toughened ceramics since the

upper temperature limit of the application should not exceed the transformation temperature and it is this transformation which is responsible for the toughness of stabilized zirconias.¹²

The tetragonal to monoclinic transformation, which was first discovered by Ruff and Ebert utilizing high temperature x-ray diffraction techniques, is unique in that it is a diffusionless, or martensitic, phase change.¹³ Not unlike the martensitic transformation which occurs in rapidly quenched steels, the martensitic transformation which occurs in zirconias is athermal. The transformation is accompanied by 4.7% increase in volume which can cause ceramics to crumble as they pass through the phase transformation.¹⁴ However, it is possible, through grain size and stabilizer control, to maintain an essentially 100% tetragonal polycrystalline zirconia through the transformation, thereby preventing a transformation to monoclinic. Typical grain sizes and stabilizer contents for tetragonal phase retention are less than 0.8 μm and 2.0 - 4.0 mol% yttria, respectively.¹⁵ In general, decreasing the grain size and increasing the yttria content increases the stability of the tetragonal phase.¹⁶

It is this ability to retain the metastable tetragonal phase that produces the high toughness of this material. When a crack with sufficient energy encounters a metastable tetragonal grain, the tetragonal grain transforms to the stable monoclinic phase. This transformation is characterized by a slight volume expansion which causes compressive stresses in the crack region. In order for the crack to propagate further it must accumulate sufficient energy to overcome the compressive stresses. It is by this mechanism that Y-TZP materials achieve such high toughness values.

1.2 Degradation of Y-TZP

The degradation of Y-TZP ceramics has many characteristics. These characteristics include:

- (1) the degradation is time-dependent and occurs at temperatures between 100 and 800°C, with the most rapid degradation occurring around 250°C;
- (2) the degradation is evidenced by an increased monoclinic content at the surface of the ceramic, creating a monoclinic layer which is severely micro- and macro-cracked;
- (3) the ceramic has a dramatic decrease in strength due to the monoclinic layer;
- (4) the degradation occurs in both liquid and gaseous environments, but quickest in liquid environments;
- (5) increasing the stabilizing content and decreasing the grain size slows the degradation; and,
- (6) degraded samples demonstrate preferred orientation, or texture, in the monoclinic and the residual tetragonal phases.

Fig. 1.2 illustrates how catastrophic the degradation can be even at low temperatures. In this figure, a comparison is made between an undegraded Y-TZP ceramic (left) to a degraded Y-TZP ceramic exposed to a 100°C 0.01 M HCl solution for approximately 260 hours (right). Fig. 1.3 schematically illustrates the degradation process of a cross-sectioned Y-TZP modulus of rupture ("MOR") test bar.

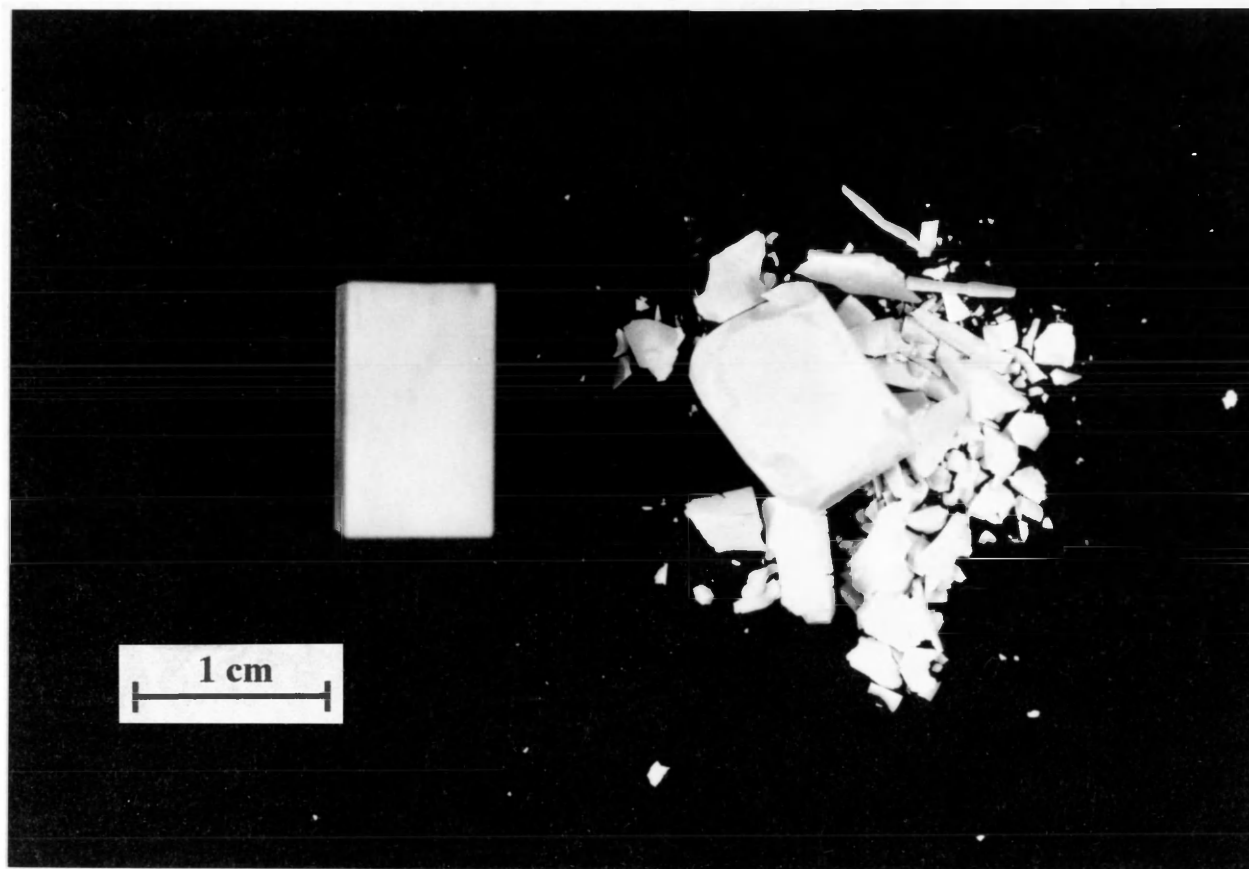


Fig. 1.2 Undegraded Y-TZP ceramic (left) and Y-TZP ceramic degraded in 100°C 0.01 M HCl solution for approximately 260 hours.

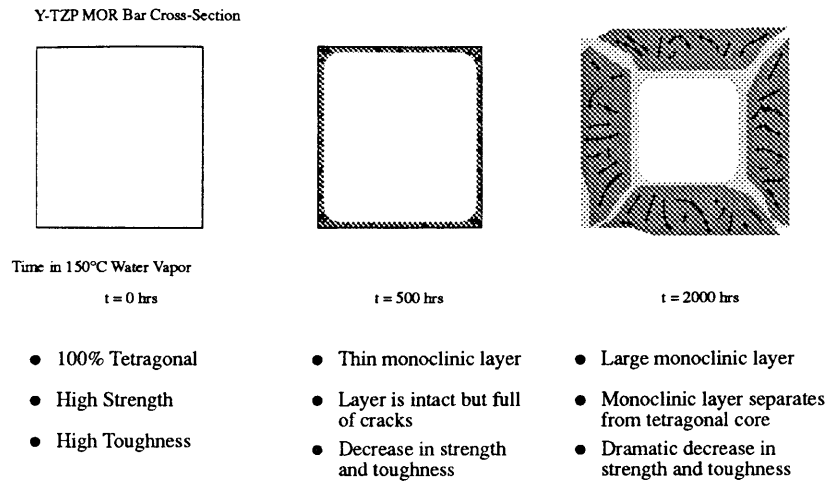


Fig. 1.3 Schematic of the degradation process of a Y-TZP MOR bar.

The degradation of Y-TZP is a time-dependent process which can be initiated in as little time as one hour.¹⁷ In addition, the monoclinic content reaches a saturation level which does not increase with further exposure to the degrading environment. Studies attempting to establish the temperature sensitivity of the process have shown that the process occurs at temperatures as low as 100°C and as high as 800°C.^{18, 19} However, the process occurs quickest at approximately 250°C.

The degradation is also evidenced by an increased monoclinic content at the surface of the ceramic. This monoclinic layer lacks structural integrity. Yet, when a monoclinic layer is created by abrading a Y-TZP ceramic, that monoclinic layer remains intact and actually improves the strength.^{20, 21} Both the aging process and the abrasion process cause the tetragonal phase to transform to monoclinic, a volume expansion of approximately 5%, but only the abrasion process creates a compressive layer. It has also been observed that abrading samples improves their resistance to degradation.^{22, 23} Jue, et al., found that when 3 mol% Y-TZP samples were polished then degraded in 275°C air they reached a monoclinic content of approximately 60% after 40 hours, whereas samples

which were machine-ground reached a maximum monoclinic content of approximately 40% after 110 hours in the same environment.²⁴

Another set of researchers not only abraded Y-TZP samples, they also annealed them at various temperatures above the transformation temperature in order to recrystallize tetragonal grains at the surface.²⁵ They found that by creating this uniform layer of ultra-fine grained tetragonal crystals at the surface they created a ceramic which was very resistant to degradation. They theorized that the inordinately stable tetragonal layer prevents the degradation from initiating at the surface and, as a result, the underlying bulk is relatively safe from aging.

The environment in which the aging occurs can drastically affect the extent of degradation. Sato and Shimada have investigated the degradation in various liquid solvents, as well as in water vapor conditions.^{26, 27} In their investigations of the effect of water vapor concentration on the degradation of Y-TZP ceramics they found that the degradation rate was directly proportional to the water partial pressure. In their investigations into the effects of various solvents on the degradation they found that solvents which contain lone pair electron orbitals opposite a proton donor site, such as water, degraded the samples the most. However, an apparent flaw is evident in this work in that their "nonaqueous" solvents contain small amounts of water yet they have shown in their water vapor experiments that the degradation is extremely sensitive to water content.

Not only is the degradation of Y-TZP ceramics strongly affected by the environment in which the aging takes place, but the microstructure and stabilizer content of the material play strong roles in determining the aging behavior. Many researchers have found that the aging behavior of Y-TZP ceramics was strongly influenced by both grain size and stabilizer content.^{28, 29, 30, 31, 32} Based on these accounts, the optimum yttria content and grain size necessary to avoid the degradation phenomena is approximately 4.0 mol% and 0.3 to 0.4 μm , respectively.

The last characteristic of the degradation to be discussed is the preferred orientation, or texture, that develops after aging and abrading. Preferred orientation occurs when

grains with a certain crystallographic orientation are present in a polycrystalline material in quantities which are greater than that found in a statistically random material.^{33, 34} The first report of such texturing occurred when Matsui, et al., observed in their XRD patterns that the monoclinic $(11\bar{1})$ peak of degraded Y-TZP ceramics was greater than expected.³⁵ Wang and Stevens explained that the preferred orientation results from the transformation of surface tetragonal grains whose (100) are perpendicular to the free surface.³⁶ Grains with this orientation initially transform more readily than other grain orientations due to a greater free energy reduction. They also found that as the degradation process proceeded, the preferred orientation phenomenon decreased as a result of the transformation of the remaining surface grains.

1.3 Degradation Models

A great deal of research has been devoted to understanding the degradation mechanism in the last ten years. Currently there are four different models which attempt to explain the degradation process. What follows are brief descriptions and discussions of these four models.

A large portion of the research conducted on the degradation of Y-TZP has occurred in Japan. A majority of this work has been undertaken by two groups, one headed by Masahiko Shimada and the other by Masahiro Yoshimura. Shimada and co-workers have proposed a degradation model which is schematically illustrated in Fig. 1.4.³⁷

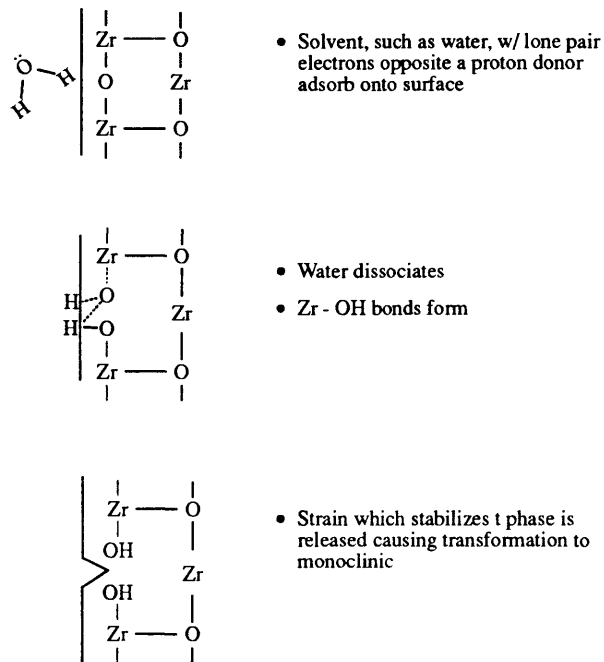


Fig. 1.4 Degradation model as described by Sato and Shimada.

According to the authors, degradation occurs when a solvent, such as water, which contains lone pair electrons opposite a proton donor site, adsorbs onto the surface of the ceramic. When water is used, the water dissociates into a proton and hydroxyl ion which enter into the lattice to form zirconium-hydroxyl bonds. The strain which is stabilizing the tetragonal grains is released and the tetragonal grain transforms to the lower energy monoclinic phase. Water penetrates into the subsurface of the ceramic via the micro-cracks and the degradation process proceeds.

Yoshimura and his group have also studied the degradation process extensively. Their model, which is similar to the Shimada model in many ways but contains a few striking contrasts, is illustrated in Fig. 1.5.³⁸

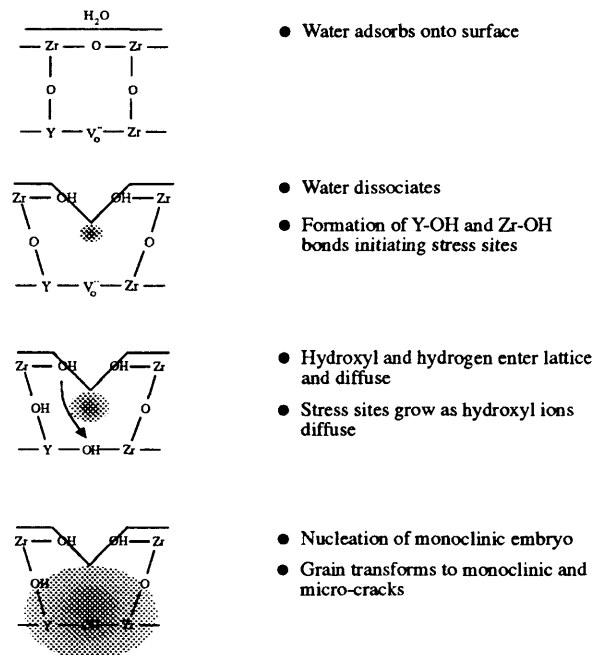
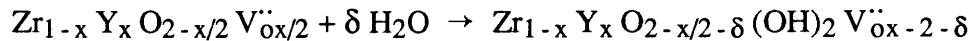


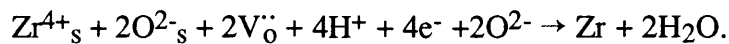
Fig. 1.5 Degradation model as described by Yoshimura, Noma, Kawabata and Somiya.

As in the Shimada model, water adsorbs onto the ceramic surface and dissociates. Yttrium and zirconium form bonds with the hydroxyl ions, initiating stress sites where there were once were zirconium, yttrium oxygen bonds. Hydroxyl ions, generated from further dissociation of water, diffuse through the lattice via oxygen sites according to the following reaction:



and increase the stress site size. This stress site serves to nucleate a monoclinic embryo which can cause the complete grain to transform from tetragonal to monoclinic if it grows beyond the critical size. Their model was supported by evidence of a weight gain and monoclinic lattice expansion after degradation, and then a weight loss and lattice contraction of these same samples after heating in a vacuum. In addition to this evidence, infrared absorption data indicated the presence of hydroxyl ions in the lattice.

A substantial amount of work on the degradation of Y-TZP has also been conducted outside of Japan. Lepisto and Mantyla have proposed a degradation model which is illustrated in Fig. 1.6.³⁹ This model proposes that water adsorbs at the ceramic's grain boundaries and dissociates into protons, electrons and diatomic oxygen. The dissociated water constituents react with the ceramic in the following reaction (The validity of this reaction is somewhat questionable since it does not follow conventional, accepted defect chemistry models and guidelines. It appears here as the authors have proposed it.):



The dissolution of the grain boundary relieves the matrix constraint that is preventing the transformation from tetragonal to monoclinic. Once this constraint is reduced or removed the grains are free to transform, resulting in micro- and macro-cracking. These cracks provide water a pathway into the interior to further the degradation.

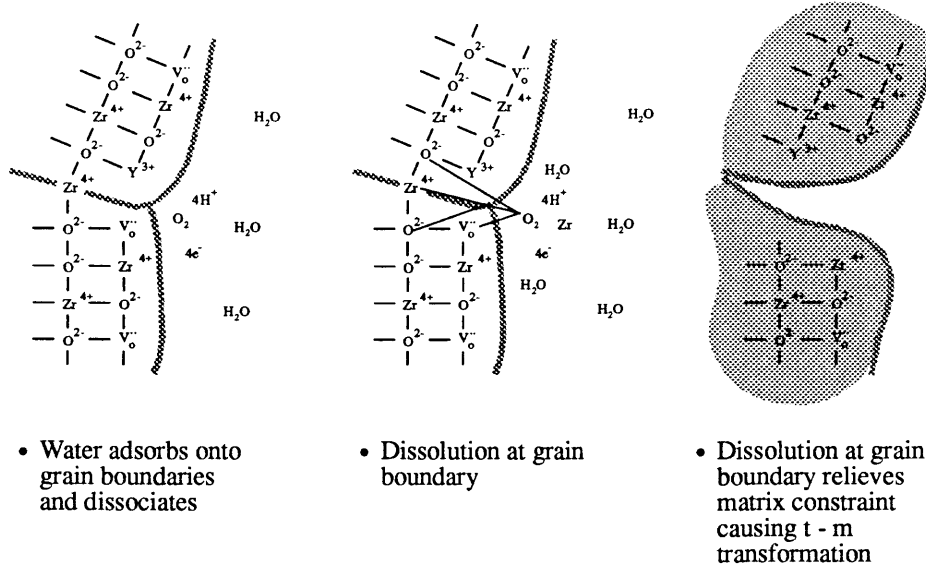


Fig. 1.6 Degradation model as described by Lepisto and Mantyla.

As with Yoshimura, et al., Lepisto and Mantyla also found evidence of OH^- ions on the ceramic surface. However, they found that the hydroxyl ions reside only on the very surface rather than throughout the degraded layer indicating that the hydroxyl ions were possibly adsorbed onto the surface rather than diffusing inward. An interesting aspect of this model, as indicated in the above reaction, is that the oxygen vacancy concentration dictates the dissolution rate. The authors propose that doping with another quadrivalent oxide, such as ceria, CeO_2 , should result in a tetragonal zirconia ceramic with very few oxygen vacancies and relatively resistant to the aging phenomena. In fact, it has been reported that stabilizing zirconia with other oxides such as ceria, titania and alumina does indeed increase the resistance to aging.^{40, 41, 42, 43, 44} Whether the increased stability is due to the decreased oxygen vacancies as predicted by Lepisto and Mantyla, or is simply due to an increased stabilizer content, is unclear. However, the validity of their model is called into question somewhat considering that increasing the yttria content improves resistance to degradation, it also increases the vacancy concentration. Their model predicts that increasing the yttria content increases the vacancy concentration, which should in turn

accelerate the degradation. Their vacancy dependent degradation model obviously has some flaws.

Another group of researchers, consisting of Lange, Dunlop and Davis have proposed another degradation model, a schematic of which is illustrated in Fig. 1.7.

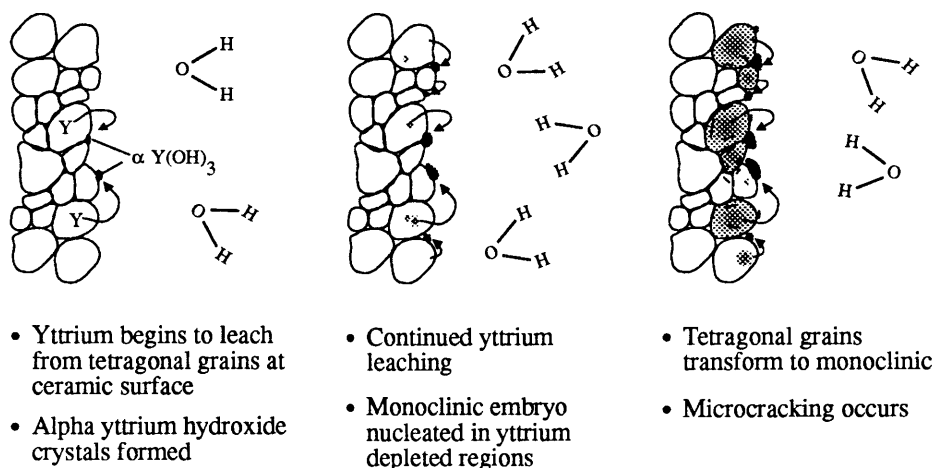


Fig. 1.7 Degradation model as described by Lange, Dunlop and Davis.

They propose that yttrium is preferentially leached from the surface tetragonal grains in contact with the solution to form alpha yttrium hydroxide. Yttrium-depleted regions in the tetragonal grains nucleate monoclinic embryos which can cause the tetragonal grains to transform to monoclinic grains if the yttrium depletion continues and the embryo grows beyond the critical size. When the grains transform to monoclinic they micro- and macro-crack, guiding water into the interior and furthering the degradation process. This group analyzed the aging behavior of a 6.6 mol% yttria-stabilized zirconia that contained cubic grains with tetragonal precipitates in a 250°C water vapor atmosphere. In their work they observed small precipitates which they identified through electron diffraction profiles as α -yttria hydroxide. Other workers have also found evidence of high yttrium contents at the surface of degraded samples and also subscribe to the Lange, et al., model.⁴⁵

1.4 Dissolution Behavior

With Lange's model in mind it is worthy to note that work has been done on the dissolution behavior of yttria-stabilized zirconia. Interestingly enough, Yoshimura, an author of one of the degradation models reviewed here, and others actually studied the dissolution of yttria-stabilized zirconia single crystals.⁴⁶ They observed that yttria fully-stabilized (14 mol%) zirconia decomposed into monoclinic zirconia in acidic solutions such as H₂SO₄ and HCl. They proposed that the dissolution mechanism was the preferential dissolution of yttrium. Unfortunately, they did not measure species concentration in the solutions to verify this. It is ironic that, even though they found evidence that yttria is preferentially leached from yttria-stabilized zirconia, they did not develop a model based on this mechanism. The reason for this, they report, is that the diffusion of yttrium in zirconia is so slow that preferential leaching of yttrium could not possibly be the mechanism responsible for the degradation.⁴⁷

The preferential leaching theory is supported by observations made by Nakajima, et al.⁴⁸ That group corroded samples with varied yttria contents in various acidic, neutral and basic solutions. Based on TEM micrographs of samples prior to and after aging, they reported corroded, transformed areas of the foil where yttria and zirconia levels were much lower than those of the samples prior to aging, indicating that the degradation process was indeed a corrosion mechanism.

The preferential dissolution of yttria from yttria-stabilized zirconia appears very probable from a thermodynamic standpoint. Stability diagrams constructed from thermodynamic data illustrate that both yttria and zirconia should not be very stable in water and especially unstable in acidic conditions.⁴⁹ Figs. 1.8 and 1.9 illustrate the various stable yttrium and zirconium compounds, respectively, as a function of pH based on thermodynamic calculations. These diagrams predict that yttria has a higher solubility than zirconium at the same pH. So, one would expect, based on these thermodynamic

predictions, that yttrium would preferentially leach from a zirconium yttrium matrix such as that found in yttria-stabilized zirconia.

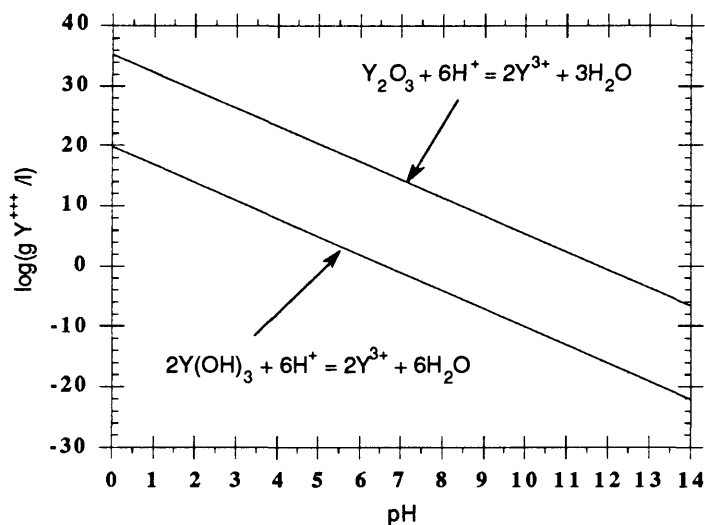


Fig. 1.8 Stable yttrium compounds and predicted solubilities as a function of pH at 25°C. (From Ref. 49)

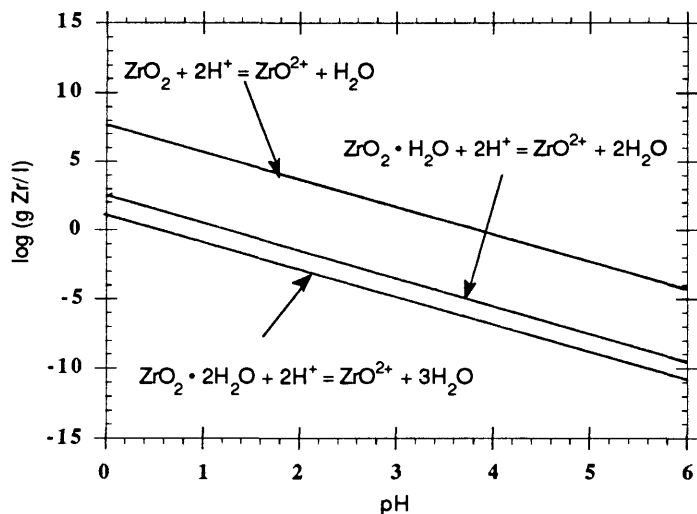


Fig. 1.9 Stable zirconium compounds and predicted solubilities as a function of pH at 25°C. (From Ref. 49)

Shafer and Roy analyzed the stability of various rare-earth oxides, including yttria, in water at various temperatures and pressures.⁵⁰ They found that two forms of yttrium compounds, $Y(OH)_3$ and $YOOH$, were the stable phases when yttria was exposed to water at temperatures between 0° and 600°C and pressures between 0.0 and 20,000 psi.

1.5 Proposed Research

Drawing on the above considerations, especially the α - $Y(OH)_3$ evidence of Lange, et al., and Winnubst, et al., the dissolution behavior observations of yttria-stabilized zirconias by Yoshimura and Nakajima, the thermodynamic predictions, and the yttria stability work by Shafer and Roy, the research conducted for this thesis will further investigate the dissolution and degradation behavior of yttria stabilized zirconia in aqueous environments.

High surface area materials will be utilized for dissolution investigations while, conventional, dense materials will be employed for morphological and mechanical investigations. All degradation experiments will occur in liquid media, specifically water, 1.0×10^{-4} M HCl and 0.01 M HCl solutions. Aqueous media were chosen because, while the degradation occurs in gaseous environments, it becomes very complex to evaluate the various transport mechanisms occurring in the gas solid system. Whereas in an aqueous system, mass transport is relatively straightforward, thereby making data interpretation much easier.

While the literature has shown that the degradation occurs quickest at 250°C, the experiments reported on in this thesis occurred at 100°C with the exception of one powder experiment which was conducted at 240°C. 100°C was chosen as a degradation

temperature because some of the experiments, specifically the mechanical mixtures needed to be carried out in 1000 ml boiling flasks. Working at temperatures much higher than 100°C would require expensive, large volume, high pressure reaction vessels. As a result, the relatively low degradation temperature was selected. The 240°C temperature was chosen because the powder was found to be very resistant to degradation at 100°C and the maximum usable temperature of the 25 ml reaction chamber was 240°C. Consequently, the 240°C temperature was chosen.

2 EXPERIMENTAL PROCEDURE

2.1 General Objectives

For the reasons discussed in the introduction, the degradation model proposed by Lange, Dunlop and Davis appears to be the most reasonable. As a result, the research conducted and reported in this thesis will focus on investigating the preferential leaching of yttrium from the Y-TZP lattice and correlating these findings with changes in the monoclinic content of the Y-TZP ceramic. Therefore, the general strategy of the research is to degrade Y-TZP samples in an aqueous solution and then measure the monoclinic content and the ionic species concentration in solution as a function of exposure time.

2.2 Materials

Three different types of yttria-stabilized zirconia ceramics were used in the degradation studies: (1) commercially available 3 mol% yttria-stabilized zirconia powder*; (2) vapor-phase-sintered 3 mol% Y-TZP samples made from the above powder; and (3) various polycrystalline dense 3 mol% Y-TZP ceramics also made from the above powder. Y-TZP powders were used since they contain both a high specific surface area, 1.8 m²/g, and approximately 60.0 vol% tetragonal phase and 40.0 vol% monoclinic phase. Vapor phase sintered samples were necessary due to problems encountered with the powders,

* HSY-3 powder, Zirconia Sales (America), Inc., Marietta, GA (404) 590-7970.

which will be explained later in the discussion. Polycrystalline samples were utilized for morphological and mechanical studies. Spectrochemical analysis for the initial 3 mol% Y-TZP powder is given in Table 2.1.

Table 2.1 Chemical composition of initial 3 mol% (5.4 wt%) Y-TZP powder ([†] - determined by X-Ray Fluorescence, * - determined by ICP-MS).

Component	Mol%	Wt %
ZrO ₂ [†]	95.1	93.2
Y ₂ O ₃ [†]	3.1	5.6
Al ₂ O ₃ [*]	0.9	0.7
SiO ₂ [†]	0.5	0.2
TiO ₂ [†]	0.3	0.2
P ₂ O ₅ [*]	0.06	0.07
MgO [*]	0.02	0.01
Fe ₂ O ₃ [*]	0.01	0.02
NaO [*]	0.01	0.003

Three aqueous solutions were used in this research -- 0.01 M HCl (pH 2), 1×10^{-4} M HCl (pH4), and distilled water. The HCl solutions were made from a commercially available* 68.6% HCl solution and distilled water. Initial yttrium, zirconium and silicon concentrations for the three solutions are given in Table 2.2.

* Reagent Grade Hydrochloric Acid, J. T. Baker Chemical Company, Phillipsburg, NJ.

Table 2.2 Initial Y, Zr and Si concentrations in aqueous solutions as determined by ICP-ES.

Solution	Y (mg/l)	Zr (mg/l)	Si (mg/l)
0.01 M HCl	0.02	< 0.01	0.06
1×10^{-4} M HCl	0.08	< 0.01	< 0.01
Water	< 0.01	< 0.01	< 0.01

2.2.1 Powder Samples

The experiments involving the various 3 mol% Y-TZP powders were conducted as follows. 4.0 g samples were weighed. Each sample was placed, along with 10 ml of the desired solution, in a 23 ml digestion bomb*. (This solids content was selected based on the need for sufficient quantities of powder for XRD analysis and the need for a fluid, low viscosity mixture.) The powder-water mixture had the consistency of milk. The samples were then placed in a drying oven at the desired temperature for the specified time. After the specified time had expired, the sample was removed and quenched to room temperature. The contents of the bomb was either centrifuged at 5000 rpm for thirty minutes or filtered through 0.45 μm and 0.1 μm tandem filters† to effectively separate the powder from the solution. The powders were then analyzed for monoclinic contents, while the solutions were analyzed for yttrium, zirconium and silicon concentrations. Fig. 2.1 is a photomicrograph of the Y-TZP powder prior to degradation.

* Bomb # 4749, Parr Instrument Company, Moline, IL 61265 (309) 762-7716

† Millipore Corporation, Bedford, MA 01730

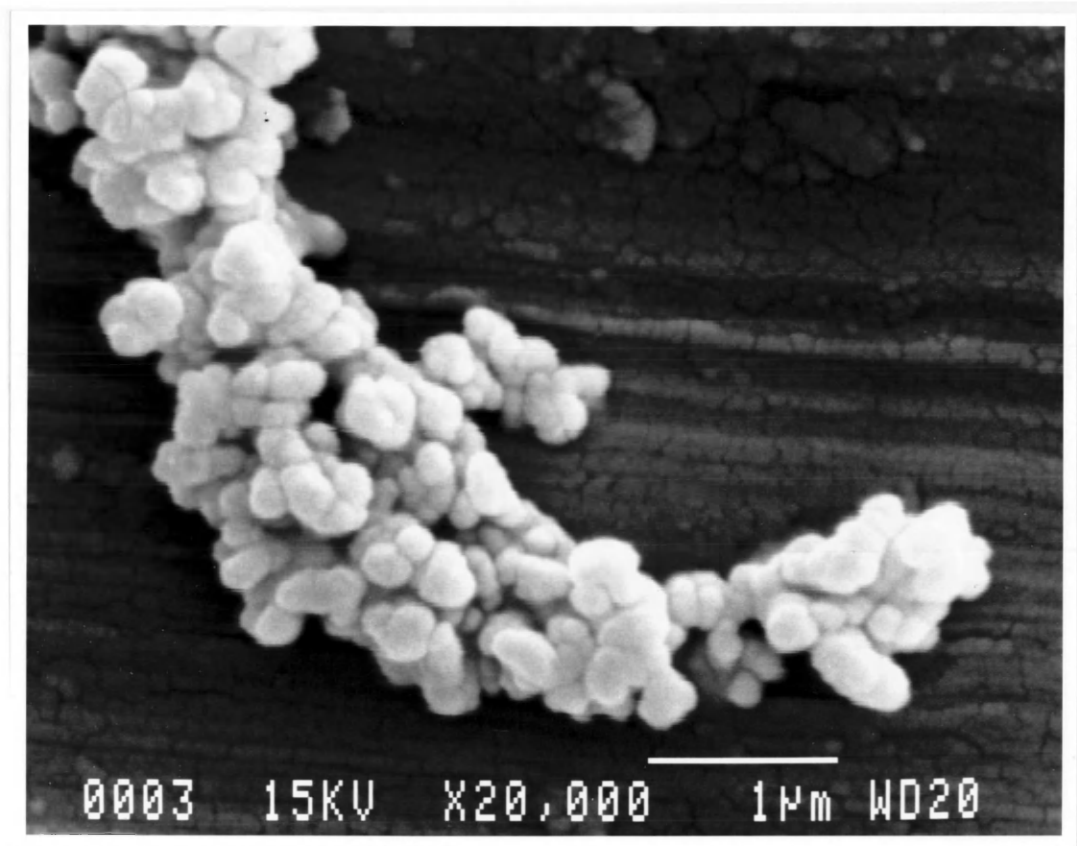


Fig. 2.1 Photomicrograph of initial 3 mol% yttria-stabilized zirconia powder.

2.2.2 Vapor Phase Sintered Samples

Vapor phase sintered samples were used due to difficulties encountered with Y-TZP powders. The details of which are discussed in the discussion. It is sufficient to state here that vapor phase sintering ("VPS") created a homogeneous, relatively unstable material which was suitable for degradation investigations. Vapor phase sintering was conducted according to the methods of Readey and Readey, who observed pure zirconia's enhanced grain growth without shrinkage by sintering zirconia in a HCl atmosphere.⁵¹ (For more details on this procedure see the reference cited.) For this research, vapor phase sintered samples were produced by pressing 3 mol% yttria-stabilized powder into 0.5 inch diameter pellets at 1400 pounds, resulting in a pressing pressure of approximately 7000 psi. Pellets were presintered at 1300°C for 1 minute to improve green strength. Samples were then placed in fused silica ampules which were closed at one end and open at the other. The ampules were then evacuated, flushed with argon numerous times, and filled with approximately 0.2 atmospheres of HCl in order to have a pressure of approximately 1.0 atmospheres at 1300°C. The sample-containing ampules were placed in a 1300°C tube furnace for thirty minutes and then removed. According to Readey and Readey, this should have resulted in a material with an approximate average grain size slightly greater than 1.0 μm . Fig. 2.2 demonstrates the typical microstructure resulting from the above-described vapor phase sintering technique. Initial, undegraded samples contained no monoclinic phase as determined by XRD.

Experiments conducted with the vapor phase sintered samples were nearly identical to the powder experiments. Each pellet was placed, along with 10 ml of the desired solution, in a digestion bomb and then placed in the drying heater for the specified amount of time. After that time expired, the bomb was removed from the oven and quenched to room temperature. The pellets were removed and dried for XRD analysis. The solutions were filtered through the 0.45 μm /0.1 μm tandem filter system to remove any powder particles and analyzed for yttrium, zirconium and silicon concentrations.

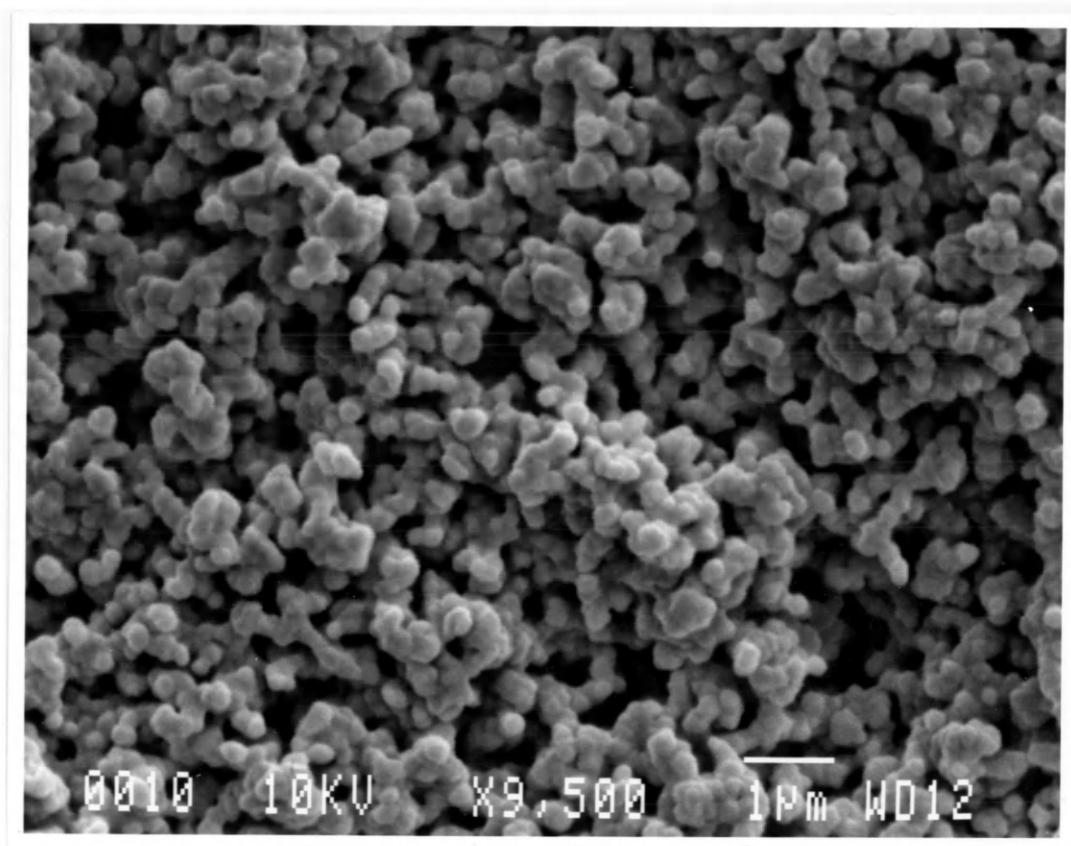


Fig. 2.2 3 mol% Y-TZP sample which was vapor phase sintered in 1 atm HCl gas at 1300°C, for thirty minutes.

The solubility of pure yttria was also investigated. Vapor phase sintered samples were prepared from a commercially available yttria powder* by pressing 2.0 g, 0.5 inch diameter pellets at 1400 pounds. Samples were sintered at 1500°C in 1.0 atm HCl. Unfortunately, the samples did not sinter as expected. Whereas previous enhanced vapor phase sintering of yttria-stabilized zirconia resulted in increased grain growth while restraining densification, vapor phase sintering of pure yttria resulted in crumbled pellets. Since the object of vapor phase sintering for this research is to repeatedly obtain a porous, controlled grain size material and these objectives can be partially achieved by under-sintering, yttria pellets were sintered in air at 1500°C for 30 minutes.

The same solubility investigation procedures were conducted for the yttria pellets as for the VPS Y-TZP material. Yttrium concentrations in the solutions were determined by ICP-ES. The yttria solubility studies were conducted in 100°C water and 100°C 0.01 M HCl solutions.

2.2.3 Polycrystalline Samples

Polycrystalline samples were used for two investigations - morphological investigations and mechanical property investigations. Polycrystalline samples for the morphological analysis were supplied by Coors Ceramics. Samples consisted of a sectioned 3 mol% Y-TZP flexural test bar which had been fired in a production kiln at 1450°C for two hours, referred to as the "as-fired" or "unpolished" samples, and polished 3 mol% Y-TZP samples. The surface area of these samples was approximately 2.5 cm². The thermal history of the polished sample is uncertain, although its fracture surface was indistinguishable from the as-fired ceramic, indicating similar microstructure and possibly similar thermal history.

* Yttria powder, Molycorp, Inc., Los Angeles, CA, (213)-977-7666.

Polycrystalline morphological studies were conducted by placing the sectioned samples, along with the desired solution, in the digestion bombs and placing the bombs in the drying oven as before. Samples were removed at the desired times and quenched to room temperature. The polycrystalline samples were removed and the solutions were once again filtered through the tandem filter system. The polycrystalline samples were analyzed for monoclinic content, as well as observed on a SEM, while the solutions were analyzed for yttrium and zirconium concentrations.

The other polycrystalline samples used for mechanical studies consisted of flexural test bars which were machined either from ingots produced at Mines or an ingot produced at Coors Ceramics. Both the ingots produced at Mines and the ingot from Coors Ceramics were produced from the same 3 mol% Y-TZP powder. The ingots produced at Mines were produced by isostatically pressing the powder at 15,000 psi, resulting in an approximately 4.5" by 5.5" compact. The green compacts were fired in a box furnace at 60°C/hour up to 300°C and held at that temperature for two hours to eliminate water and burn out any possible organics. The temperature was then ramped up at the same rate to 1000°C and held for two hours and then ramped as quickly as possible up to 1550°C. This temperature was held for two hours, after which time the furnace was shut off. The density of the Mines material as measured by the Archimedes technique was 6.0 g/cc. The reason for the differences in density and microstructure between the Coors and Mines material is unclear. Both materials were isopressed at the same pressure and the Mines firing schedule was supposedly the same as the Coors schedule. It would appear that the firing schedules were not as similar as originally thought to be.

The ingot supplied by Coors was also produced by isopressing the powder at 15,000 psi, yielding a cylindrical ingot approximately 3.0" in diameter and 4.5" in length. This ingot was then fired in a production kiln at 1550°C for approximately 3.5 hours. The density of the Coors material as measured by the Archimedes technique was 5.7 g/cc.

Flexural test bars, measuring 0.25" x 0.125" x 2.0" were machined from the ingots, 25 of which originated from the Coors ingot; the remaining 101 originated from the

Mines produced ingots.* Flexural test bars were both rough and fine ground parallel to the major axis to remove any surface damage induced by cutting or previous grinding steps. In addition, the four long edges of the bars were chamfered at 45° angles. All MOR bar samples were dye checked in order to observe any surface cracks. Dye checking involved submerging a bar in a red organic dye which, when washed away, remains in cracks and pores making their detection much easier. Any bars containing surface cracks or imperfections were discarded. The microstructure of all ingots were characterized by observing polished and thermally etched surfaces of representative initial flexural bars. The microstructure of the material produce at Mines is illustrated in Figs. 2.3 and 2.5, while the microstructure of the Coors supplied material is illustrated in Figs. 2.4. and 2.6

Initial flexural test bar XRD patterns indicated a 9.4 vol% monoclinic content for both materials. This amount of monoclinic phase was due to transformation which occurred during machining. In order to convert the monoclinic back into tetragonal phase the bars needed to be annealed above the transformation temperature. This was accomplished by annealing the bars at 1000°C for one hour. After the annealing process, no monoclinic content was detected by x-ray diffraction.

Polycrystalline flexural test bars were divided into four groups. An initial group containing three bars from the Mines material and three bars from the Coors material were not placed in any degrading environment. The three other groups were degraded in either water, 0.01 M HCl or 1.0×10^{-4} M HCl solutions. These samples were placed in 1000 ml boiling flasks with approximately 800 ml of the desired solution. The flasks were heated to and maintained at 100°C by rheostat controlled heating elements. The solution vapors were retained through use of water cooled, reflex condenser coils. Five samples were removed from each flask at the desired times, labeled and set aside for flexural testing. Of the five samples, four were from the Mines-produced material and one was from the Coors material.

* Machining performed by Bomass Machine Specialties, Inc., Sommerville, MA.

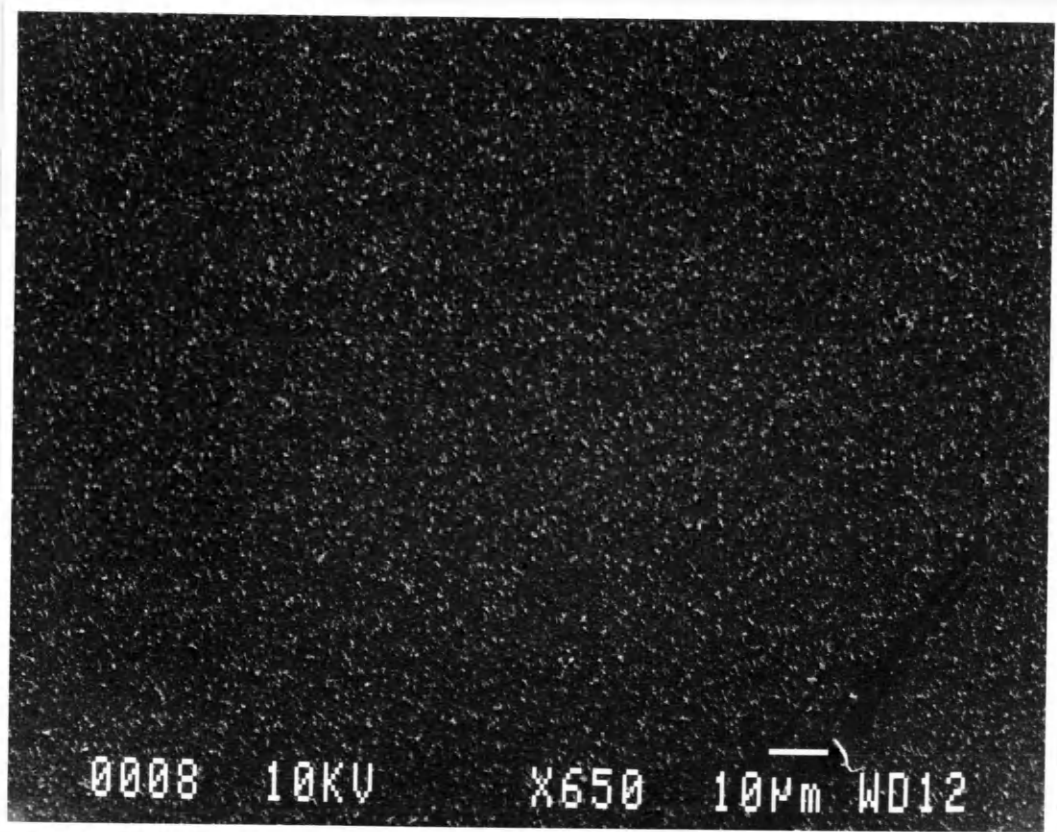


Fig. 2.3 Low magnification micrograph of Mines produced Y-TZP flexural test bar (polished and thermally etched at 1450°C for twenty minutes). White specks on the surface are some form of surface contamination and are not part of the ceramic microstructure.

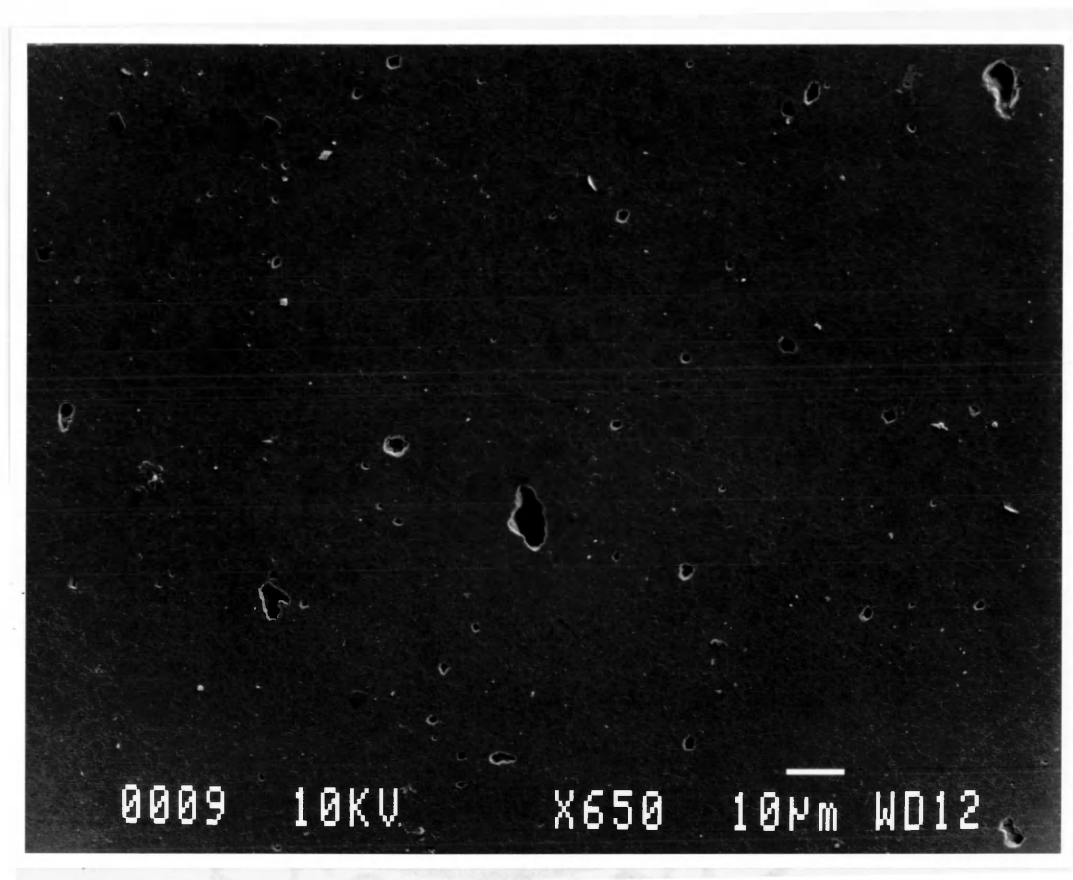


Fig. 2.4 Low magnification micrograph of Coors produced Y-TZP flexural test bar (polished and thermally etched at 1450°C for twenty minutes).

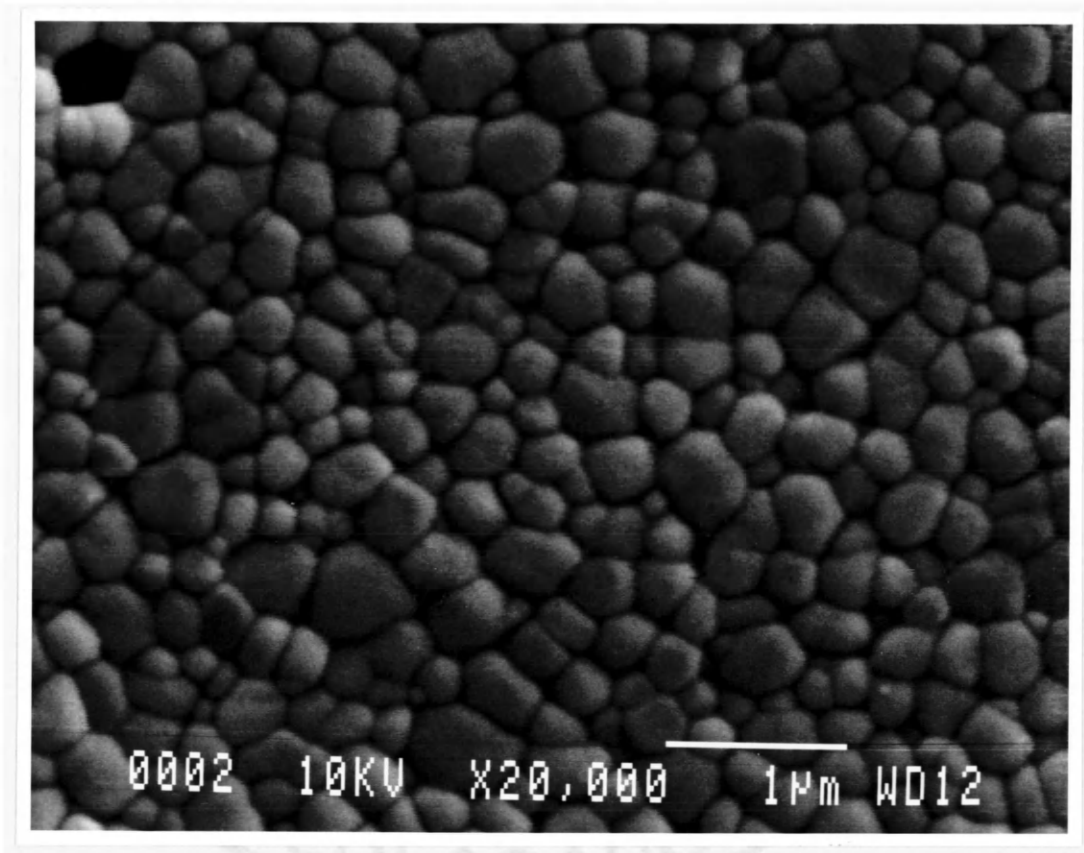


Fig. 2.5 High magnification micrograph of Mines produced Y-TZP flexural test bar. Average grain size as determined by image analysis -- $0.3 \mu\text{m}$.

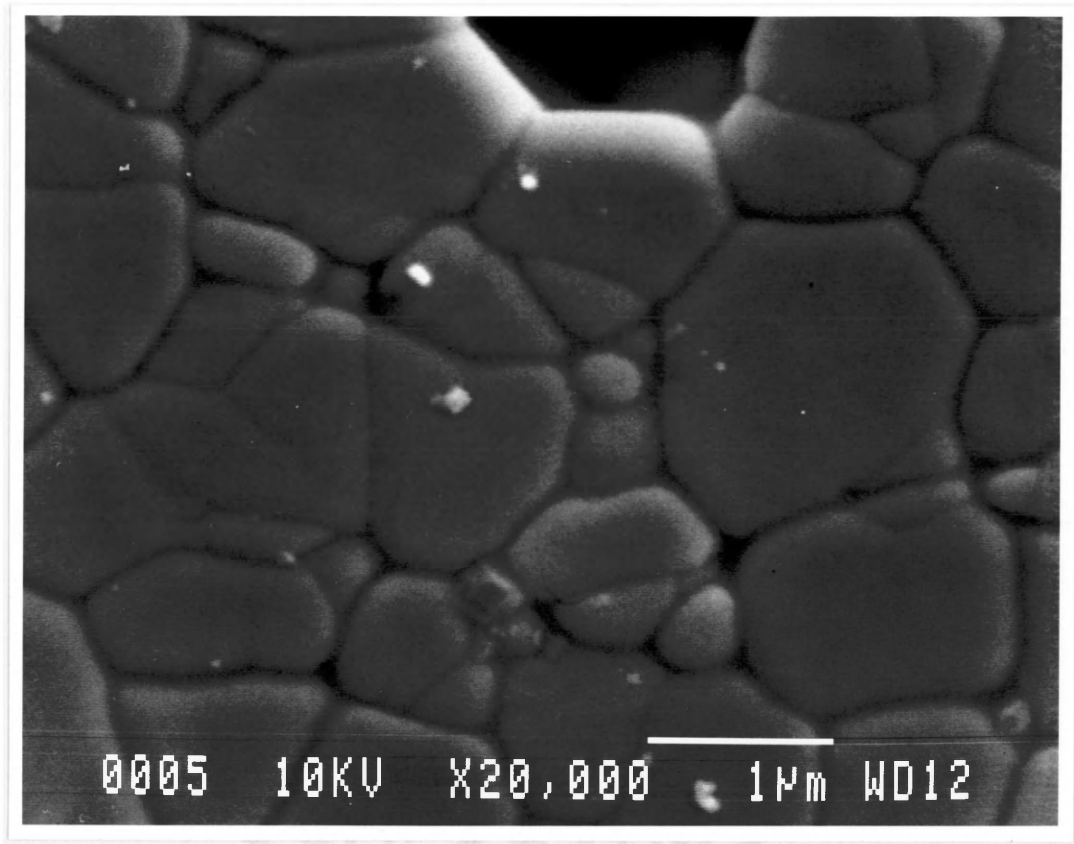


Fig. 2.6 High magnification micrograph of Coors produced Y-TZP flexural test bar. Average grain size as determined by image analysis -- $0.9 \mu\text{m}$.

Standard four point flexural tests were conducted according to ASTM standard C 1161 (1991). The following parameters were utilized: sample size was 0.125" x 0.25" x 2.0"; lower span - 20.0 mm; upper span - 40 mm; and crosshead speed - 0.01"/min. Test bar bending strengths were calculated from simple four point - 1/4 point beam loading analysis. The resulting equation utilized to determine the maximum tensile strength of the bar based on the load at fracture is:

$$S = \frac{3 P L}{2 w t^2} \quad (2.1)$$

where,

S ≡ strength of the beam;

P ≡ load at failure;

L ≡ outer span distance;

w ≡ specimen width; and

t ≡ specimen thickness.

Data points were generated by averaging the strengths of the five samples for each respective time. Error bars for the data points represent plus and minus one standard deviation based on the five sample population.

2.2.4 Miscellaneous Materials

Other ceramic powders used included commercially available unstabilized zirconia* and 8 mol% yttria-stabilized zirconia.† These were used for the x-ray diffraction calibration curve. Fig. 2.7 diagrams the various combinations of powder, VPS and polycrystalline samples and the degradation solutions used during this research.

* SC-30 monoclinic powder, Magnesium Elektron Inc., Flemington, N. J., (201) 782-5800.

† HSY-8 powder, Zirconia Sales (America), Inc., Marietta, GA (404) 590-7970.

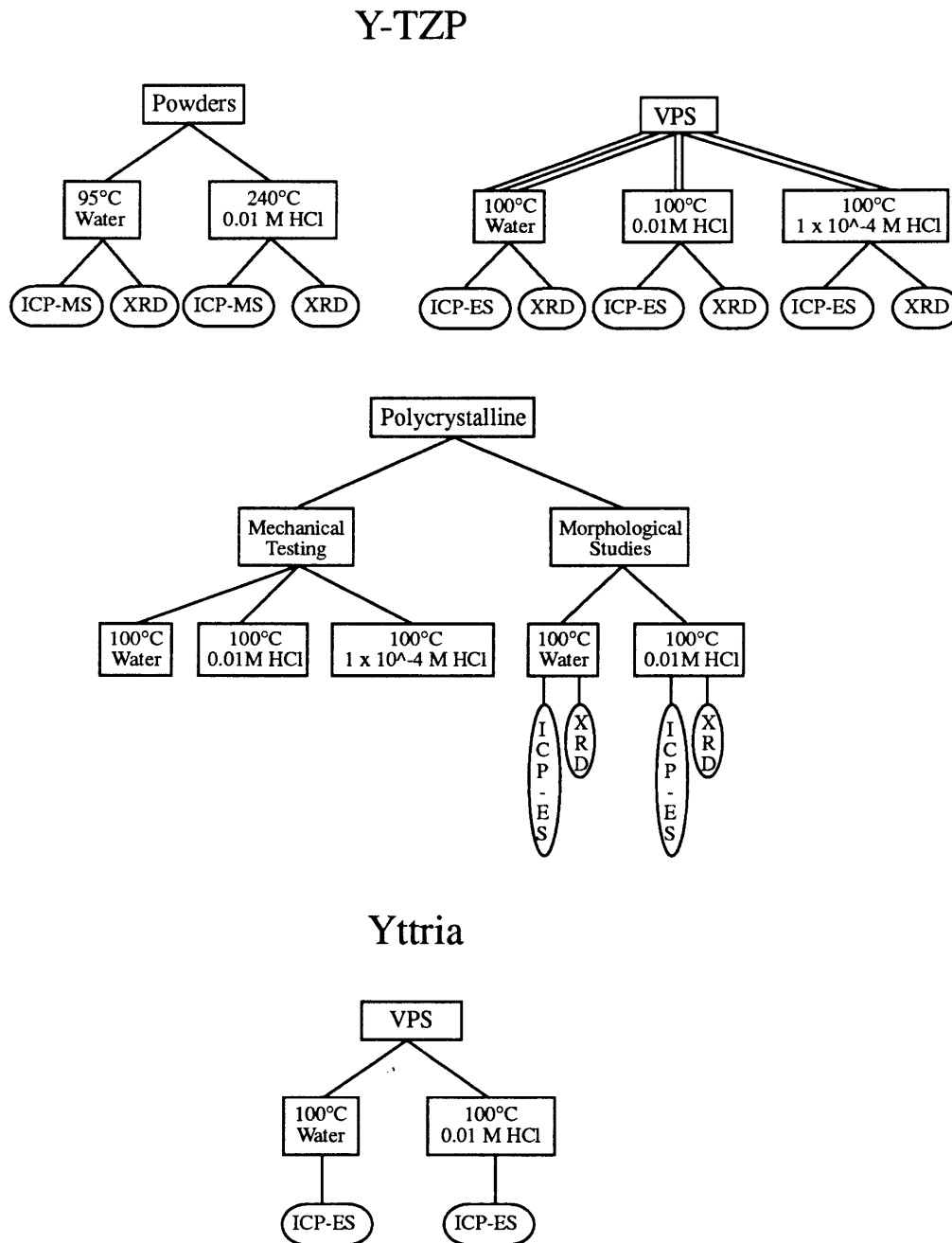


Fig. 2.7 Experimental matrix for degradation studies. Multiple lines represent the number of times the experiment was conducted.

2.3 X-Ray Diffraction Analytical Techniques

Various analytical techniques can be employed to quantitatively determine phase contents in Y-TZP. X-ray diffraction was utilized as the phase analysis technique in this research due to its wide acceptance, ease of use and established methodologies.

2.3.1 Equipment, Settings, and Sample Mounting Techniques

For this research, a Rigaku rotating anode diffractometer with monochromated copper K α radiation was employed. The various x-ray machine settings include a divergence slit opening of 1.0°, a Soller slit entrance opening of 2.0° and a receiving slit opening of 0.15". Data acquisition was conducted by interfacing an IBM personal computer with the output from the XRD unit. Diffraction patterns were obtained by step-scanning through the desired 2 θ range and recording the data onto floppy disks. The data was then analyzed with another software program; the details of the analysis will be discussed later.

XRD samples were in either powder or polycrystalline pellet or bar form. Powder samples were either back-fill mounted with the standard aluminum holders or sprinkled onto double sticky sided tape on glass slides. Polycrystalline samples were held parallel and flat with the diffraction plane by placing the sample face down in an aluminum holder and then securing the sample with double sticky sided tape and modeling clay.

Full XRD scans for the three polymorphs of zirconia are shown in Fig. 2.8. To illustrate how the three phases can be present in a sample, a scan for undegraded 3 mol% Y-TZP powder is also included in the figure.

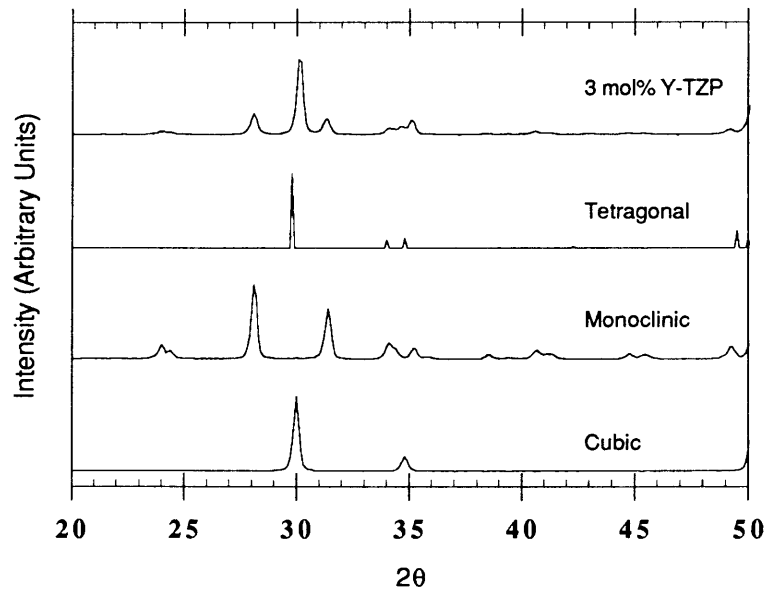


Fig. 2.8 XRD scans of cubic zirconia (8 mol% yttria), monoclinic zirconia (pure zirconia) and undegraded 3 mol% TZP powder. Scanned from 20 to 80° 2θ, 0.01°/step, 4 sec/step. Tetragonal pattern is a calculated pattern by Smith, JCPDS Card # 24-1164.

2.3.2 Analysis of XRD Data

In this research it is necessary to quantitatively determine the monoclinic content of the samples. The polymorph technique, a method originally devised by Garvie and Nicholson, calculates the monoclinic content from the integrated intensities of the

monoclinic ($11\bar{1}$), monoclinic (111) and cubic/tetragonal (111) peaks.⁵² The cubic/tetragonal notation is used since it is difficult to separate the tetragonal and cubic phases due to peak overlap*. As a consequence, researchers generally discuss the tetragonal peak of Y-TZP materials even though small amounts of the cubic phase may be present. In general, the objective is to determine the change in monoclinic content. A sample XRD pattern with the monoclinic ($11\bar{1}$), monoclinic (111) and cubic/tetragonal (111) peak locations is shown in Fig. 2.9.

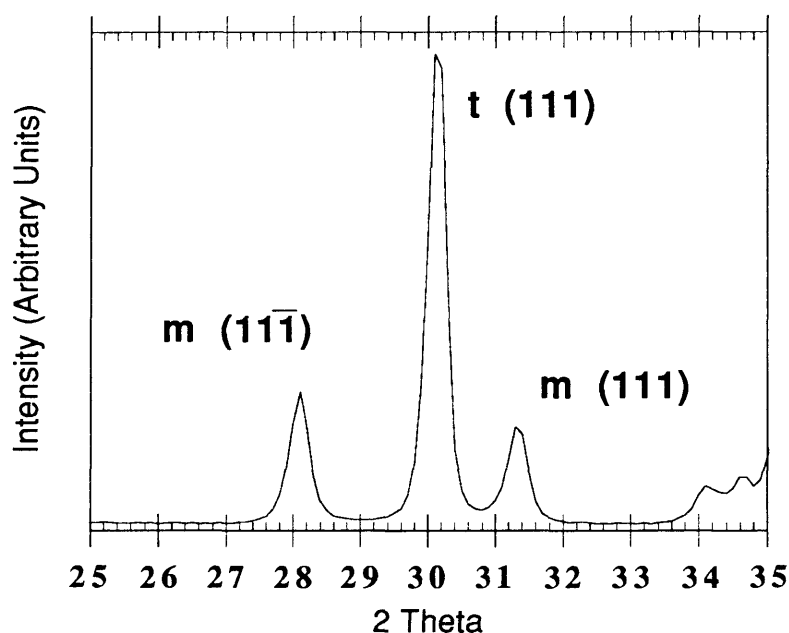


Fig. 2.9 X-ray diffraction pattern for initial 3 mol% yttria-stabilized zirconia powder illustrating important monoclinic and tetragonal peak location.

From mixtures of monoclinic and cubic zirconia of known phase composition, Garvie and Nicholson established a calibration curve between the monoclinic phase volume fraction, calculated from the intensity ratios of the monoclinic (111), monoclinic ($11\bar{1}$) and

* d-spacings for t(111) and c(111) are 0.296 nm and 0.293 nm respectively (JCPDS cards 17-923 and 27-997).

cubic (111) peaks, and the known monoclinic contents. Equation (2.2) is the intensity ratio relationship used by Garvie and Nicholson to determine the volume fraction of monoclinic.

$$V_m = \frac{I_{m(111)} + I_{m(11\bar{1})}}{I_{m(111)} + I_{m(11\bar{1})} + I_{c(111)}} \quad (2.2)$$

Where,

V_m \equiv volume fraction monoclinic phase;

$I_{m(111)}$ \equiv integrated intensity from monoclinic (111) peak;

$I_{m(11\bar{1})}$ \equiv integrated intensity from monoclinic (111) peak; and

$I_{c(111)}$ \equiv integrated intensity from cubic (111) peak.

While Garvie and Nicholson's work involved separating the monoclinic content from the cubic content, the work discussed in this thesis separates the monoclinic content from the tetragonal content. However, it is possible to simply replace the intensity of the cubic (111) peak with the tetragonal (111) peak and use the same equation due to the peak overlap discussed earlier.

There have been updates to the polymorph technique, most notably by Heuer, et al., and Yoshimura, et al. Heuer and Porter pointed out that the relationship established by equation (2.2) is not necessarily linear with respect to the monoclinic content and that the intensity difference between the cubic/tetragonal phase and the monoclinic phase needs to be accounted for.⁵³ The result of their work is a relationship presented in equation (2.3).

$$V_m = \frac{1.603 [I_{m(111)}]}{1.603 I_{m(111)} + I_{c/t(111)}} \quad (2.3)$$

where,

V_m \equiv volume fraction monoclinic phase;

$I_{m(111)}$ \equiv integrated intensity from monoclinic (111) peak; and

$I_{c/t(111)}$ \equiv integrated intensity from the combined cubic/tetragonal (111) peak.

The latest update to the polymorph technique was presented by Yoshimura and his group in 1984.⁵⁴ This group determined a calibration equation relying on theoretical calculations of reflection intensities based on hkl reflection multiplicity, linear absorption, Bragg angle, structure factor, unit cell volume and polarization corrections. These theoretical results were compared with experimental results and a calibration equation was determined. Their calibration equations are:

$$X_m = \frac{I_{m(111)} + I_{m(11\bar{1})}}{I_{m(111)} + I_{m(11\bar{1})} + I_{c/t(111)}} \quad (2.4)$$

where,

X_m \equiv intensity ratio;

$I_{m(111)}$ \equiv integrated intensity from monoclinic (111) peak;

$I_{m(11\bar{1})}$ \equiv integrated intensity from monoclinic (111) peak; and

$I_{c/t(111)}$ \equiv integrated intensity from the combined cubic/tetragonal (111) peak.

The volume fraction monoclinic, V_m , is given as:

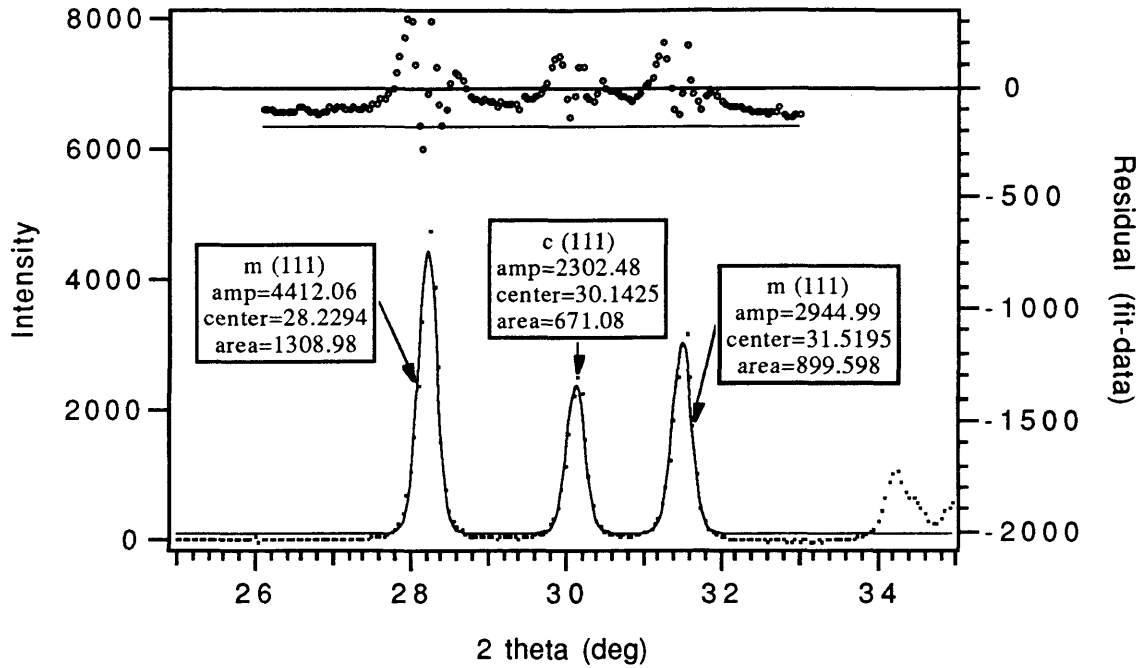
$$V_m = \frac{1.311 X_m}{1 + 0.311 X_m} \quad (2.5)$$

All of the above techniques require that the integrated intensities of the specific peak be evaluated. This is simply not the peak height but the area underneath the peak. As a result, a technique is needed whereby an area under the peak can be deduced from the digital XRD data.

There are various techniques which accomplish just this task. Numerical integration and curve fitting and integration are two such techniques. Of these two techniques, the curve fitting and integration technique is the most common. The technique used for this research was to fit a Gaussian curve to the peak and calculate the area from known properties of Gaussian curves.

A commercial software program called Igor*, along with a Macintosh II computer, was employed to determine peak areas for the quantitative phase analysis. Fig. 2.10 illustrates a typical Gaussian fit and resulting area as well as a fit residual for a XRD scan.

* WaveMetrics, P. O. Box 2088, Lake Oswego, OR 97035, (503) 620-3001



$$X_m = \frac{A_{m(11\bar{1})} + A_{m(111)}}{A_{m(11\bar{1})} + A_{m(111)} + A_{c(111)}}$$

$$= \frac{1309.0 + 899.6}{1309.9 + 899.6 + 671.1}$$

$$= 0.766$$

$$V_m = \frac{1.311 X_m}{1.0 + 0.311 X_m}$$

$$= \frac{1.311 (0.766)}{1.0 + 0.311 (0.766)}$$

$$= 0.811$$

Fig. 2.10 Typical analysis of XRD data from a mechanical mixture containing 20.0 vol% cubic and 80 vol% monoclinic zirconia.

In order to determine which of the quantitative phase analysis methods should be employed for this research, a calibration curve was developed for each of the three techniques. Mechanical mixtures of powder containing 0.0 vol%, 21.0 vol%, 41.5 vol%, 61.5 vol%, 81.0 vol% and 100.0 vol% monoclinic were constructed by combining the appropriate weights of 100% cubic 8 mol% yttria-stabilized zirconia powder, 100% monoclinic zirconia powder and 10 ml alcohol in a milling jar with alumina grinding media and milling for 16 hours. The samples were dried and XRD patterns were obtained using the following parameters: 50.0 kV; 75.0 mA; 0.05°/step; and 4.0 secs/step. The XRD patterns for these standards are presented in Fig. 2.11.

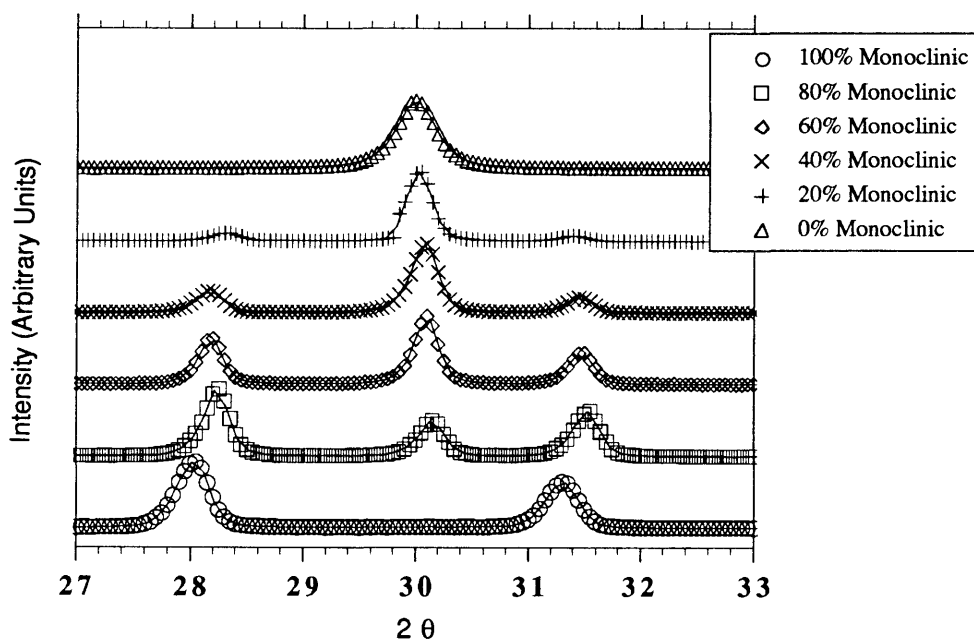


Fig. 2.11 XRD patterns for various monoclinic/cubic mixtures.

When the intensities for the appropriate peaks are calculated, the volume fraction of monoclinic can be calculated by one of the three techniques given above. The results of these calculations are given in Fig. 2.12.

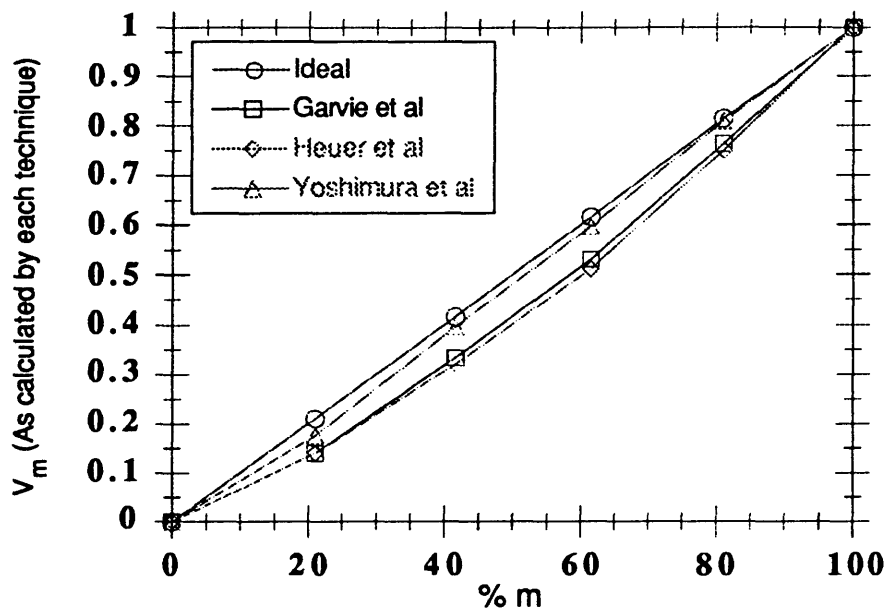


Fig. 2.12 Comparison of volume fraction monoclinic calculations between Garvie, et al., Heuer, et al., Yoshimura, et al., and the ideal situation.

As indicated by Fig. 2.12, the monoclinic contents calculated by the Yoshimura technique corresponds closest to the standards. As a result, all monoclinic contents presented in this thesis were evaluated by first determining integrated intensities utilizing Igor and then calculating monoclinic volume fractions with the Yoshimura technique (equations (2.4) and (2.5)).

2.4 ICP - MS and ICP - ES

Solution species concentrations were determined by one of two analytical techniques, either inductively coupled plasma mass spectroscopy ("ICP-MS")* or inductively coupled plasma emission spectroscopy ("ICP-ES")† . These techniques were selected due to the relative refractory nature of the yttrium and zirconium and the relative difficulty encountered when attempting to excite these species in other analytical techniques. Since the equipment necessary was not available at The Colorado School of Mines, species concentration was conducted at Coors Analytical Labs.** Both techniques were found to give comparable results, as indicated in Fig. 2.13. However, analyses conducted by ICP-ES required less time, and thus less resources, so the majority of concentrations were determined by ICP-ES.

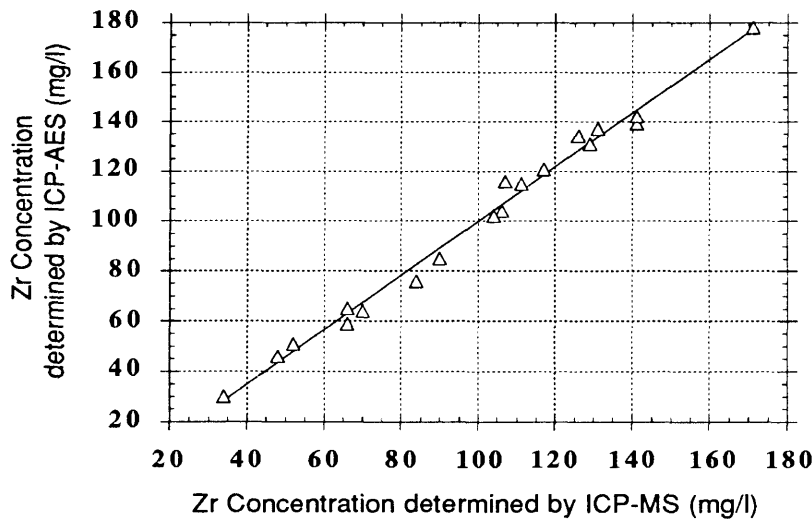


Fig. 2.13 Comparison of data as determined by ICP-MS and ICP-ES.

* VG Elemental PQ2+ Inductively Coupled Argon Plasma Mass Spectrometer

† Jarrell Ash Atom-Comp 1100 Inductively Coupled Argon Plasma Emission Spectrometer

** Coors Analytical Laboratories, Golden, CO (303) 277-5439.

One of the difficulties encountered with the above-described analytical techniques results from the relatively small digestion bomb volume, 23 ml, which limits the amount of solution available for analysis. The initial solution volume was 10 ml and some solution was unavoidably lost during filtration. The final volume submitted for analysis was on the order of 5.0 - 7.0 ml. This small volume prevented the analyst from repeating the analysis and thus establishing data confidence. As a result, various standards were submitted along with the unknown samples to establish some confidence in the data. Standards were produced from yttrium nitrate pentahydrate* and distilled water, 1000 mg/l zirconium reference standard† or 1000 mg/l silicon reference standard**. The actual concentration of these samples and the concentration as determined by Coors Analytical are listed in Table 2.3. In general, the analysis conducted by Coors Analytical was very good with the exception of the occasional detection of a species which should not have been present. However, this may have been the result of contamination during standard production.

Table 2.3 Standards submitted to Coors Analytical to establish data confidence.

Standard Sample Name	Species Concentration (mg/l)			Species Concentration (mg/l) as Determined by Coors Analytical		
	Y	Zr	Si	Y	Zr	Si**
BAN1	0.0	1000.0	0.0	0.214	1060.0	-
BAN2	0.0	10.0	0.0	0.004	10.1	-
BAN3	0.0	0.1	0.0	0.004	0.091	-
1NIT	1000.0	0.0	0.0	928.0	0.096	-
2NIT	10.0	0.0	0.0	9.87	0.026	-
3NIT	0.1	0.0	0.0	0.280	0.015	-
1NITB	1000.0	0.0	0.0	760.0	< 0.05	-
BAN3B	0.0	0.1	0.0	< 0.05	0.099	-

** Silicon concentration was not requested.

* EM Science, Gibbstown, NJ

† Anderson Laboratories, Inc. Fort Worth, TX

** VWR Scientific, Denver, CO

Error bars for the solution data were generated by submitting a set of standards of typical high and low concentrations to Coors Analytical for analysis. These standards and the concentrations as determined by Coors Analytical are presented in Table 2.4 below. Error bars were created from this data by determining the average and the standard deviation of the series. The upper and lower limit of the error bar for a given solution concentration data point then represent plus and minus one standard deviation, respectively. One obvious disparity occurred at the low zirconia concentration (0.03 mg/l) where the error is approximately 82%. The reason for this large error is most likely due to the fact that these low concentration levels are near the quantifiable detection limits of the analysis machine.

Table 2.4 Standards from which error bars were determined.

	Species Concentration (mg/l)			Species Concentration (mg/l) as Determined by Coors Analytical		
High Concentrations						
Sample	Y	Zr	Si	Y	Zr	Si
HSTAN1	333.3	3.3	333.3	416.0	3.55	425.0
HSTAN2	333.3	3.3	333.3	266.0	3.05	334.0
HSTAN3	333.3	3.3	333.3	405.0	3.36	453.0
HSTAN4	333.3	3.3	333.3	235.0	2.14	311.0
HSTAN5	333.3	3.3	333.3	344.0	3.26	365.0
Average				333.2	3.19	377.6
Standard Deviation				72.5	0.28	53.7
Percent Error				21.8	8.8	14.2
Low Concentrations						
Sample	Y	Zr	Si	Y	Zr	Si
LSTAN1	3.3	0.03	3.3	3.35	0.04	3.5
LSTAN2	3.3	0.03	3.3	2.96	<0.01	3.39
LSTAN3	3.3	0.03	3.3	4.33	0.04	3.64
LSTAN4	3.3	0.03	3.3	3.08	0.1	3.41
LSTAN5	3.3	0.03	3.3	3.15	<0.01	3.51
Average				3.37	0.04	3.49
Standard Deviation				0.49	0.03	0.09
Percent Error				14.5	75.5	2.6

3 RESULTS

3.1 Powder Results

Y-TZP powders were degraded in two different situations -- 95°C water and 240°C 0.01M HCl solution. The results from the 95°C water investigations will be presented first. The change in monoclinic content as a function of exposure time for the 95°C run are presented in Fig. 3.1. The yttrium and zirconium concentrations as a function of exposure time are presented in Fig. 3.2.

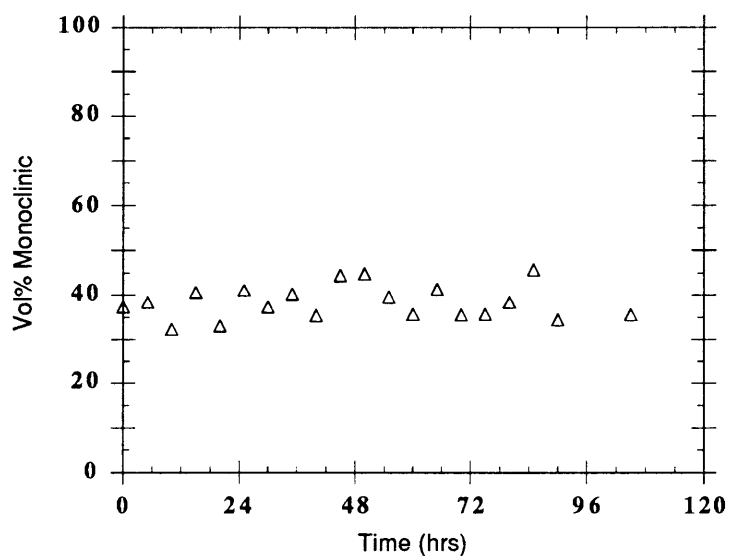


Fig. 3.1 Monoclinic contents of Y-TZP powder samples exposed to 95°C water.

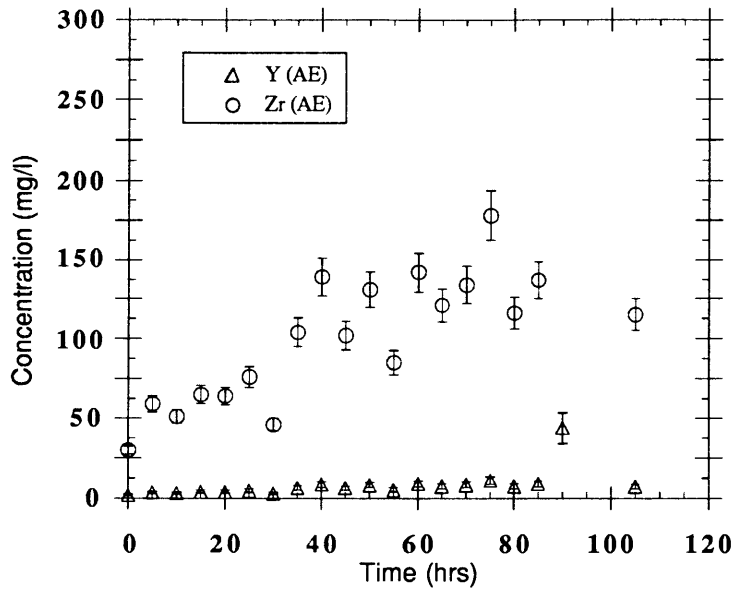


Fig. 3.2 Yttrium and zirconium concentrations in solutions for Y-TZP powder samples in 95°C water. There is a spurious zirconium concentration data point at 700 mg Zr/l which has been removed.

Since little degradation was achieved during the 95°C water investigations, a much harsher degradation environment was desired. Therefore, the powder was then exposed to 240°C 0.01 M HCl solution. The monoclinic content of the powders exposed to these conditions are illustrated in Fig. 3.3. The yttrium and zirconium concentrations found in the solution as a function of time are presented in Fig. 3.4.

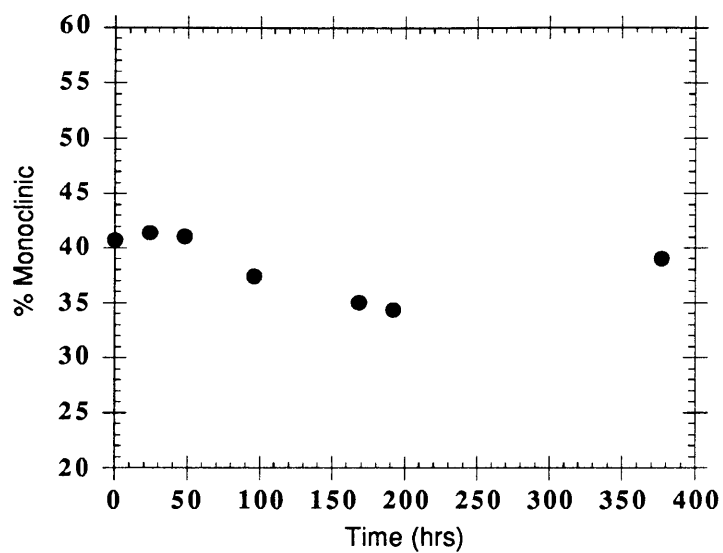


Fig. 3.3 Monoclinic contents of Y-TZP powder samples exposed to 240°C 0.01M HCl solution.

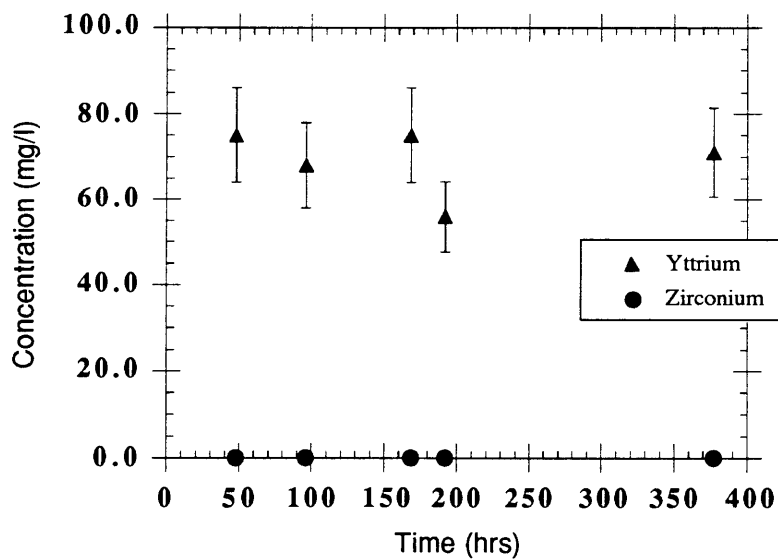


Fig. 3.4 Yttrium and zirconium concentrations in solutions for Y-TZP powder samples in 240°C 0.01M HCl solution.

3.2 Vapor Phase Sintered Results

Vapor phase sintered Y-TZP degradation investigations were conducted at 100°C in three different solutions -- water, 1×10^{-4} M HCl solutions and 0.01 M HCl solutions. The surface area of the initial VPS samples for all the experiments as determined by BET analysis at Coors Analytical Laboratories, are presented in Table 3.1.

Table 3.1 Surface areas of Y-TZP powder and vapor phase sintered samples as determined by BET analysis.

Sample ID	Comments	Surface Area (m ² /g)	Calculated Grain Size (nm)*
3 mol% Y-TZP powder	Starting powder	7.5	133
0V2AHCl	Initial sample for 1st 0.01 M HCl run	1.25	800
0V2BHCl	Initial sample for 2nd 0.01 M HCl run	1.71	585
0V4AHCl	Initial sample for 1st 1.0×10^{-4} M HCl run	2.24	446
0V4BHCl	Initial sample for 2nd 1.0×10^{-4} M HCl run	1.7	588
0VAH ₂ O	Initial sample for 1st H ₂ O run	1.63	613
0VBH ₂ O	Initial sample for 2nd H ₂ O run	1.61	621
0VCH ₂ O	Initial sample for 3rd H ₂ O run	2.59	386
0YSOL100	Initial sample for yttria water and 0.01 M HCl runs	1.19	840

* Grain sizes are calculated assuming spherical grains and a monodisperse size distribution.

Since the surface area of the VPS samples varied somewhat, and dissolution can be strongly dependent on the surface area, all the concentration data presented for the VPS Y-TZP samples have been normalized to unit surface area. The surface areas given in Table 3.1, above, were employed to normalize the respective concentrations.

The yttrium concentrations per unit surface area for the VPS yttria samples exposed to 100°C water and 0.01 M HCl are presented in Fig. 3.5.

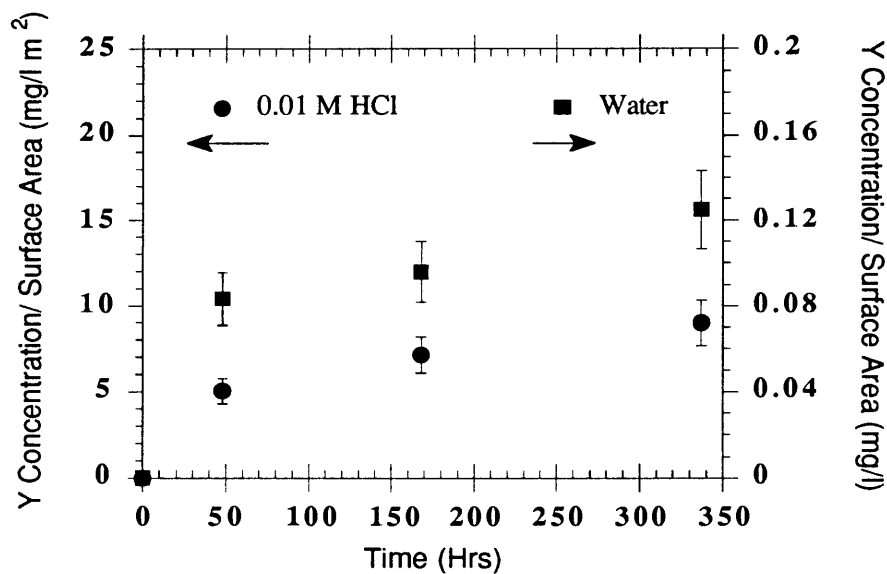


Fig. 3.5 Yttrium concentrations per unit surface area in solution for pure yttria samples exposed to 100°C water and 0.01 M HCl solution.

The change in monoclinic content for the VPS Y-TZP exposed to 100°C water is illustrated in Fig. 3.6. Figs. 3.7, 3.8 and 3.9 present the yttrium, zirconium and silicon concentrations per unit surface area for the 100°C water investigations.

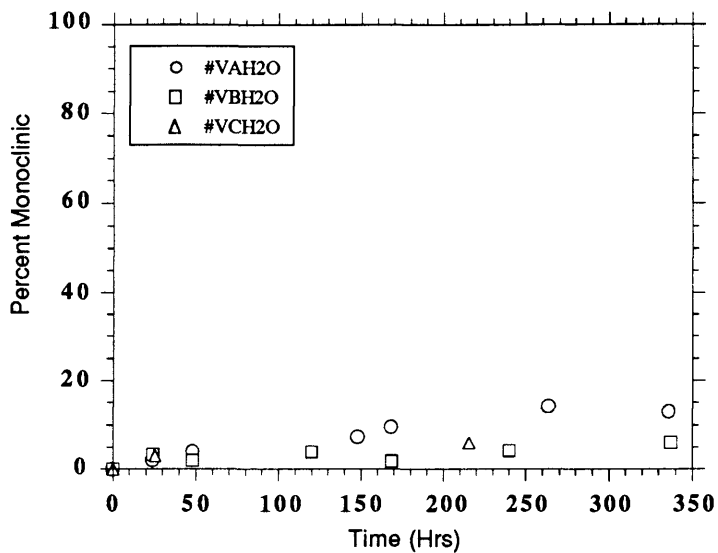


Fig. 3.6 Monoclinic contents of Y-TZP VPS samples exposed to 100°C water.

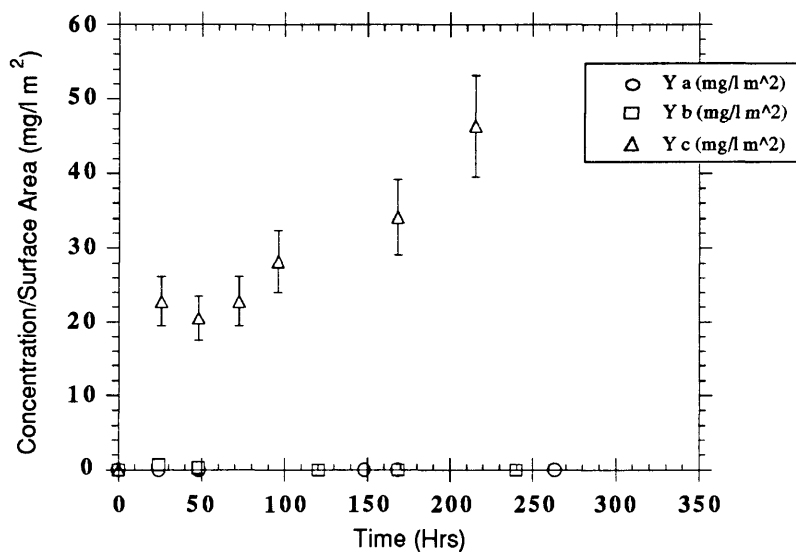


Fig. 3.7 Yttrium concentration in solution per unit surface area for Y-TZP VPS samples in 100°C water.

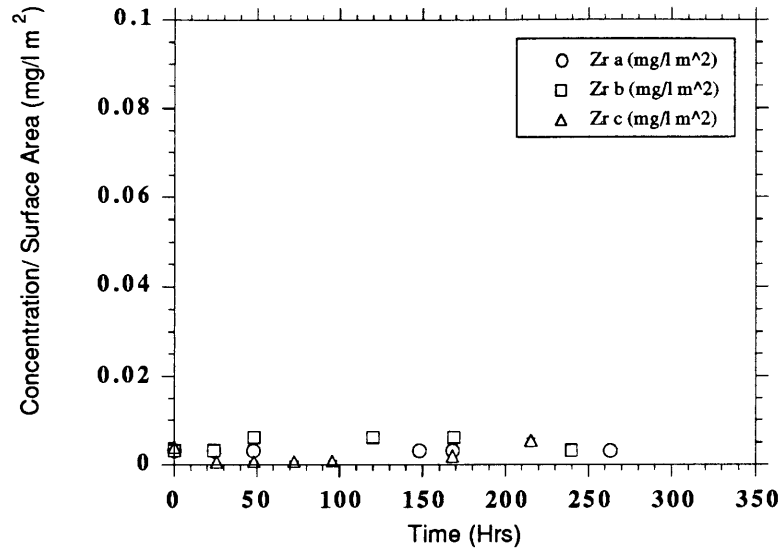


Fig. 3.8 Zirconium concentration in solution per unit surface area for Y-TZP VPS samples in 100°C water.

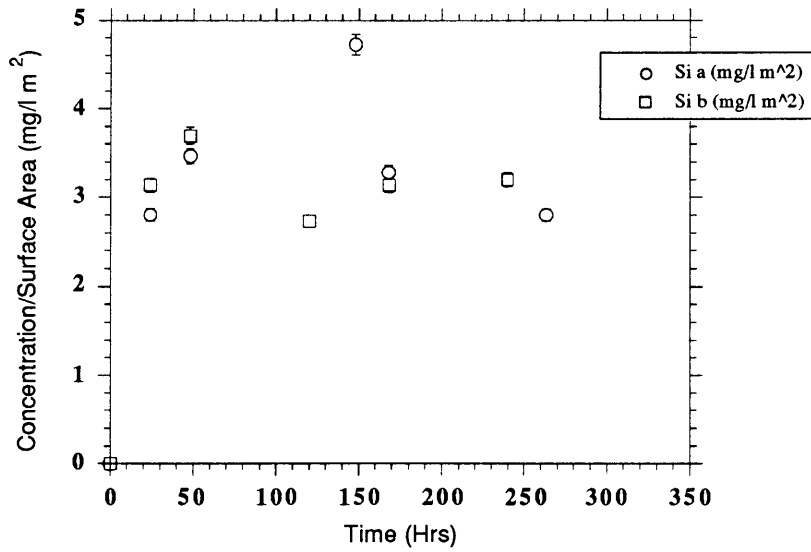


Fig. 3.9 Silicon concentrations in solution per unit surface area for Y-TZP VPS samples in 100°C water.

The monoclinic content of VPS Y-TZP as a function of exposure time to 100°C, 1.0×10^{-4} M HCl solution is depicted in Fig. 3.10. Yttrium, zirconium and silicon concentrations per unit surface area are presented in Figs. 3.11, 3.12 and 3.13, respectively.

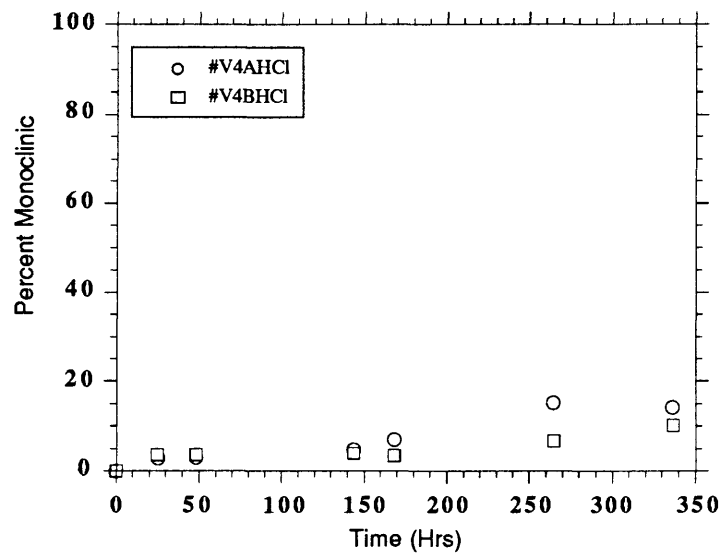


Fig. 3.10 Monoclinic contents of Y-TZP VPS samples exposed to 1.0×10^{-4} M HCl solution.

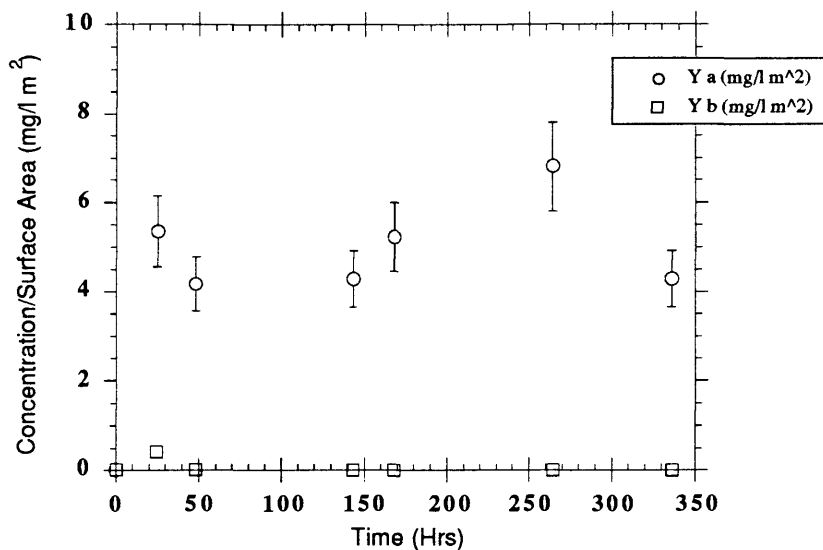


Fig. 3.11 Yttrium concentration in solution per unit surface area for Y-TZP VPS samples in 1.0×10^{-4} M HCl solution.

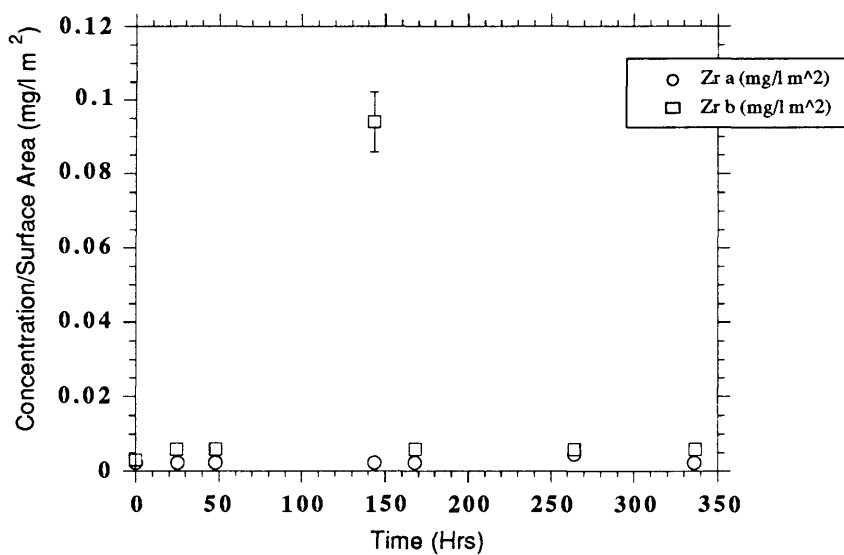


Fig. 3.12 Zirconium concentration in solution per unit surface area for Y-TZP VPS samples in 1.0×10^{-4} M HCl solution.

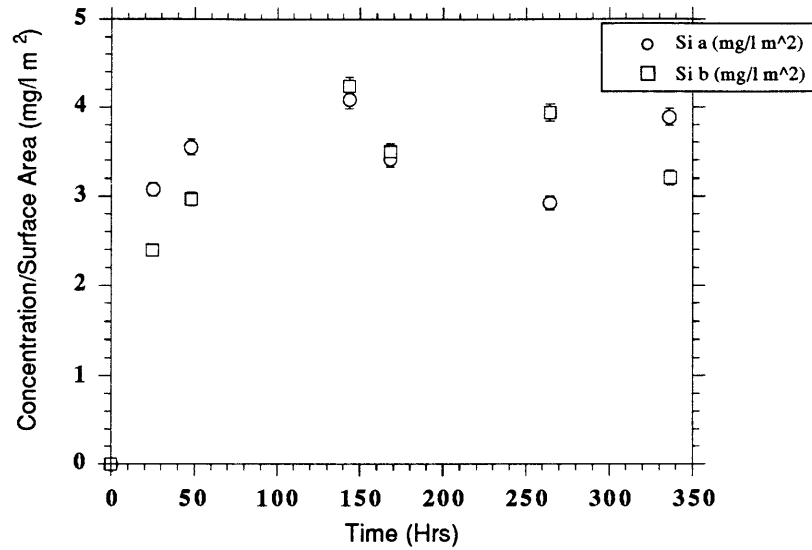


Fig. 3.13 Silicon concentration in solution per unit surface area for Y-TZP VPS samples in 1.0×10^{-4} M HCl solution.

Monoclinic content of VPS Y-TZP as function of exposure time to 100°C, 0.01 M HCl solution is depicted in Fig. 3.14. Yttrium, zirconium and silicon concentrations per unit surface area for VPS Y-TZP in a 100°C, 0.01 M HCl solution are given in Figs. 3.15, 3.16 and 3.17, respectively.

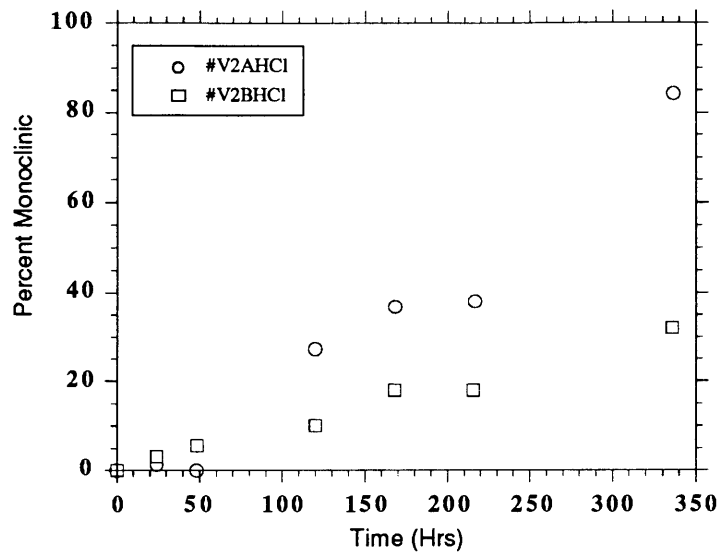


Fig. 3.14 Monoclinic contents of Y-TZP VPS samples exposed to 0.01 M HCl solution.

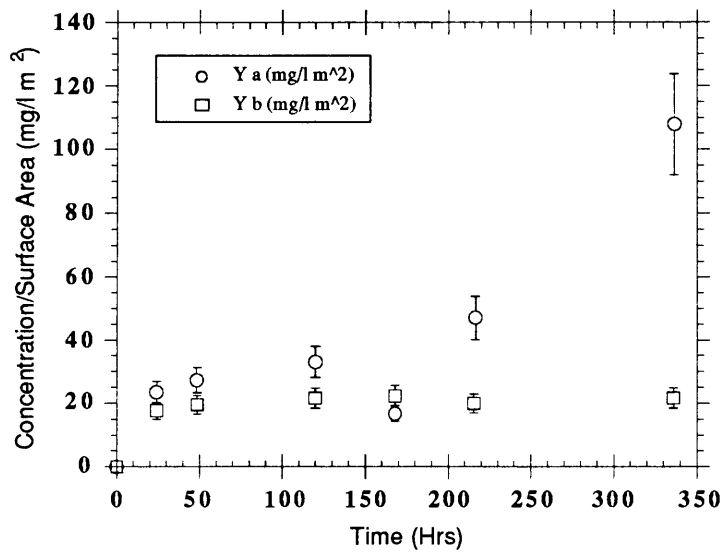


Fig. 3.15 Yttrium concentration in solution per unit surface area for Y-TZP VPS samples in 0.01 M HCl solution.

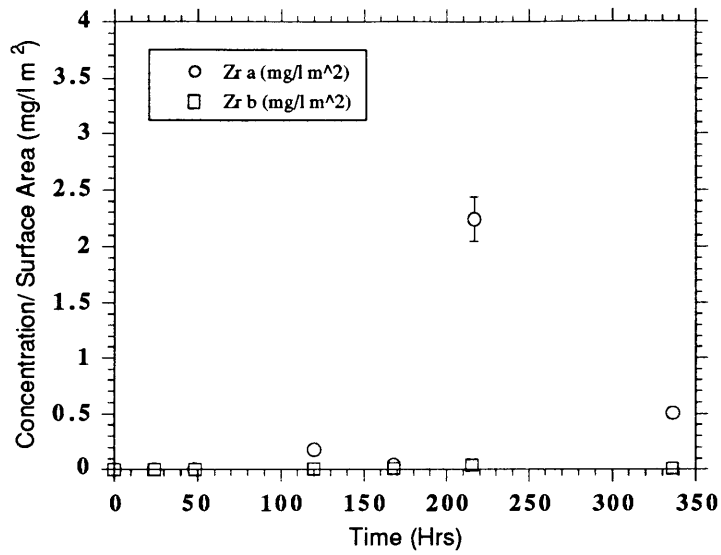


Fig. 3.16 Zirconium concentration in solution per unit surface area for Y-TZP VPS samples in 0.01 M HCl solution.

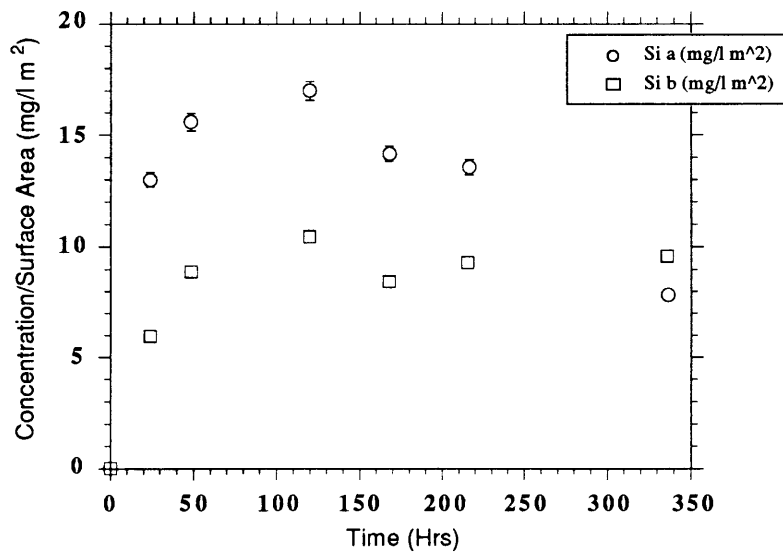


Fig. 3.17 Silicon concentration in solution per unit surface area for Y-TZP VPS samples in 0.01 M HCl solution.

3.3 Polycrystalline Results

3.3.1 Morphological

Morphological investigations were conducted on unpolished and polished, dense Y-TZP samples in 100°C water and 100°C, 0.01 M HCl solution. The goal of this investigation is to monitor the monoclinic content and the yttrium and zirconium concentrations, as well as understand the morphological development occurring during degradation.

The monoclinic content of the unpolished samples as a function of exposure time to 100°C water are depicted in Fig. 3.18. Yttrium and zirconium concentrations are presented in Fig. 3.19. Figs. 3.20-3.23 illustrate the morphological changes occurring during the degradation of the unpolished Y-TZP samples in 100°C water. Fig. 3.24 is a TEM micrograph from a two-stage replica from an unpolished Y-TZP sample which was degraded in 100°C water for 125.0 hours. Fig. 3.25 is a thin foil TEM micrograph of the undegraded, unpolished material.

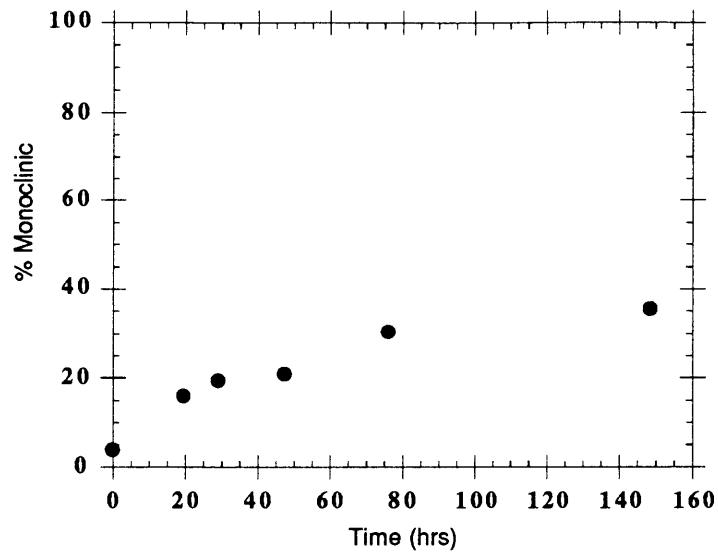


Fig. 3.18 Monoclinic content of unpolished Y-TZP polycrystalline samples exposed to 100°C water.

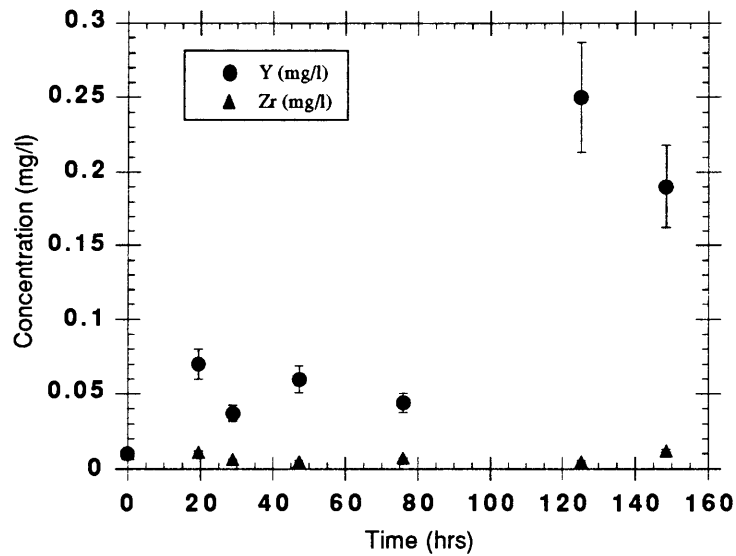


Fig. 3.19 Yttrium and zirconium concentrations in solutions from unpolished Y-TZP polycrystalline samples in 100°C water.

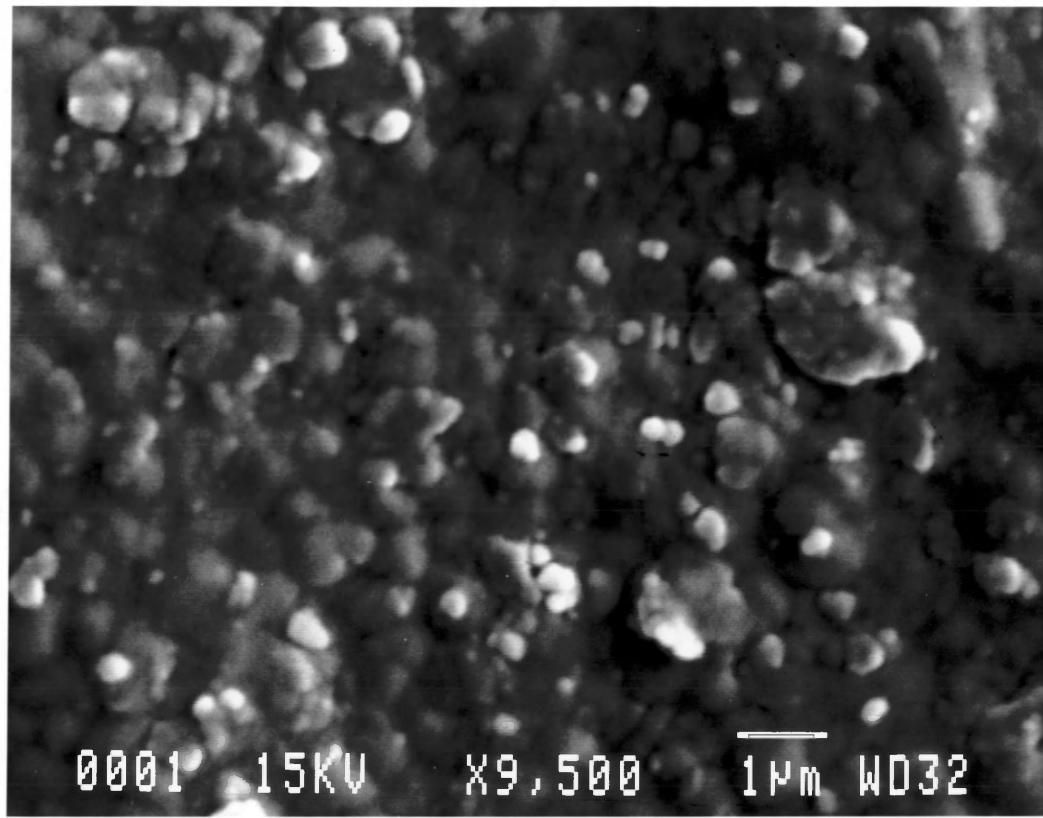


Fig. 3.20 SEM micrograph of unpolished Y-TZP sample which was exposed to 100°C water for 19.5 hours.

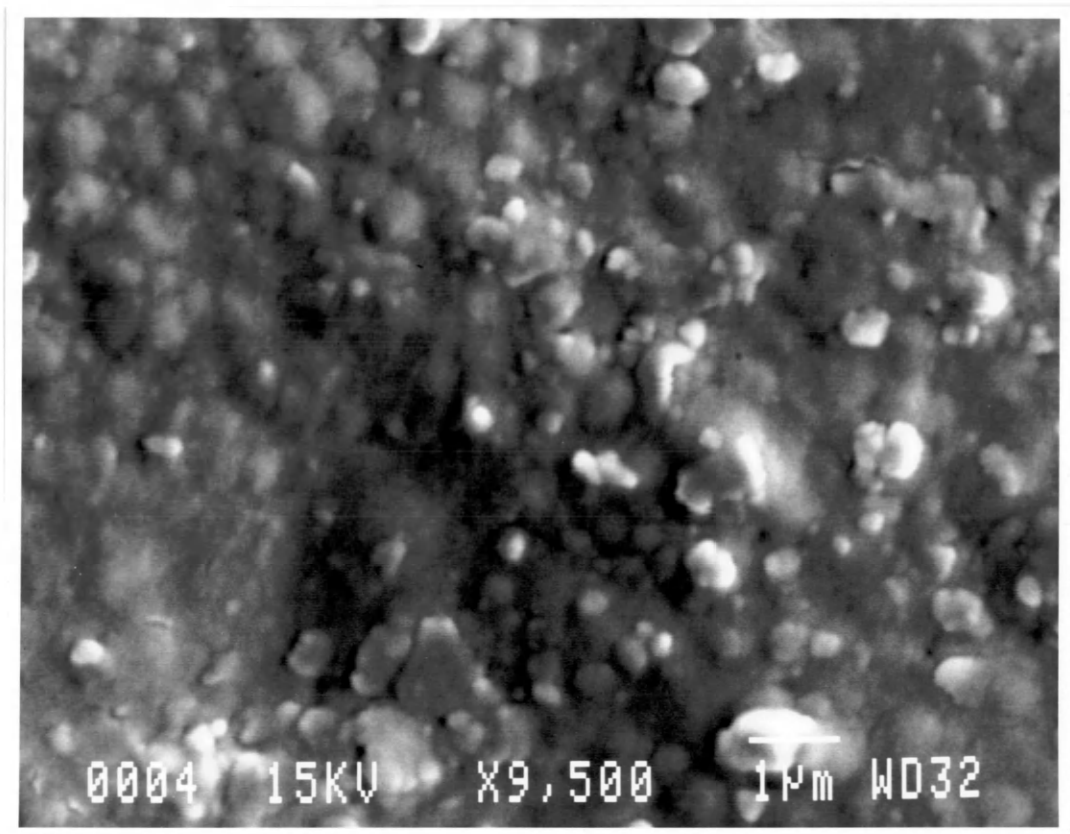


Fig. 3.21 SEM micrograph of unpolished Y-TZP sample which was exposed to 100°C water for 29.0 hours.

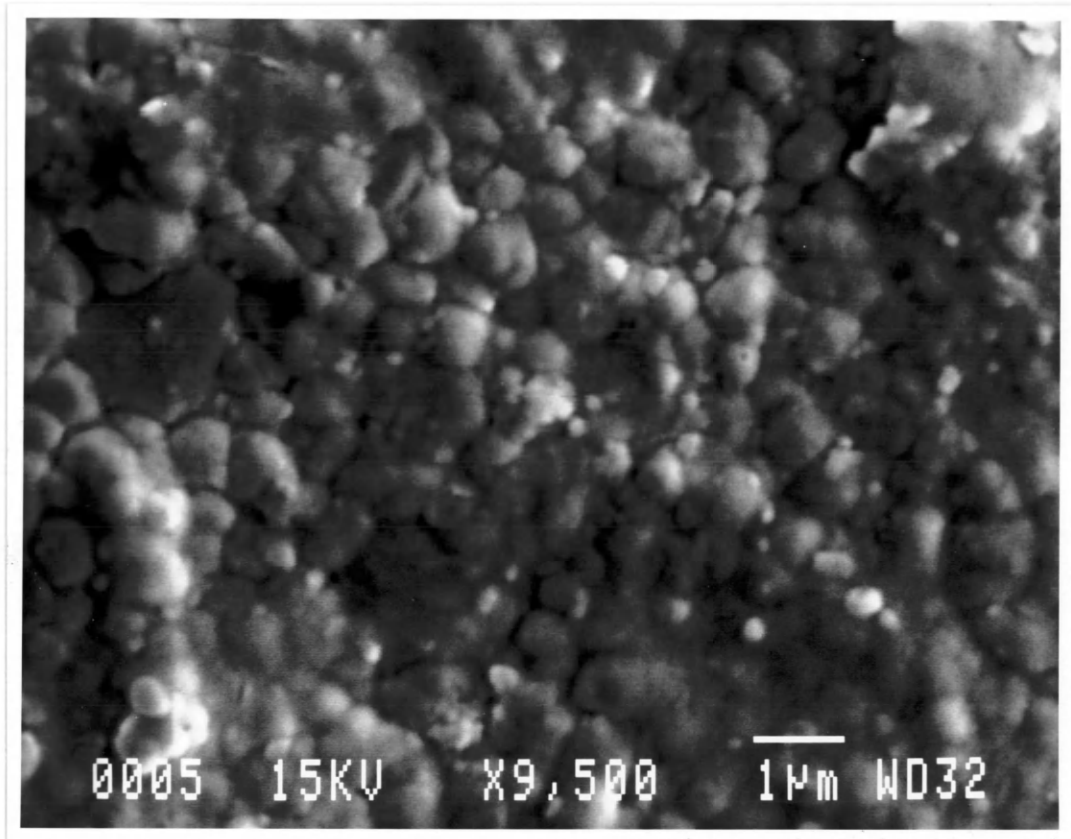


Fig. 3.22 SEM micrograph of unpolished Y-TZP sample which was exposed to 100°C water for 47.3 hours.

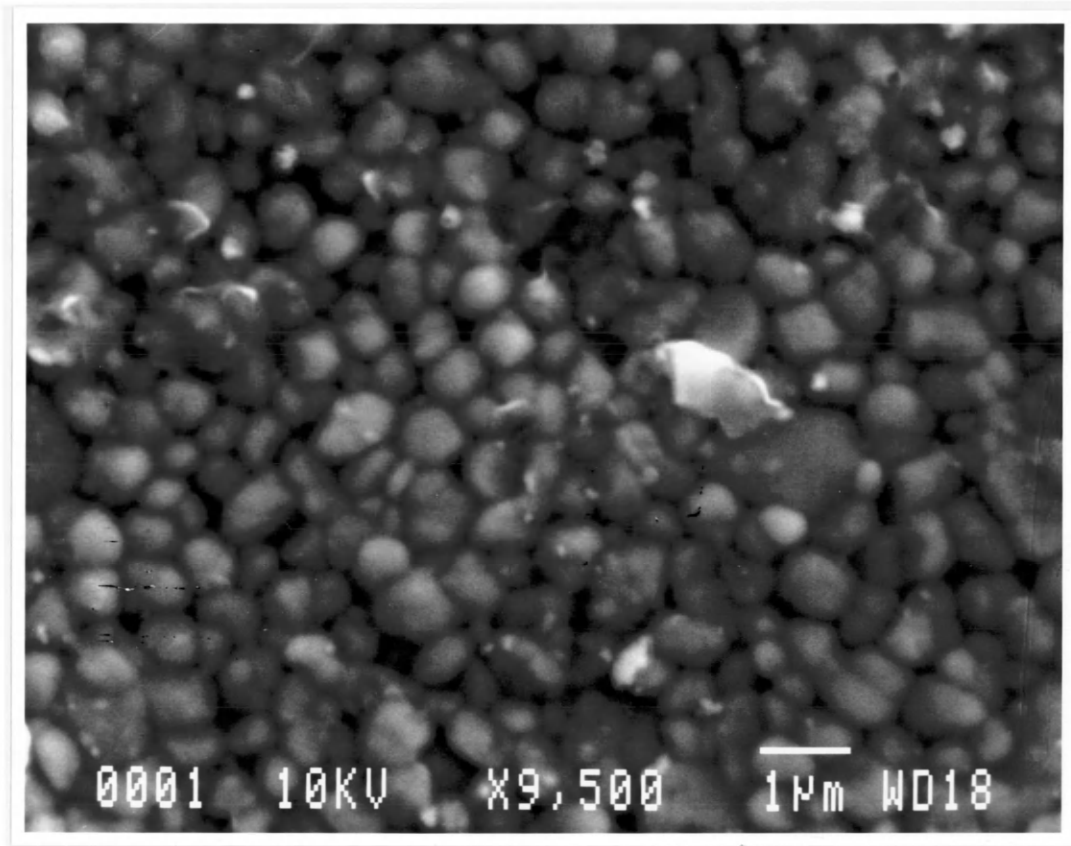


Fig. 3.23 SEM micrograph of unpolished Y-TZP sample which was exposed to 100°C water for 125.0 hours.

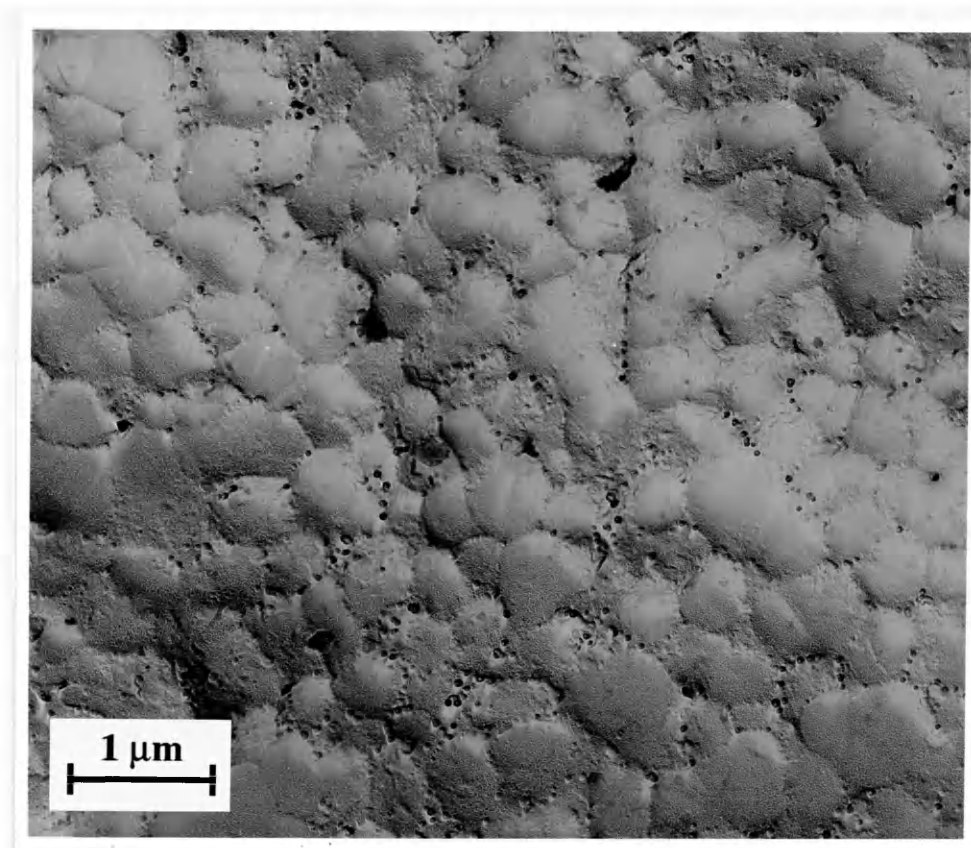


Fig. 3.24 TEM micrograph of two-stage replica from unpolished Y-TZP sample which was exposed to 100°C water for 125.0 hours.

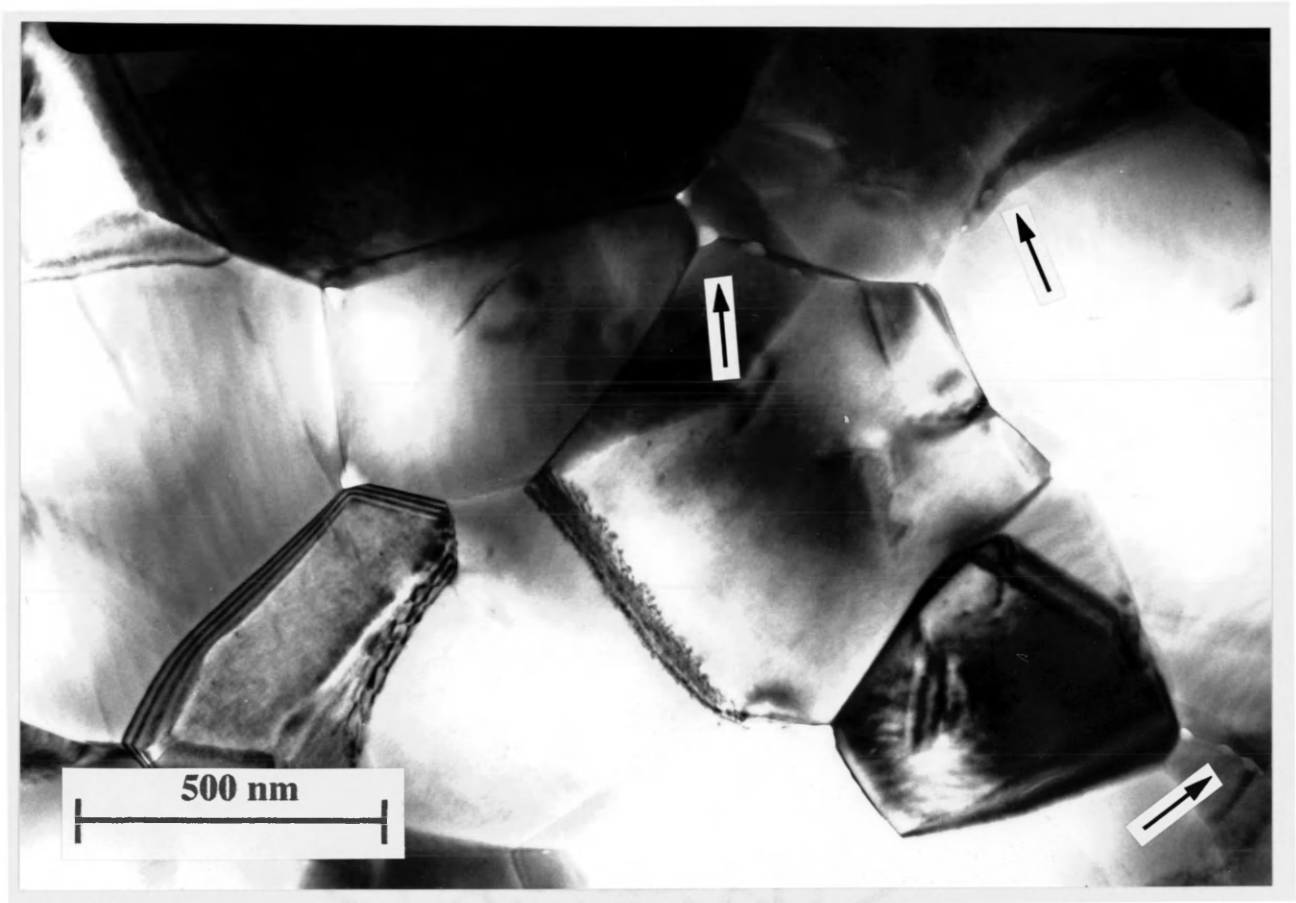


Fig. 3.25 TEM micrograph of thin foil section of unpolished Y-TZP material.

The monoclinic contents of polished, dense Y-TZP samples as a function of exposure time to 100°C, 0.01 M HCl solution are given in Fig. 3.26. Yttrium and zirconium concentrations for the 0.01 M HCl investigations are depicted in Fig. 3.27. Fig 3.28 depicts the morphological changes which occurred during the degradation of an polished sample exposed to 100°C, 0.01 M HCl solution for 169 hours.

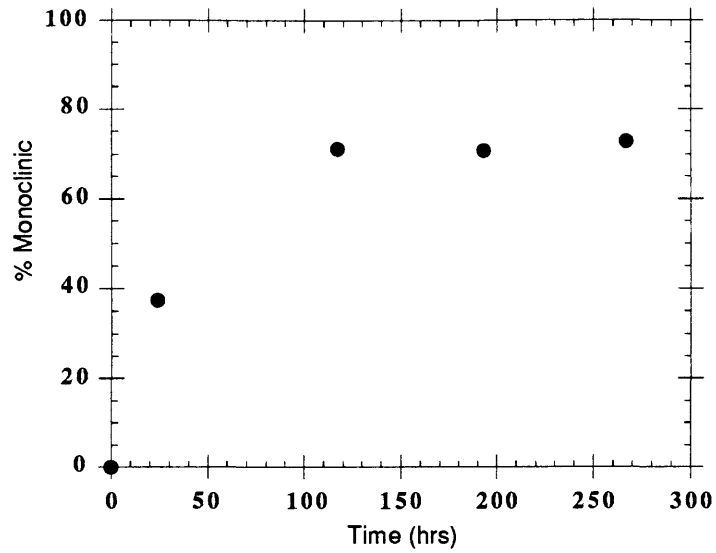


Fig. 3.26 Monoclinic content of polished Y-TZP polycrystalline samples exposed to 100°C 0.01 M HCl solution.

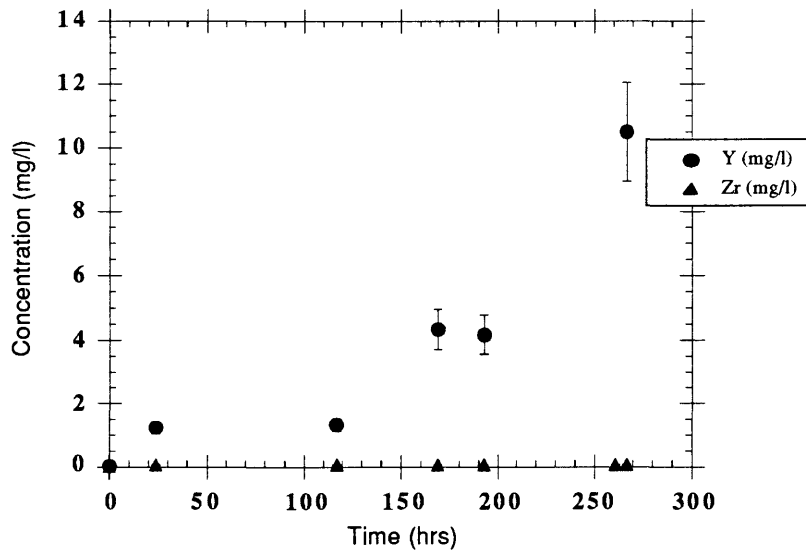


Fig. 3.27 Yttrium and zirconium concentrations in solutions from polished Y-TZP polycrystalline samples in 100°C 0.01 M HCl solution.

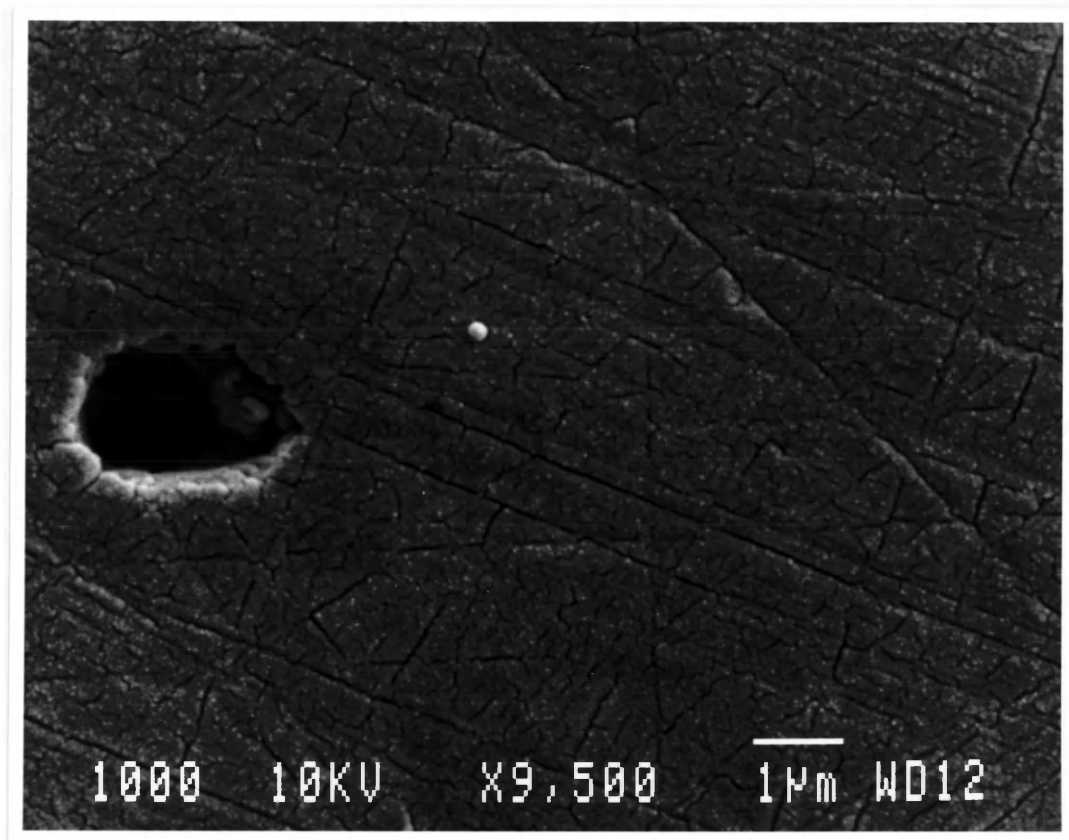


Fig. 3.28 SEM micrograph of polished Y-TZP sample which was exposed to 100°C 0.01 M HCl solution for 169.0 hours.

3.3.2 Mechanical Testing

Flexural tests were conducted on dense Y-TZP samples which had been degraded in 100°C water, 100°C 1.0 x 10⁻⁴ M HCl solutions, or 100°C 0.01 M HCl solutions. Samples consisted of fine grained and coarse grained materials, the details of which were discussed in the experimental procedure.

The bending strengths of initial and degraded samples are shown in Figs. 3.29, 3.30 and 3.31. The monoclinic contents of the flexural bars are illustrated in Fig. 3.32, 3.33 and 3.34. Cross-sections indicating the monoclinic layers for both the Mines and the Coors materials are illustrated in the micrographs in Figs. 3.35 and 3.36, respectively.

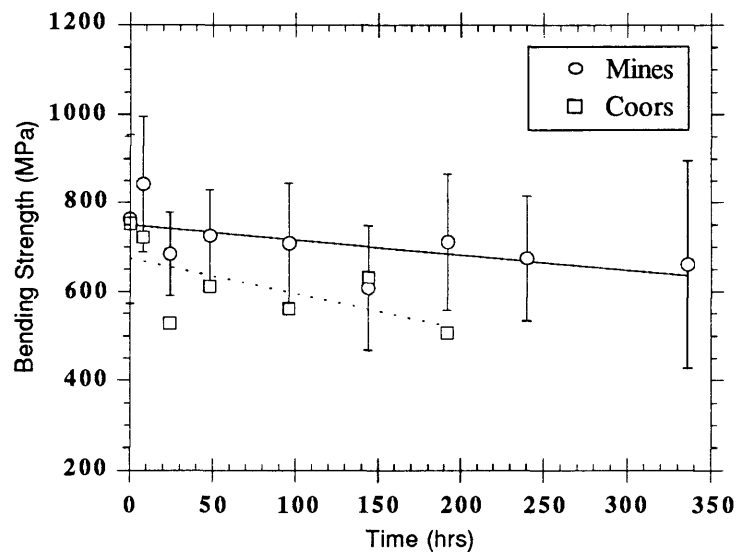


Fig. 3.29 Bending strengths of Y-TZP flexural test bars after degrading in 100°C water.

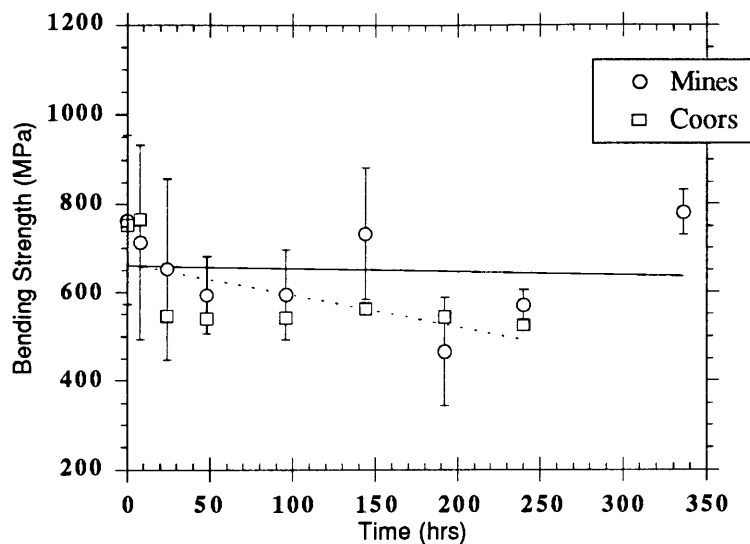


Fig. 3.30 Bending strengths of Y-TZP flexural test bars after degrading in 100°C 1.0 x 10⁻⁴ M HCl solution.

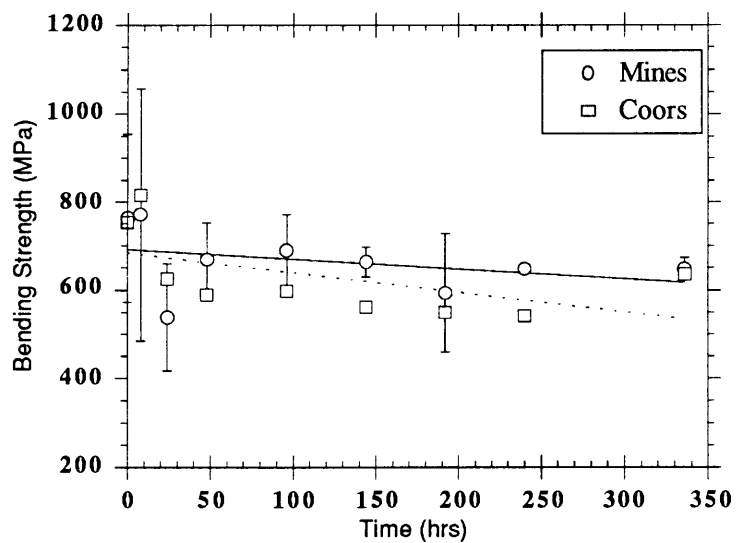


Fig. 3.31 Bending strengths of Y-TZP flexural test bars after degrading in 100°C 0.01 M HCl solution.

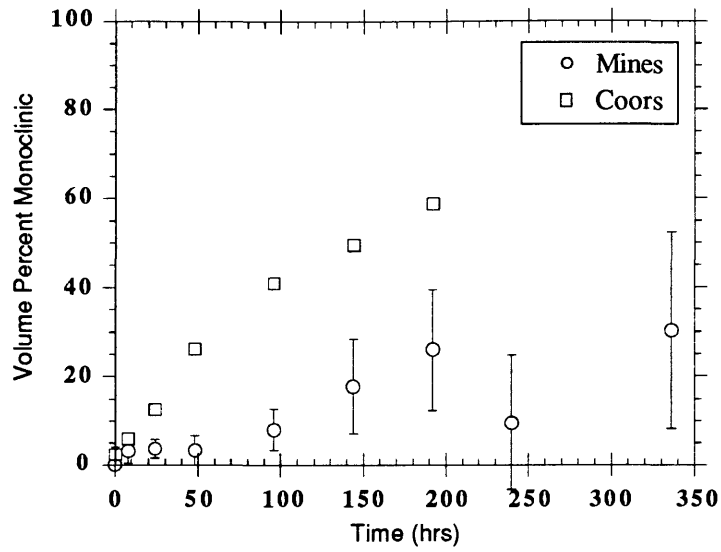


Fig. 3.32 Monoclinic contents of flexural test bars degraded in 100°C water.

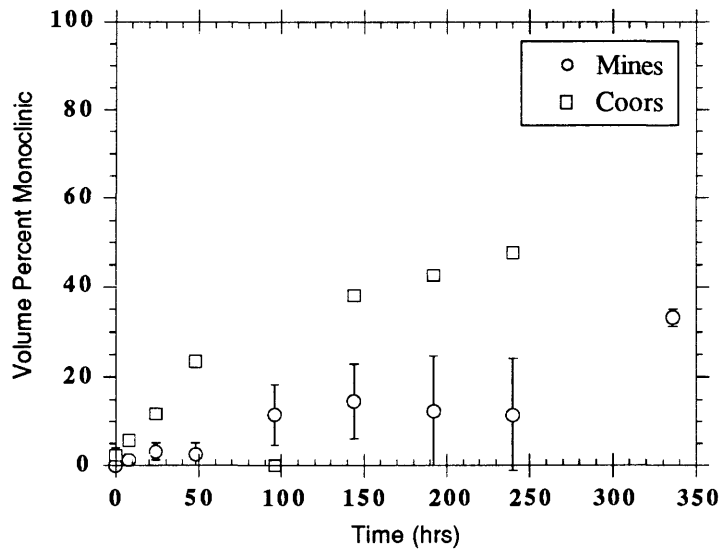


Fig. 3.33 Monoclinic contents of flexural test bars degraded in 100°C 1.0 x 10⁻⁴ M HCl solution.

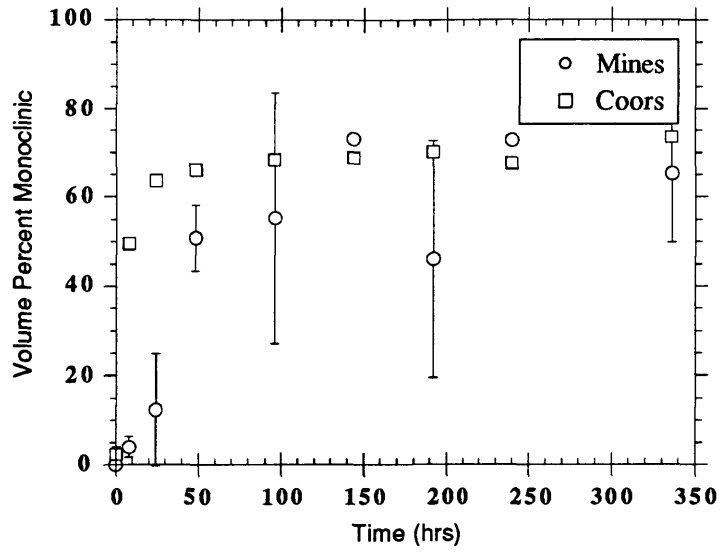
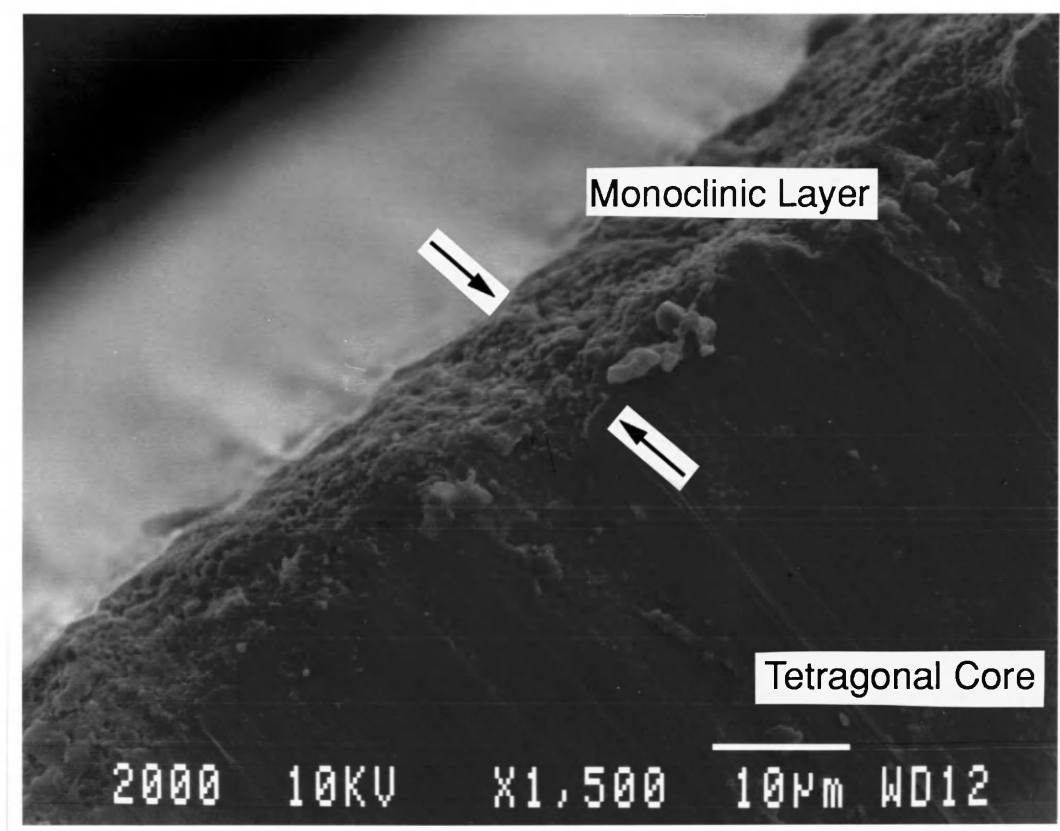


Fig. 3.34 Monoclinic contents of flexural test bars degraded in 100°C 0.01 M HCl solution.



MOR Bar Cross-Section

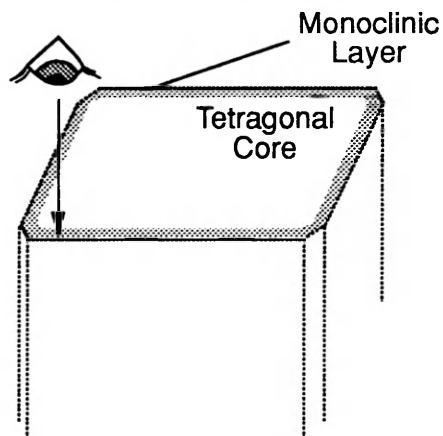


Fig. 3.35 SEM micrograph of cross-section of Mines MOR bar which was degraded for 50 hours in 100°C 0.01 M HCl solution.

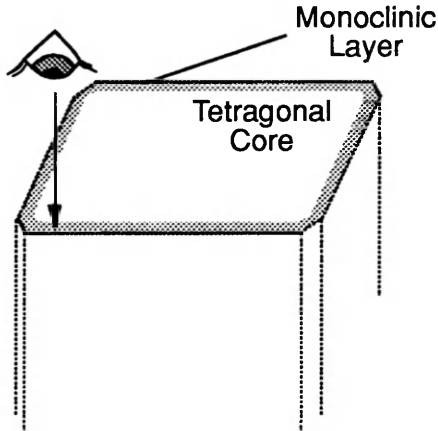
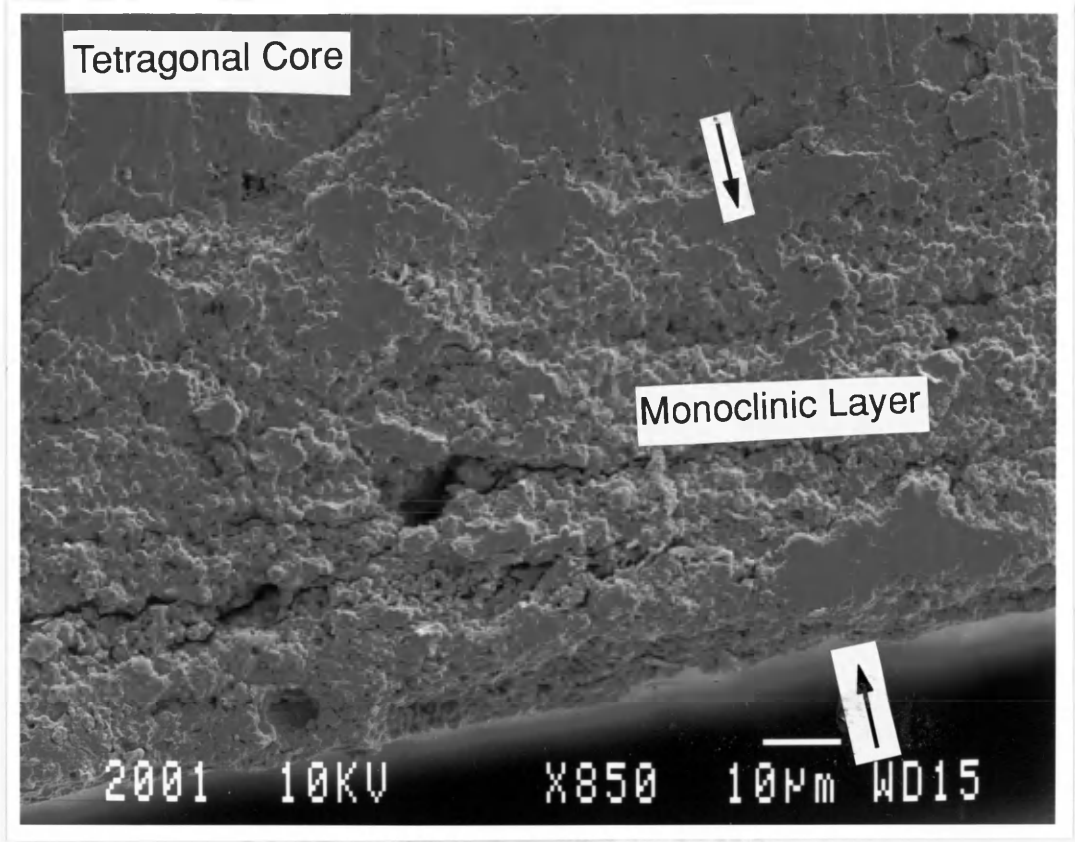


Fig. 3.36 SEM micrograph and schematic of cross-section of Coors MOR bar which was degraded for 50 hours in 100°C, 0.01 M HCl solution.

4 DISCUSSION

Initially the goal of this research was to investigate the degradation of yttria-stabilized zirconia in aqueous solutions and, from these investigations, determine the mechanisms causing the degradation. It was hypothesized that the degradation occurred due to preferential dissolution of yttrium from the crystal lattice, causing the metastable tetragonal phase to destabilize and transform to the stable monoclinic phase.

The dissolution characteristics of the Y-TZP powder proved to be interesting, and somewhat perplexing. Whereas it was predicted that the yttrium should selectively dissolve, the 95°C water data depicted in Fig. 3.2 does not support this prediction. If the yttrium were to dissolve preferentially, a plot of the yttrium concentration in solution versus the zirconium concentration would show very high yttrium to zirconium ratios. However, when the data is plotted in this manner, as in Fig. 4.1, the yttrium to zirconium weight ratio is nearly 6.0%. Calculations show (Appendix A) that a stoichiometric weight ratio between yttrium and zirconium is approximately 6.0%. Therefore, the data for the 95°C water investigations would indicate that yttrium does not dissolve preferentially but rather stoichiometrically.

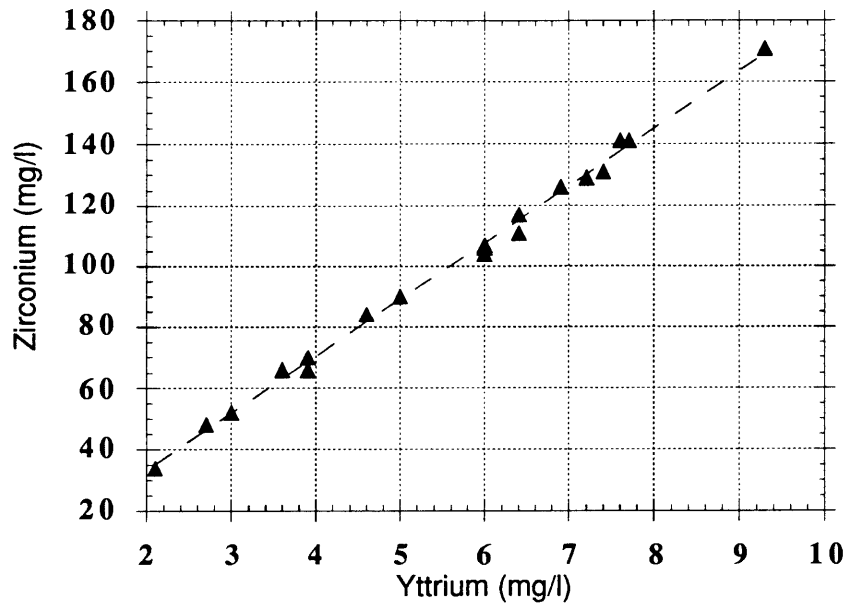


Fig. 4.1 Correlation between yttrium and zirconium concentrations in solution for Y-TZP samples exposed to 95°C water.

In contrast, when the temperature was raised to 240°C and the solution made acidic, as the experimental data illustrated in Fig. 3.4 indicates, that yttrium dissolved preferentially.

This Y-TZP powder, like most of the fine-grained Y-TZP powders commercially available, is synthesized employing a coprecipitation process. During this process, a hydrolyzed mixture of $ZrOCl_2$ and YCl_3 is precipitated to form a zirconium/yttrium hydroxide compound which is then dried and calcined at approximately 850-950°C.⁵⁵ If carefully controlled, this process should lead to an oxide which has yttrium and zirconium uniformly distributed on the atomic scale. However, if the process has not successfully homogenized the material, residual yttrium and zirconium chlorides, most likely in near stoichiometric ratios, will remain. Provided the chlorides are soluble in water, their dissolution would lead to stoichiometric yttrium-zirconium ratios in the solution that increase with passing time. While this explanation does account for the exact stoichiometric ratios in the 95°C water experiments, it does not explain the dissolution

behavior at higher temperature in more acidic solutions. One would expect similar, although perhaps faster, dissolution behavior at higher temperatures and in acidic solutions than in lower temperature, less acidic solutions. Unfortunately, the 240°C 0.01 M HCl data, Fig. 3.4, do not support this theory. It is possible that two different mechanisms occur in these solutions. However, considerably more data needs to be collected at different temperatures and pHs before speculating about these mechanisms.

One result is clear from the powder investigations, the tetragonal phase in the powder is very stable, even at high temperatures, and in acidic solutions. The essentially unchanged monoclinic content of the powder in both 95°C water, Fig. 3.1, and 240°C 0.01 M HCl solution, Fig. 3.3, provide evidence of this stability. On the one hand, this should not be surprising considering that the literature states that a Y-TZP ceramic containing an average grain size of 300 nm is considered relatively resistant to degradation and the Y-TZP powder has an effective average grain size of 133 nm. However, the studies discussed in the introduction focused on polycrystalline materials in which grains are surrounded by a matrix of other grains, not on relatively unconstrained particles found in powders. Consequently, prior to these studies the degradation behavior, i. e., stability, of these powders was uncertain. It is important to state here that fine grained Y-TZP powders do not make suitable materials for degradation investigations for two reasons. One, they may be incompletely calcined and homogenized and, two, due to their fine particle size, they remain very stable and do not readily exhibit degradation behavior.

Due to these difficulties encountered with powders, VPS Y-TZP samples were employed. Vapor phase sintering at 1300°C for thirty minutes in 1 atm HCl produced a more homogeneous material, more typical of polycrystalline materials without sacrificing the large surface areas afforded by powders. As indicated by the average grain sizes in Table 3.1, and the visual confirmation from SEM micrographs such as Figs. 2.1 and 2.2, vapor phase sintering increased the grain size from 133 nm for the powder to approximately 600 nm for the VPS samples, while the surface area was only slightly reduced from approximately 7.5 m²/g for the powder to approximately 1.7 m²/g for the VPS samples.

An interesting note should be made here concerning the kinetics of vapor phase sintering of yttria containing zirconias and pure zirconias. Qualitatively, the vapor phase sintering kinetics of 3 mol% Y-TZP were considerable slower than that of pure zirconia observed in the literature. Whereas the Y-TZP particle size grew from 150 nm to 600 nm after sintering for 30 minutes at 1300°C in 1.0 atm HCl, the pure zirconia⁵¹ grew from 200 nm to over 1.0 μm during the same treatment. The slower kinetics might be the result of the yttrium or, possibly, some other impurity. This is an area for further work.

The dissolution results for yttria shown in Fig. 3.5 demonstrate that it is indeed soluble, but not nearly to the extent that the thermodynamics predict. The thermodynamics, as illustrated in Figs. 1.7 and 1.8, predict that yttria is essentially infinitely soluble in acidic solutions at 25°C, yet Fig. 3.5 shows yttrium contents in 100°C water on the order of 0.3 mg/l and yttrium contents in 100°C 0.01M HCl on the order of 20 mg/l. Although the yttrium levels in solution are not as high as predicted, the data do show that yttria is soluble and that the amount dissolved in a given time increases with increased acidity.

The most striking result from the VPS Y-TZP data is that yttrium definitely leaches preferentially. Not only does yttrium leach out preferentially, its dissolution rate increases as the solution's acidity increases. Unfortunately, the yttrium concentration data for each solution varied considerably from run to run. Sometimes, as indicated in the water results, Fig. 3.7, and the 1.0×10^{-4} M HCl solution results, Fig. 3.11, the yttrium concentration varied by as much as two orders of magnitude. Unfortunately, there does not appear to be a reasonable explanation for these data. However, if these two stray data sets, the "Yc" run in Fig. 3.7, and the "Ya" run in Fig. 3.11, are removed, a qualitative correlation between the amount of yttrium leached and the monoclinic content is seen. As the acidity of the solution increased, the amount of yttrium leached increased and the monoclinic contents increased. Unfortunately, due to the inconsistent data, it impossible to conduct quantitative kinetic evaluations, thereby making it equally impossible to determine dissolution mechanisms.

Silicon levels in the solutions were monitored for two reasons. First, the starting powder contains a considerable amount of silicon (Table 2.1) and, secondly Heuer, et. al.,

have found that nearly all Y-TZP ceramics contain a glassy intergranular phase which is high in silicon and yttrium.⁵⁶ Although the vapor phase sintered ceramics are very porous, they still contain grain boundaries at the necks between the particles. Data from the 100°C water, Fig. 3.9; the 100 °C 1.0×10^{-4} M HCl solution, Fig. 3.13 and the 100°C 0.01 M HCl solution, Fig. 3.17 all show substantial silicon concentrations in solution. In addition, a silicon concentration saturation limit which increased with increased acidity was observed in all the solutions. Correlations between silicon concentrations in solution and the amount of silicon in the material as determined by x-ray fluorescence, Table 2.1, show that even in the 0.01 M HCl solution where the silicon levels were the highest at approximately 45 mg/l, the amount of silicon removed from the material is approximately 12%. Therefore, the remaining silicon must either be tied up in the ceramic grain interior, or the silicon is indeed available but a solubility limit has been reached. As with the yttrium, the amount of silicon concentrations in solution appear to be directly proportional to the monoclinic content.

The zirconium concentrations in the water, Fig. 3.8; 1.0×10^{-4} M HCl, Fig. 3.12 and 0.01 M HCl, Fig. 3.16, are all quite low, nearly at the detection limits in some instances. Although, the zirconium levels increase with decreasing acidity as the thermodynamics predicts, the consistently low zirconium levels yet increasing monoclinic contents would indicate that zirconium's role in the degradation is minimal.

To summarize the vapor phase sintered experiments, three interesting phenomena were observed: (1) the monoclinic contents were essentially the same for the water and 1.0×10^{-4} M HCl solutions, Figs. 3.6 and 3.10, respectively, but the monoclinic levels for the 0.01 M HCl solutions, Fig. 3.14, increased dramatically; (2) the monoclinic content of the 0.01 M HCl solution did not exhibit the saturation behavior seen in dense polycrystalline materials; and, if, as discussed earlier, the stray data in the water and 1.0×10^{-4} M HCl solution are ignored, monoclinic contents appear to be directly proportional to yttrium, and possibly to silicon levels in solution. Based on these observations, the degradation appears to be related to not only the amount of yttrium leached, but also to the amount of silicon leached from the Y-TZP material.

The polycrystalline morphological investigations provided morphological information as well as additional solubility data. Since the unpolished and polished materials have a similar composition and microstructure, it can be assumed that the materials have a similar degradation resistance. The solubility data for the unpolished Y-TZP, Fig. 3.19, and the polished Y-TZP, Fig. 3.27, demonstrates both the preferential dissolution of yttrium as well as increased yttrium solubility in acidic solutions. An important observation to be made from the polycrystalline data is that the yttrium concentrations in solutions, Figs. 3.19 and 3.27, coincided with higher monoclinic contents, Figs. 3.18 and 3.26. Zirconium levels in the polycrystalline solutions were near the detection limit of the ICP-ES machine. Zirconium's role in the degradation is uncertain, however, the low levels would indicate that it is negligible. Qualitatively, these data and the VPS data would indicate that the preferential leaching of yttrium and possible silicon* appear to be important degradation mechanisms.

The SEM micrographs of the unpolished samples, Figs. 3.20-3.23, indicate that the grain boundaries are being preferentially attacked. The TEM micrograph of the replica, Fig. 3.24, provided an order of magnitude higher resolution in order to better observe what is occurring at the grain boundaries. The micrograph indicates that the grain boundary attack appears to be very localized, resulting in pitting along the grain boundaries and at grain triple points. It is possible that some of the observed pits might in fact be residual porosity, however, it is unlikely that all the pits are pores. The TEM micrograph of the thin foil section shows the presence of a small amount of glassy phase at the grain boundaries and triple points. When the two TEM micrographs are compared the pits in the replica micrograph correlate well with the glass pockets in the thin foil section. Considering Heuer's observations and the silicon levels present in the original powder (Table 2.1), it is most likely that the polycrystalline Y-TZP used in these investigations also contained a high yttrium, silicon glassy phase. Without the silicon concentrations it is difficult to emphatically state that the degradation is caused by grain boundary dissolution

* Silicon levels in solution were not requested for these investigations since at the time they were being conducted, silicon's role in the degradation was not considered. It would have been very interesting to have these data and compare it to the VPS sample levels.

where silicon and yttrium are dissolved from the grain boundary glassy phase, but that appears to be the case.

It is appropriate at this point to summarize the dissolution investigations. The Y-TZP powder results are unclear making it difficult to compare to the VPS and polycrystalline results. Both the VPS and the polycrystalline results indicate the preferential dissolution of yttrium, while the VPS results show high levels of silicon.

Two possible yttrium, silicon sources should be considered, the bulk material and the grain boundaries. If the source of the yttrium were the bulk material, dramatic increases in exposed surface area should lead to dramatic increases in dissolved species in solution. The VPS and polycrystalline results do not support this notion. The difference in yttrium levels between the VPS, 100°C 0.01 M HCl solution, Fig. 3.15, and the polycrystalline, 100°C 0.01 M HCl solution, Fig. 3.27, was only a factor of ten, yet the surface areas, VPS $\approx 3 \text{ m}^2$, polycrystalline $\approx 3 \times 10^{-4} \text{ m}^2$, differed by four orders of magnitude. This indicates that yttrium levels are not related to the exposed surface areas of the materials.

Whereas the surface area is a measurable quantity, the grain boundary concentration in a sample is not and must be calculated based on idealized models. The assumptions and calculations for grain boundary concentration models for VPS and dense, polycrystalline Y-TZP materials are presented in Appendix B. It is sufficient to state here that the polycrystalline sample is modeled as a dense cube containing cubic grains and the vapor phase sintered sample is modeled as cubic packed spherical grains. Based on these models, the polycrystalline sample has a calculated grain boundary concentration of approximately 10^5 cm , while the VPS sample calculated concentration was approximately 10^8 cm . Once again, the difference in yttrium concentrations in solution between VPS Y-TZP and dense, polycrystalline Y-TZP, Figs. 3.15 and 3.27, is a factor of ten yet the calculated grain boundary concentration between VPS and polycrystalline Y-TZP differ by nearly four orders of magnitude. This would indicate that the yttrium concentrations in solution are not related to the available grain boundaries. However, certain assumptions were made in the models which may have been too idealized. Examples of these possible poor assumptions include (1) the polycrystalline material is not 100% dense but contains

porosity which opens up subsurface grain boundaries to exposure and (2) polycrystalline materials contain a distribution of spherical grain sizes rather than monodisperse square grains increasing the grain density and thus the grain boundary concentration. Whether these factors are sufficient to bring the grain boundary concentrations within one order of magnitude is uncertain. Much more sophisticated models might provide the answer. Unfortunately, that would be beyond the scope of this research.

The polycrystalline mechanical investigation yielded mixed results. As the literature points out, fine grained Y-TZP ceramics should resist strength degradation better than coarser grained materials. This is in fact what was discovered as the bending strength of the fine-grained, denser Mines material decreased less than the relatively coarse-grained Coors material. In addition, the increase of the monoclinic content of the Mines material was less than that of the Coors material. In light of this, the literature states^{16-19, 25-30} that the strength degradation of Y-TZP materials is a result of the monoclinic layer which develops. It is curious to note that while the monoclinic contents increased dramatically, the bending strengths did not show similar dramatic reductions.

Two things need to be considered before making a conclusion on the monoclinic content-bending strength dilemma, (1) x-ray penetration depth and (2) the effect of the thickness of the monoclinic layer on strength. The x-ray penetration is a function of the radiation used for diffraction and the material it is diffracting from and experimental geometry. This research utilized $\text{CuK}\alpha$ as a radiation source and, of course, the material was yttria-stabilized zirconia. The probe depth can be calculated from the X-ray absorption of the material which is given as:

$$I_x = I_0 e^{-\mu x} \quad (4.1)$$

where,

I_x \equiv intensity after absorption;

I_0 \equiv initial intensity;

μ \equiv linear absorption coefficient; and

x \equiv sample thickness.

Typically, linear absorption coefficients are not found in the literature, but mass attenuation coefficients, $\frac{\mu}{\rho}$, where ρ is the density of the species, are. When these are used, equation (4.1) becomes:

$$I_x = I_0 \exp^{-\frac{\mu}{\rho} \rho x} \quad (4.2)$$

Since Y-TZP is a mixture of yttrium, zirconium and oxygen atoms, it is necessary to use a weighted average of the mass attenuation coefficients based on the weight fractions of the species in the mixture. The mass attenuation coefficients for yttrium, zirconium and oxygen are $127.1 \text{ m}^2 \text{ kg}^{-1}$, $136.8 \text{ m}^2 \text{ kg}^{-1}$ and $11.03 \text{ m}^2 \text{ kg}^{-1}$, respectively.³³ A plot of the relative intensity ratio as a function of sample thickness determined from equation (4.2) is plotted in Fig. 4.3. Since x-rays must travel in and out of the sample during diffraction, and this distance depends on the rotation angles, the thickness in Fig. 4.3 would need to account for both these distances. Fig. 4.3 would indicate that even at normal incidence, where maximum penetration occurs, only the top 10.0 microns of the sample are probed.

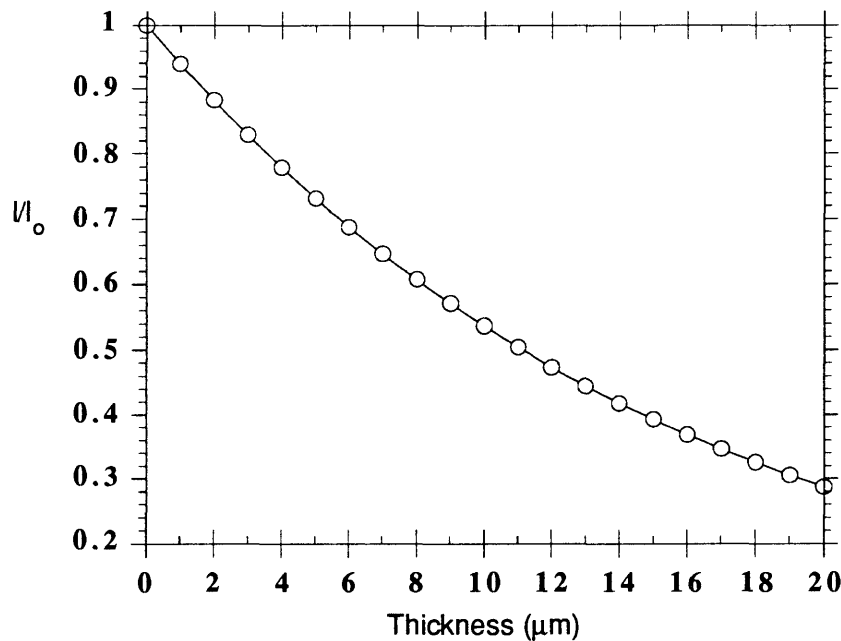


Fig. 4.3 X-ray absorption as a function of Y-TZP thickness.

Therefore, if the x-ray data is only revealing surface monoclinic contents, then it is quite possible that a very thin monoclinic layer is present on the sample which does not adversely affect the strength of the sample. This hypothesis would seem to explain the behavior of the degraded Y-TZP flexural bars.

The photomicrographs and schematics of degraded Mines and Coors flexural bars in Figs. 3.40 and 3.41, respectively, further support this hypothesis. As indicated by a porous, severely cracked layer in the micrographs, the monoclinic layer in the Mines material appears to be on the order of 10 μm , whereas the monoclinic layer for the Coors material appears to be approximately 70 μm . The monoclinic content of the Mines material was approximately 50 vol%, while the Coors monoclinic content was approximately 65 vol%, yet the strength decrease for the Mines material was only approximately 150 MPa, and the strength decrease for the Coors material was approximately 225 MPa. Therefore, even though the XRD data would suggest severe degradation as evidenced by very high

monoclinic contents, the actual strength degradation for these material was not as dramatic. It is possible that, had the bars been left to degrade for significantly longer time, there would have been a greater strength degradation

Based on the data presented and discussed here, the degradation appears to be the result of preferential dissolution of yttrium and silicon from the grain boundaries. This dissolution reduces the matrix restraint from metastable tetragonal grains allowing them to transform to the monoclinic phase. When the grains transform, micro- and macro-cracks develop which guide the degrading solution into the interior allowing further degradation to occur.

5 CONCLUSIONS

The following conclusions and observations were made during these investigations:

- flexural investigations of Y-TZP samples exposed to 100°C water, 1.0×10^{-4} M HCl and 0.01 M HCl solutions show slight strength degradation yet dramatic increases in monoclinic contents in thin surface layers that did not adversely effect the strength;
- fine-grained Y-TZP showed less strength degradation and less monoclinic content than coarse-grained Y-TZP;
- yttrium dissolves preferentially from Y-TZP vapor phase sintered and dense polycrystalline ceramics;
- high silicon concentrations were found in the solutions in which vapor phase sintered ("VPS") samples were degraded;
- yttrium levels in the solutions in which VPS and dense polycrystalline samples were degraded do not appear to correlate to the exposed surface area;
- yttrium levels do not correlate well to idealized grain boundary concentration calculations, however, due to the assumptions made, correlations may exist;
- both SEM and TEM micrographs of polycrystalline Y-TZP indicate that grain boundary dissolution is occurring;
- pure yttria is soluble in water and 0.01 M HCl solutions, showing higher solubility in the acid solution; and,
- Y-TZP powders are unsuitable for degradation investigations due to their extraordinary stability and possible chemical inhomogeneity.

Based on the data presented and discussed in this thesis, the following qualitative degradation model is proposed: initial degradation is caused by the preferential dissolution of yttrium and silicon from grain boundaries; this dissolution reduces the matrix restraint

from metastable tetragonal grains allowing them to transform to the monoclinic phase; when the grains transform, micro- and macro-cracks develop which guide the degrading solution into the interior allowing further degradation to occur.

6 SUGGESTED FUTURE WORK

There is a considerable amount of work to be done on the degradation of zirconia. The next logical step, which would complement the data presented here, would be to conduct solubility, morphological and mechanical investigations at higher temperatures. A factor which was not considered in these investigations but could be very important is the effect the chlorine anion has on the dissolution of Y-TZP. These investigations could be carried out by creating solutions of the same acidity as used in this investigation, yet make the solutions from acids other than HCl, for example HF or H₂SO₄. Finally, as mentioned in the thesis, it would be interesting to develop a more realistic dense, polycrystalline model from which grain boundary concentrations could be determined. From these data, and the grain boundary calculations determined from the VPS models, possible correlations might be observed between the yttrium levels in solution between polycrystalline and vapor phase sintered samples.

7 REFERENCES

1. T. Masaki and K. Sinjo, "Mechanical Properties of Highly Toughened ZrO₂-Y₂O₃," *Ceram. Int.*, **13** 109-12 (1987).
2. R. C. Garvie, "Structural Applications of ZrO₂-Bearing Materials," 465-79 *Advances in Ceramics Vol. 12, Science and Technology of Zirconia II*, edited by N. Claussen, M. Ruhle and A. H. Heuer, American Ceramic Society, Columbus, OH (1983).
3. R. Stevens, "Zirconia and Zirconia Ceramics," Magnesium Elektron Publication No. 113 (1986).
4. D. J. Green, R. H. J. Hannink and M. V. Swain, *Transformation Toughening of Ceramics*, 138-145 CRC Press, Inc., Boca Raton, FL (1989).
5. O. T. Masaki, H. Kuwashima, and K. Kobayashi, "Phase Change and Mechanical Properties of ZrO₂-Y₂O₃ Solid Electrolyte After Aging," *Solid State Ionics*, **3/4**, 489-95 (1981).
6. D. J. Green, R. H. J. Hannink and M. V. Swain, *Transformation Toughening of Ceramics*, CRC Press, Inc., Boca Raton, FL (1989).
7. E. C. Subbarao, "Zirconia-an overview," 1-13 *Advances in Ceramics Vol. 3, Science and Technology of Zirconia*, edited by H. A. Heuer, L. W. Hobbs, American Ceramic Society, Columbus, OH (1981).
8. R. Stevens, "Zirconia and Zirconia Ceramics," Magnesium Elektron Publication No. 113 (1986).
9. Phase diagram taken from M. Ruhle, N. Claussen and A. H. Heuer, "Microstructural Studies of Y₂O₃-Containing Tetragonal ZrO₂ Polycrystals (Y-TZP)," 352-70 *Advances in Ceramics Vol. 12, Science and Technology of Zirconia II*, edited by N. Claussen, M. Ruhle and A. H. Heuer, American Ceramic Society, Columbus, OH (1983).
10. C. Grain, "Phase Relations in the ZrO₂-MgO System," *J. Am. Ceram. Soc.*, **50** [6] 288-290 (1967).
11. V. Stubican and J. Hellmann, "Phase Equilibria in Some Zirconia Systems," 25-36 *Advances in Ceramics Vol. 3, Science and Technology of Zirconia*, edited by H. A. Heuer, L. W. Hobbs, American Ceramic Society, Columbus, OH (1981).

12. D. L. Porter and A. H. Heuer, "Mechanism of Toughening Partially Stabilized Zirconia (PSZ)," *J. Am. Ceram. Soc.* **60** [1-2] 183 (1977).
13. O. Ruff and F. Ebert, "Refractory Ceramics: I, The Forms of Zirconium Dioxide," *Z. Anorg. Allg. Chem.*, **180** [1] 19-41 (1929)
14. M. Ruhle and A. H. Heuer, "Phase Transformations in ZrO₂-Containing Ceramics: II, The Martensitic Reaction in t-ZrO₂," 14-32 *Advances in Ceramics Vol. 12, Science and Technology of Zirconia II*, Edited by N. Claussen, M. Ruhle and A. H. Heuer, American Ceramic Society, Columbus, OH (1983).
15. A. H. Heuer, R. Chaim and V. Lanteri, "Review: Phase transformations and Microstructural Characterization of Alloys in the System Y₂O₃-ZrO₂," *Advances in Ceramics Vol. 24, Science and Technology of Zirconia III*, edited by. S. Somiya, N. Yamamoto and H. Yanagida, American Ceramic Society, Inc., Westerville, OH (1988).
16. T. Masaki, "Mechanical Properties of Toughened ZrO₂-Y₂O₃ Ceramics," *J. Am. Ceram. Soc.*, **69** [8] 638-40 (1986).
17. T. Sato and M. Shimada, "Transformation of Ytria-Doped Tetragonal ZrO₂ Polycrystals by Annealing in Water," *J. Am. Ceram. Soc.*, **68** [6] 356-59 (1985).
18. T. Sato and M. Shimada, "Transformation of Ytria-Doped Tetragonal ZrO₂ Polycrystals by Annealing in Water," *J. Am. Ceram. Soc.*, **68** [6] 356-59 (1985).
19. T. Sato, S. Ohtaki, T. Endo and M. Shimada, "Changes in Crystalline Phase and Microstructure on the Surface of Ytria-Doped Tetragonal Zirconia Polycrystals by Annealing in Humid Conditions," 501-508 *Advances in Ceramics Vol. 24, Science and Technology of Zirconia III*, edited by. S. Somiya, N. Yamamoto and H. Yanagida, American Ceramic Society, Inc., Westerville, OH (1988).
20. F. Lange and A. Evans, "Erosive Damage Depth in Ceramics: A Study on Metastable, Tetragonal Zirconia," *J. Am. Ceram. Soc.*, **62** [1-2] 62-65 (1979).
21. J. Reed and A. Lejus, "Affect of Grinding and Polishing on Near-Surface Phase Transformations in Zirconia," *Mat. Res. Bull.*, **12** [10] 949-954 (1977).
22. P.J. Whalen, F. Reidinger and P. F. Antrim, "Prevention of Low Temperature Surface Transformation by Surface Recrystallization in Ytria Doped Tetragonal Zirconia," *J. Am. Ceram. Soc.*, **72** [2] 319-21 (1989).
23. J. F. Jue, J. Chen and A. Virkar, "Low-Temperature Aging of t'-Zirconia: The Role of Microstructure on Phase Stability," *J. Am. Ceram. Soc.*, **74** [8] 1811-20 (1991).
24. Ibid.

25. P.J. Whalen, F. Reidinger and P. F. Antrim, "Prevention of Low Temperature Surface Transformation by Surface Recrystallization in Ytria Doped Tetragonal Zirconia," *J. Am. Ceram. Soc.*, **72** [2] 319-21 (1989).
26. T. Sato and M. Shimada, "Transformation of Ytria-Doped Tetragonal ZrO₂ Polycrystals by Annealing in Water," *J. Am. Ceram. Soc.*, **68** [6] 356-59 (1985).
27. T. Sato and M Shimada, "Transformation of Ytria-Doped Tetragonal ZrO₂ Polycrystals by Annealing under Controlled Humidity Conditions," *J. Am. Ceram. Soc.*, **68** [12] C-320-322 (1985).
28. M. Watanabe, S. Iio and I Fukuura, "Aging Behavior of Y-TZP," 391-98 *Advances in Ceramics Vol. 12, Science and Technology of Zirconia II*, edited by. N. Claussen, M. Ruhle and A. H. Heuer, American Ceramic Society, Columbus, OH (1983).
29. A. Winnubst and A. Burggraaf, "The Aging Behavior of Ultra-Fined Grained Y-TZP in Hot Water," 39-47, *Advances in Ceramics Vol. 24, Science and Technology of Zirconia III*, edited by. S. Somiya, N. Yamamoto and H. Yanagida, American Ceramic Society, Columbus, OH (1988).
30. N. Hecht, S. Jang and D. McCullum, "Environmental Effects on Toughened Zirconia Ceramics," 133-144, *Advances in Ceramics Vol. 24, Science and Technology of Zirconia III*, edited by. S. Somiya, N. Yamamoto and H. Yanagida, American Ceramic Society, Columbus, OH (1988).
31. T. Arai, T. Yamamoto and K. Tsuji, "Transition-Free Zirconia Ceramics," 517-522, *Advances in Ceramics Vol. 24, Science and Technology of Zirconia III*, edited by. S. Somiya, N. Yamamoto and H. Yanagida, American Ceramic Society, Columbus, OH (1988).
32. M. Wakamatsu and N. Takeuchi, "Effect of Firing Atmosphere on the Sintering of ZrO₂," 1023-1031, *Advances in Ceramics Vol. 24, Science and Technology of Zirconia III*, edited by. S. Somiya, N. Yamamoto and H. Yanagida, American Ceramic Society, Columbus, OH (1988).
33. B. D. Cullity, *Elements of X-Ray Diffraction, 2nd Edition*, 295-317 Addison-Wesley Publishing Company, Inc., Reading, MA (1956).
34. L. Schwartz and J. Cohen, *Diffraction from Materials*, 202-203 Springer-Verlag, Berlin (1977).
35. M. Matsui, T. Soma and I. Oda, "Stress-Induced Transformation and Plastic Deformation for Y₂O₃-Containing Tetragonal Zirconia Polycrystals," *J. Am. Ceram. Soc.*, **69** [3] 198-202 (1986).
36. J. Wang and R. Stevens, "Preferred ZrO₂(t) - ZrO₂(m) Transformation on the Aged Surface of Y-TZP Ceramics," *J. Mater. Sci. Lett.*, **8** 1195-98 (1989).

37. T. Sato and M. Shimada, "Transformation of Yttria-Doped Tetragonal ZrO₂ Polycrystals by Annealing in Water," *J. Am. Ceram. Soc.*, **68** [6] 356-59 (1985).
38. M. Yoshimura, T. Noma, K. Kawabata and S. Somiya, "Role of H₂O on the Degradation Process of Y-TZP," *J. Mater. Sci. Lett.*, **6** 465-67 (1987).
39. T. Lepisto and T. Mantyla, "A Model for Structural Degradation of Y-TZP Ceramics in Humid Atmosphere," *Ceram. Eng. Sci. Proc.*, **10** [7-8] 658-67 (1989).
40. N. Hecht, S. Jang and D. McCullum, "Environmental Effects on Toughened Zirconia Ceramics," 133-144 Advances in Ceramics Vol. 24, Science and Technology of Zirconia III, edited by. S. Somiya, N. Yamamoto and H. Yanagida, American Ceramic Society, Columbus, OH (1988).
41. T. Sato and M. Shimada, "Transformation of Ceria-Doped Tetragonal Zirconia Polycrystals by Annealing in Water," *Am. Ceram. Soc. Bull.*, **64** [10] 1382-84 (1985).
42. T. Sato, S. Ohtaki, T. Endo and M. Shimada, "Improvement of Thermal Stability of Yttria-Doped Tetragonal Zirconia Polycrystals by Alloying with Various Oxides," *Int. J. High Tech. Ceram.*, **2** 167-77 (1986).
43. T. Sato and M. Shimada, "Control of the Tetragonal-to-Monoclinic Phase Transformation of Yttria Partially Stabilized Zirconia in Hot Water," *J. Mat. Sci.*, **20** 3988-3992 (1985).
44. M. Hirano, H. Inada, "Hydrothermal Stability of Yttria- and Ceria-Doped Tetragonal Zirconia-Alumina Composites," *J. Mat. Sci.*, **26** 5047-5052 (1991).
45. A. Winnubst and A. Burggraaf, "The Aging Behavior of Ultrafine-Grained Y-TZP in Hot Water," 39-47 Advances in Ceramics Vol. 24, Science and Technology of Zirconia III, edited by. S. Somiya, N. Yamamoto and H. Yanagida, American Ceramic Society, Columbus, OH (1988).
46. M. Yoshimura, T. Hiuga and S. Somiya, "Dissolution and reaction of Yttria-Stabilized Single Crystals in Hydrothermal Solutions," *J. Am. Ceram. Soc.*, **69** [7] 583-84 (1986).
47. M. Yoshimura, T. Noma, K. Kawabata and S. Somiya, "Role of H₂O on the Degradation Process of Y-TZP," *J. Mater. Sci. Lett.*, **6** 465-67 (1987).
48. K. Nakajima, K. Kobayashi and Y. Murata, "Phase Stability of Y-PSZ in Aqueous Solutions," 399-407 Advances in Ceramics Vol. 12, Science and Technology of Zirconia II, edited by. N. Claussen, M. Ruhle and A. H. Heuer, American Ceramic Society, Columbus, OH (1983).

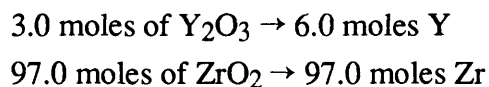
49. Thermodynamic data taken from M. Pourbaix, Atlas of Electrochemical Equilibria in Aqueous Solutions, 177-182 & 223-229 Pergamon Press, New York (1966).
50. M. Shafer and R. Roy, "Rare-Earth Polymorphism and Phase Equilibrium in Rare-Earth Oxide-Water Systems," *J. Am. Ceram. Soc.*, **42** [11] 563-70 (1959).
51. Readey and Readey, "Sintering of ZrO₂ in HCl Atmospheres," *J. Am. Ceram. Soc.* **69** [7] 580 (1986).
52. R. C. Garvie and P. S. Nicholson, "Phase Analysis in Zirconia Systems," *J. Am. Ceram. Soc.* **55** [6] 303-305 (1972).
53. D. L. Porter and A. H. Heuer, "Microstructural Development in MgO-Partially Stabilized Zirconia (Mg-PSZ)," *J. Am. Ceram. Soc.*, **62** [5-6] 298-305 (1979).
54. H. Toraya, M. Yoshimura and S. Somiya, "Calibration Curve for Quantitative Analysis of the Monoclinic-Tetragonal ZrO₂ System by X-Ray Diffraction," *J. Am. Ceram. Soc.*, **67** [6] C-119-C-121 (1984).
55. R. Stevens, "Zirconia and Zirconia Ceramics," Magnesium Elektron Publication No. 113 (1986).
56. M. Ruhle, N. Claussen and A. Heuer, "Microstructural studies of Y₂O₃-Containing Tetragonal ZrO₂ Polycrystals (Y-TZP)," 352-370 Advances in Ceramics Vol. 12, Science and Technology of Zirconia II, edited by N. Claussen, M. Ruhle and A. H. Heuer, American Ceramic Society, Columbus, OH (1983).

8 APPENDICES

Appendix A

To determine the stoichiometric yttrium to zirconium weight ratio, it is necessary to first determine the yttrium and zirconium contents in the starting material.

For a 3.0 mol% yttria-stabilized zirconia,



The yttrium/zirconium molar ratio is 6.2%.

In terms of the mass ratio,

$$\frac{(6.0 \text{ moles } Y)(88.90 \text{ g } Y/\text{mol})}{(97.0 \text{ moles } Zr)(91.22 \text{ g } Zr/\text{mol})} = 6.0 \%$$

Therefore, the stoichiometric mass yttrium to zirconium ratio for a 3.0 mol% yttria-stabilized zirconia is 6.0%.

Appendix B

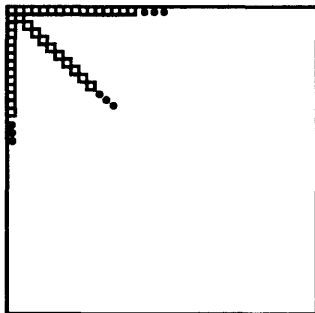
Comparison of Grain Boundary Distance Available from Dense Polycrystalline Material and VPS Material

For a polycrystalline material:

Assumptions:

- (1) Sample is 100% dense
- (2) Grains are square and they have $0.5 \mu\text{m}$ edges
- (3) Grain boundaries have negligible thickness and can be considered lines
- (4) Sample is perfect cube
- (5) Sample mass is 2.0 g
- (6) Density is 5.9 g cm^{-3}

Cube Geometry:



Cube Face

Need cube dimensions first:

$$\text{Volume} = \frac{2.0 \text{ g}}{5.9 \text{ g cm}^{-3}} = 0.339 \text{ cm}^3$$

$$\text{Cube side length} = \sqrt[3]{0.339 \text{ cm}^3} = 0.697 \text{ cm}$$

The number of 0.5 μm grains per edge:

$$\frac{0.697 \text{ cm}}{0.5 \times 10^{-4} \text{ cm}} \approx 14,000 \frac{\text{grains}}{\text{edge}}$$

The number of grains per face:

$$14,000 \frac{\text{grains}}{\text{edge}}^2 = 2.0 \times 10^8 \frac{\text{grains}}{\text{face}}$$

The number of grains on all six faces:

$$6 \cdot 2.0 \times 10^8 \frac{\text{grains}}{\text{face}} = 1.2 \times 10^9 \frac{\text{grains}}{\text{surface}}$$

The grain boundary distance is then:

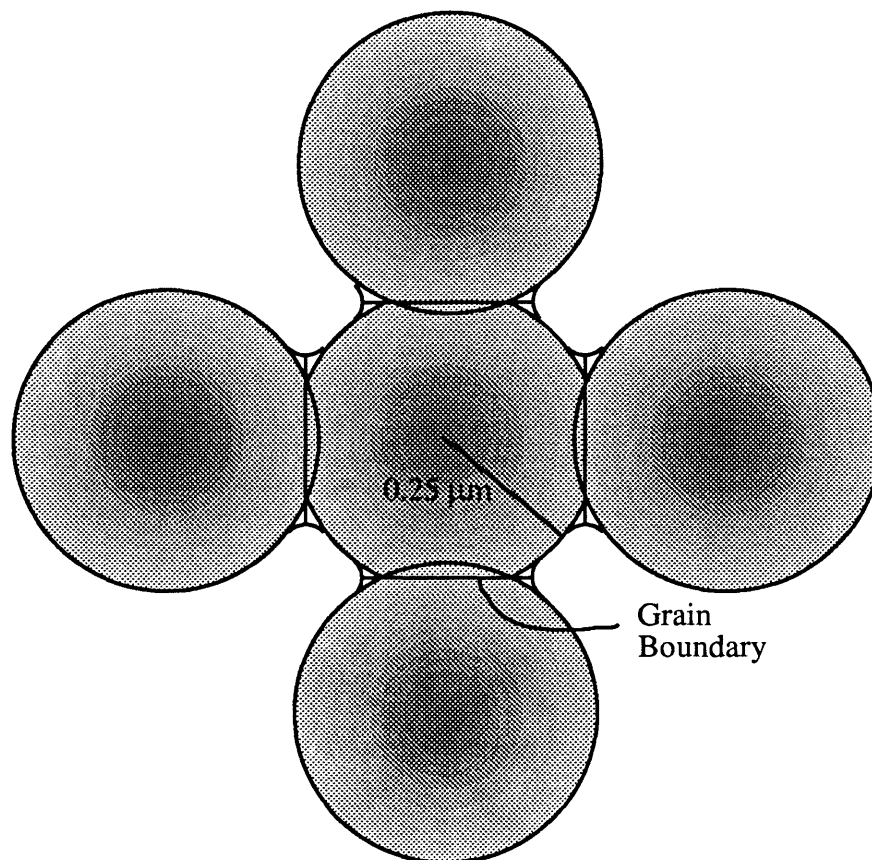
$$6 \cdot 2 \cdot 14,000 \frac{\text{grains}}{\text{edge}} \cdot 0.697 \text{ cm} = 1.2 \times 10^5 \text{ cm per sample}$$

For a Vapor Phase Sintered sample:

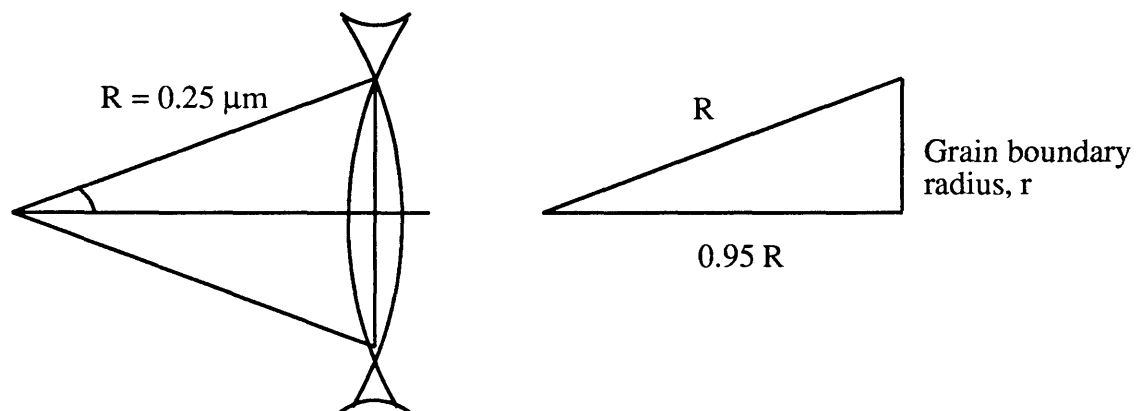
Assumptions:

- (1) Grain size is 0.5 μm
- (2) Sample mass is 2.0 g
- (3) Grains are spheres
- (4) Spheres are packed in a cubic configuration
- (5) Linear shrinkage is approximately 5% (observed experimentally)

Sample Geometry:



Close-Up of Grain Boundary Geometry:



Grain boundary is considered the perimeter of the neck region between the spheres.
Need to calculate this distance:

From the above geometries and some simple trigonometry:

$$r^2 + (0.95 R)^2 = R^2$$

$$r = 0.31R$$

For a radius, R, of 0.25 μm :

$$r = 0.08 \mu\text{m}$$

Then the neck perimeter is:

$$2 \pi 0.08 \mu\text{m} = 0.5 \mu\text{m}$$

If there are three grain boundaries per grain, then the grain boundary distance per grain is:

$$3 (0.5 \mu\text{m}) = 1.5 \mu\text{m GB grain}^{-1}$$

Now, need the number of grains per sample:

$$\text{Specific surface area} = \frac{3}{r R} = \frac{3}{5.9 \times 10^6 \text{ g m}^{-3} 0.25 \times 10^{-6} \text{ m}} = 2.0 \text{ m}^2 \text{ g}^{-1}$$

The surface area for a 2.0 g sample is twice the A_{sp} , or, 4.0 m^2 .

The surface area occupied by the remaining sphere (see sample geometry) is:

$$= 4 \pi R^2 - 6(2 \pi R 0.05 R)$$

$$= 3.4 \pi R^2$$

$$= 0.67 \mu\text{m}^2 = 6.7 \times 10^{-13} \text{ m}^2 \text{ grain}^{-1}$$

The number of grains is then:

$$\frac{4.0 \text{ m}^2}{6.7 \times 10^{-13} \text{ m}^2 \text{ grain}^{-1}} = 6.0 \times 10^{12} \text{ grains}$$

The grain boundary distance in a VPS sample is then:

$$6.0 \times 10^{12} \text{ grains } 1.5 \times 10^{-6} \text{ m grain}^{-1} = 9.0 \times 10^6 \text{ m} = 9.0 \times 10^8 \text{ cm per sample}$$